The Dissertation Committee for Shannon Doane Lewis Certifies that this is the approved version of the following dissertation:

Chemical Vapor Sensing with Novel Coupled-Channel Field-Effect Transistors

Committee:

Ananth Dodabalapur, Supervisor

Jack C. Lee

Seth Bank

Chih-Kang "Ken" Shih

David Vanden Bout

Chemical Vapor Sensing with Novel Coupled-Channel Field-Effect Transistors

by

Shannon Doane Lewis

Dissertation

Presented to the Faculty of the Graduate School of

The University of Texas at Austin

in Partial Fulfillment

of the Requirements

for the Degree of

Doctor of Philosophy

The University of Texas at Austin

December 2018

Dedication

To my family.

Acknowledgements

I owe special debt of thanks to my advisor, Prof. Ananth Dodabalapur, and the administrative staff at the University of Texas Electrical Engineering Department, in particular Melanie Gulick. I would also like to thank my committee members and group members including Jaewon Shim, Dr. Chen-Guan Lee, Dr. Davianne Duarte, Dr. Christopher Lombardo, Dr. Daniel Fine, Damilare Ajibade, and Kelly Liang. A very special thanks to those scientists I worked most closely with including Deepak Sharma, Sebastian Schoefer, and Dr. Soumya Dutta.

Furthermore, many thanks to Dr. Joseph Nuffer, III, and Dr. Sara Saylor for invaluable editing.

I would also like to thank the Atomic and Molecular Imaging of Interfaces/Defects in Electronic, Spintronic, and Organic/Inorganic Materials IGERT and its principal investigators Prof. Ken Shih and Prof. Jack Lee for funding.

This material is based upon work supported by the National Science Foundation Graduate Research Fellowship under Grant No. DGE-054917, The Welch Foundation (F-1631), and the National Science Foundation ECCS Division (CHE-0847763).

Chemical Vapor Sensing with Novel Coupled-Channel Field-Effect Transistors

Shannon Doane Lewis, Ph.D.

The University of Texas at Austin, 2018

Supervisor: Ananth Dodabalapur

Chemical vapor sensing has numerous practical applications. Many small polar organic molecules, from alcohols to explosives, are tested for in ambient atmosphere every day as part of security and air quality monitoring. However, many of these tests require expensive monitoring equipment. This work explores organic and inorganic oxide semiconductors as room-temperature low-cost chemical vapor sensors.

Organic semiconductors have well-known chemical vapor sensing capabilities that arise from the grain boundaries and charge transport in their non-crystalline structure. However, organic semiconductors suffer from the bias stress effect in atmosphere and low mobilities. Inorganic oxide semiconductors also display sensitivity to polar vapor molecules and are transparent at visible wavelengths, which makes them of interest to the display industry.

Coupling disordered semiconductors with silicon channels can produce the detection range of organic and inorganic oxide semiconductors combined with the stability of electrical characteristics of silicon semiconductor devices. This work discusses three different device geometries designed to allow organic and inorganic oxide semiconductors to influence the current in a complementary silicon semiconductor channel. The four-terminal device is a novel device geometry developed to function in a

chemical memory mode that produces a one hundred-fold increase in silicon drain current in response to polar analyte vapor exposure. Thin film transistor (TFT) geometry relies on a silicon substrate to function as a bottom gate and processing platform. The bilayer device geometry also uses a silicon substrate as a bottom gate and processing platform, but then relies on the interaction of an inorganic oxide semiconductor and organic semiconductor in a planar heterojunction to produce a sensing event. The sensing mechanisms and responses for these devices are discussed in this work.

Table of Contents

List of Tables

List of Figures

Chapter 1: Organic Semiconductors

The first electrically conductive polymers were discovered by Hideki Shirakawa, Alan MacDairmid and Alan Heger in 1977—a discovery for which they won the Nobel Prize in Chemistry in 2000 [1]. Shirakawa, MacDairmid and Heger used iodine doping to create conductive polyacetylene (the polymerization of acetylene won Karl Zeigler and Guilo Natta the Nobel Prize in Chemistry in 1963).

Mott calculated the minimum metallic conductivity for an electron gas in an electric field with a lattice constant a (in Angstrom) to be

$$\sigma_{min} \sim \frac{610}{a} \Omega^{-1} cm^{-1}$$

at zero temperature where $E_F = E_C$ [2]. For Mott's ideal metal, the valence and conduction band overlap. He refers to "metallic" conductivities on the order of 150-400 $\Omega^{-1} cm^{-1}$, which are certainly achievable in doped organics, as shown below.

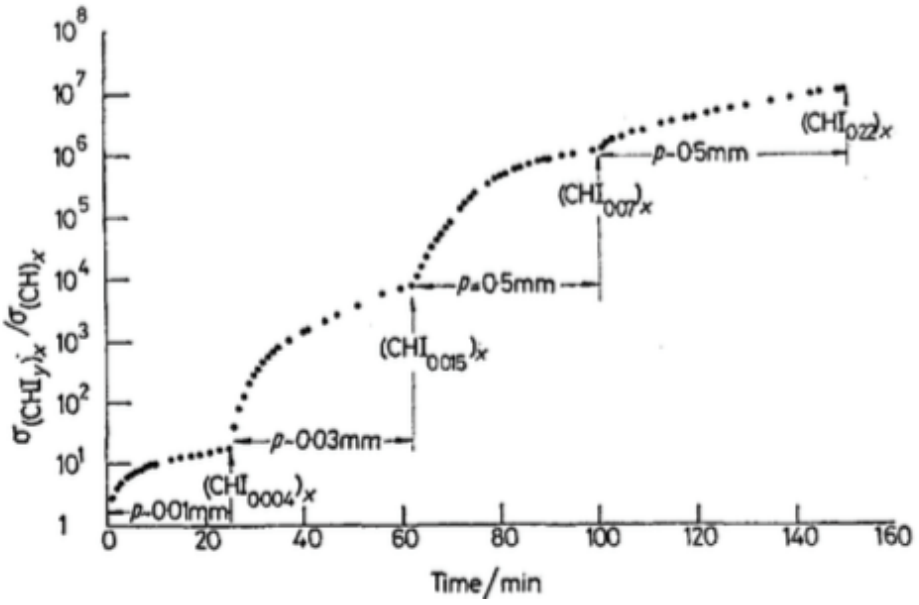

Figure 1.1: Conductivity in polyacetylene as a function of iodine exposure time, from Shirakawa *et al* [3].

The polymerization of acetylene in the presence of a concentrated Zeigler-Natta catalyst, $Ti(O\text{-}n\text{-}C_4H_9)_4/(C_2H_5)_3Al$, led to the formation of a matted precipitate film of polyacetylene. Shirakawa *et al* [3] demonstrated the production of iodine-doped conductive polyacetylene, a metallic polyacetylene with conductivity greater than Mott's minimum metallic conductivity.

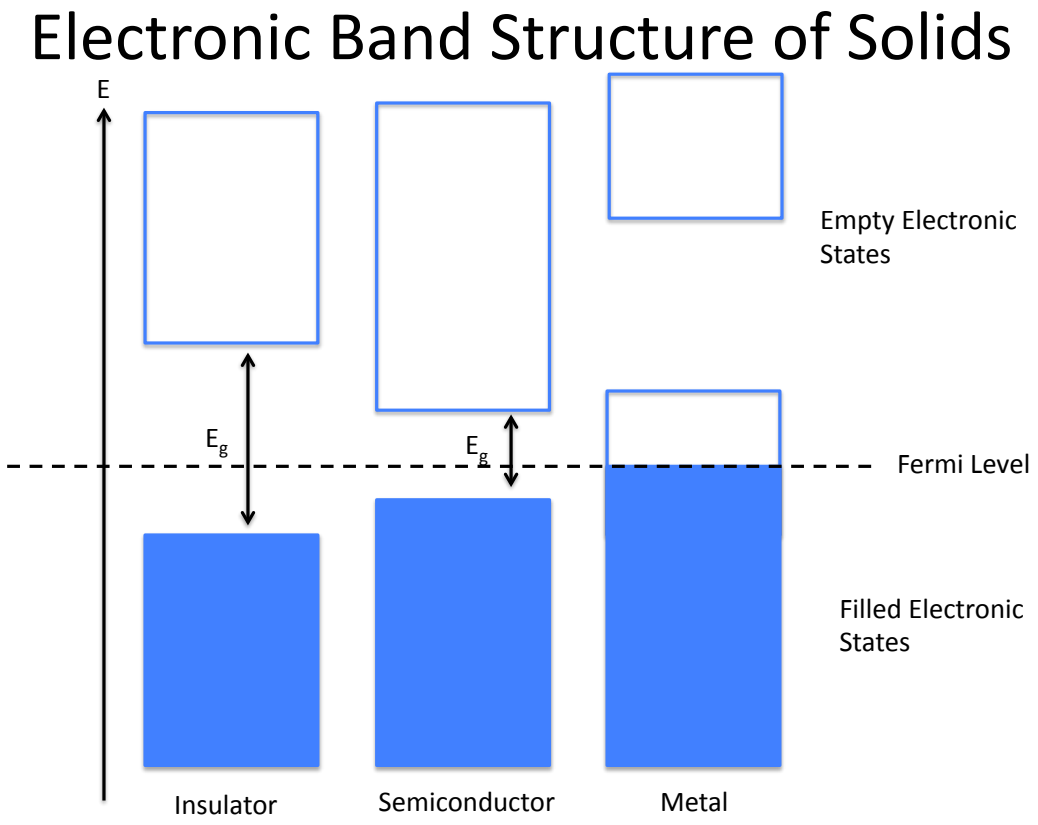

Figure 1.2: Schematic band diagrams for insulators, semiconductors, and metals.

Organic semiconductors are useful in applications for which physical flexibility, cost, and low-temperature large-area deposition is needed. While organic semiconductors have electrical properties that are inferior to crystalline silicon, these organic materials have several advantages. The polymeric flexible amorphous bonds

between molecules make organic semiconductors invulnerable to repeat flexing and stressing. Solution and evaporative deposition of these semiconductors is a cheap, low-temperature process in large area applications. Furthermore, unlike bulk crystalline semiconductors, organic semiconductors are functionalizable and sensitive to vapor and liquid chemicals. In order to understand the sensing properties of organics, the classes and charge carrier transport modes of these materials must be described.

1.1 Conductive Organic Polymers

Polyacetylene is an organic molecule consisting of a chain of π-conjugated, sp^2-hybridized carbon atoms. Polyacetylene forms a quasi-one-dimensional semiconductor in its natural state—albeit a semiconductor with a small electronic bandwidth for both the valence and conduction bands.

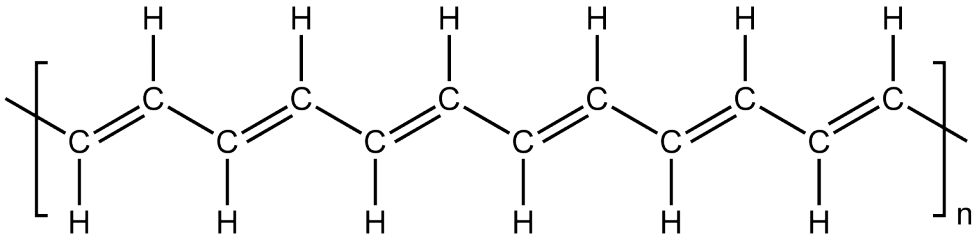

Figure 1.3: The chemical structure of polyacetylene.

Polyacetylene functions as a semiconductor because the π orbitals are exactly half-filled. For polyacetylene chains of infinite length, the double and single bonds between carbon atoms are indistinguishable due to resonance. Each monomer unit has a single uniform bond length, and the strength of this bond is approximately equal to the strength of a 1.5 carbon-carbon bond: stronger than a σ bond, but weaker than a σ bond and a π bond. If each carbon-carbon bond is at least partially a π bond, then the π bonds are spread over the entire carbon chain—a distance equal to approximately twice the

distance covered by π bonds, if the polymer has truly alternating double and single bonds. This effect means that the π bonds are only half as strong over twice the distance. If each carbon-carbon π bond holds only one electron, then each π bond is half-filled. The HOMO (highest occupied molecular orbital) and LUMO (lowest unoccupied molecular orbital) are separated by the energy needed to add one more electron to the half-filled π orbital.

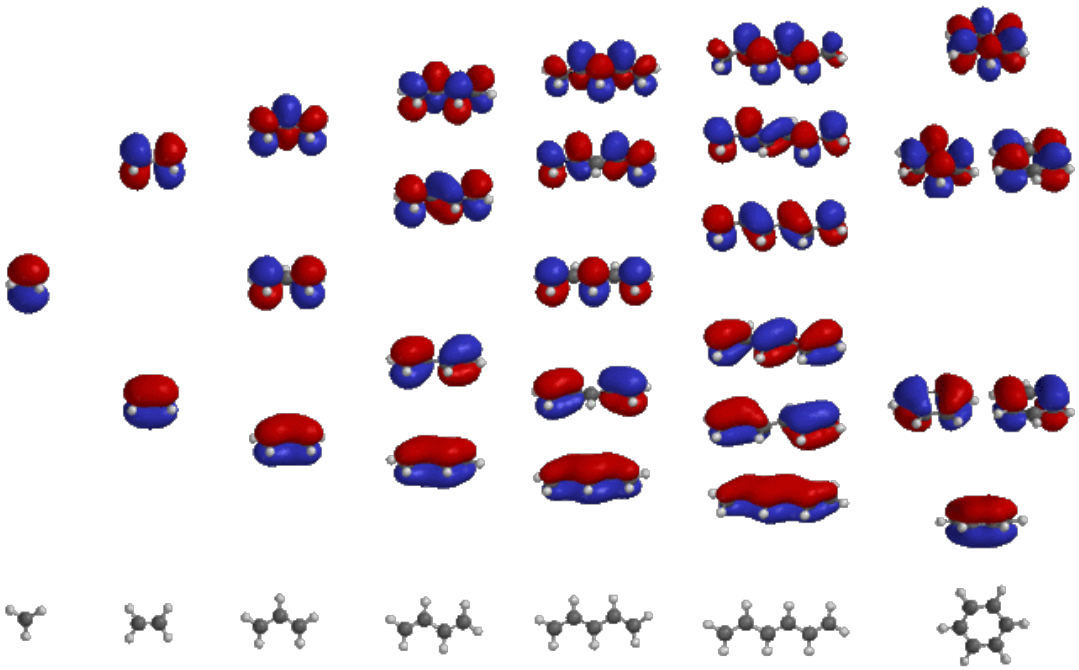

Figure 1.4: The π bonding and antibonding orbitals for ethylene, allyl, butadiene, pentadienyl, hexatriene, and benzene. From http://courses.chem.psu.edu/chem210/mol-gallery/pi-systems/pisystems.html [4].

For undoped polyacetylene, the band gap lies in the large energy gap between the half-filled π orbital (as described above) and the over-filled π orbital that could represent an alkene chain. This large intrinsic energy gap is characteristic of an insulator.

Shirakawa *et al*. doped polyacetylene with halogens, particularly iodine, to form conductive polymers. The addition of electron-rich halide atoms to the carbon backbone leads to the accumulation of charge in the bands. The Fermi energy level is shifted from the natural band gap into the partially filled valence band. The halides function as electron-withdrawing charge-transfer salts and accept (or pull) electron density from the neighboring carbon atoms [5]. These halides produce a hole conduction channel along the axial direction of the polymer. Charge conduction is unidirectional in a single molecule but may be anisotropic or quasi-isotropic for a poly-molecular film depending upon intra-molecular charge transfer and orientation.

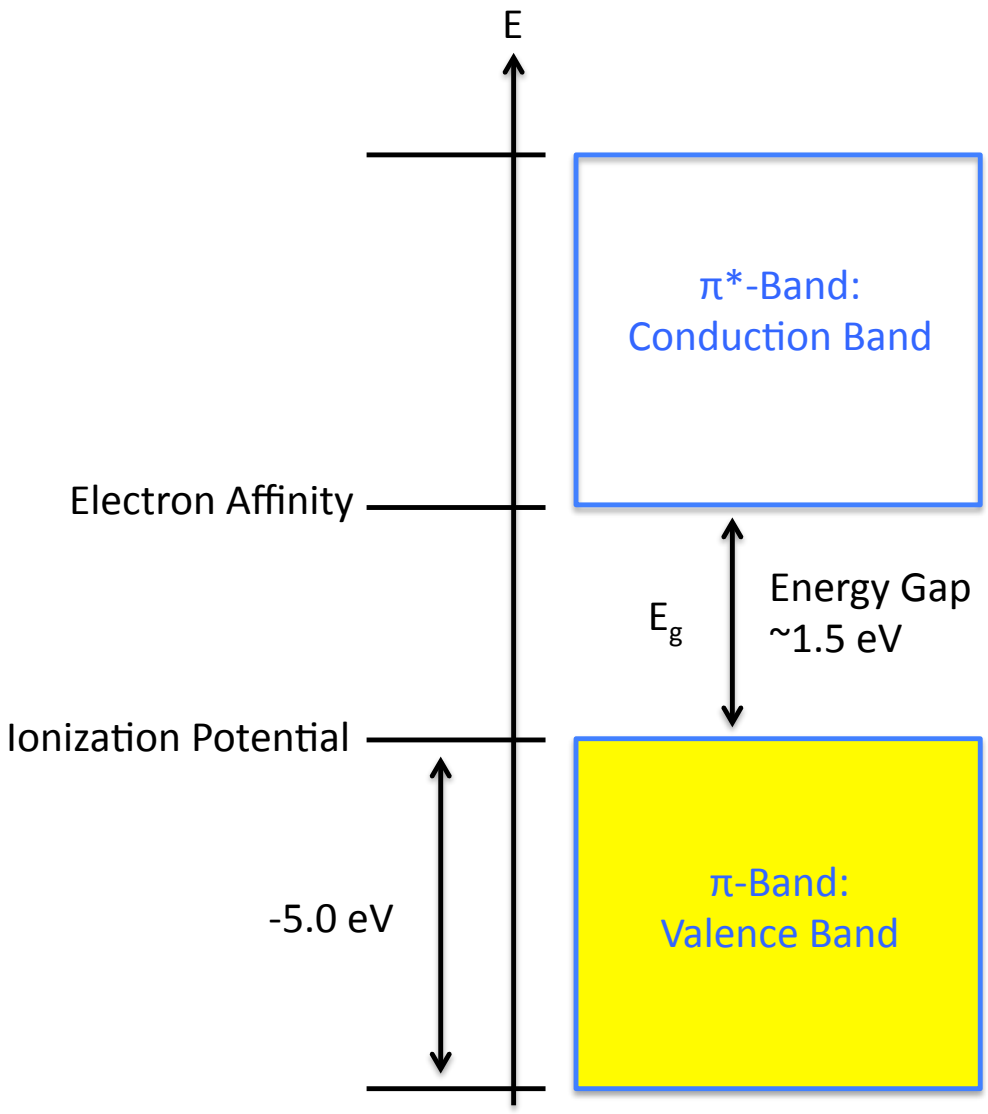

Figure 1.5: The electronic band structure of polyacetylene showing the bandgap between bonding and antibonding π orbitals.

Polyacetylene is not the only organic semiconductor. The same delocalized, half-filled π-bond energy levels occur in benzene rings, polyacetylene derivatives, and both large and small molecules containing these structures.

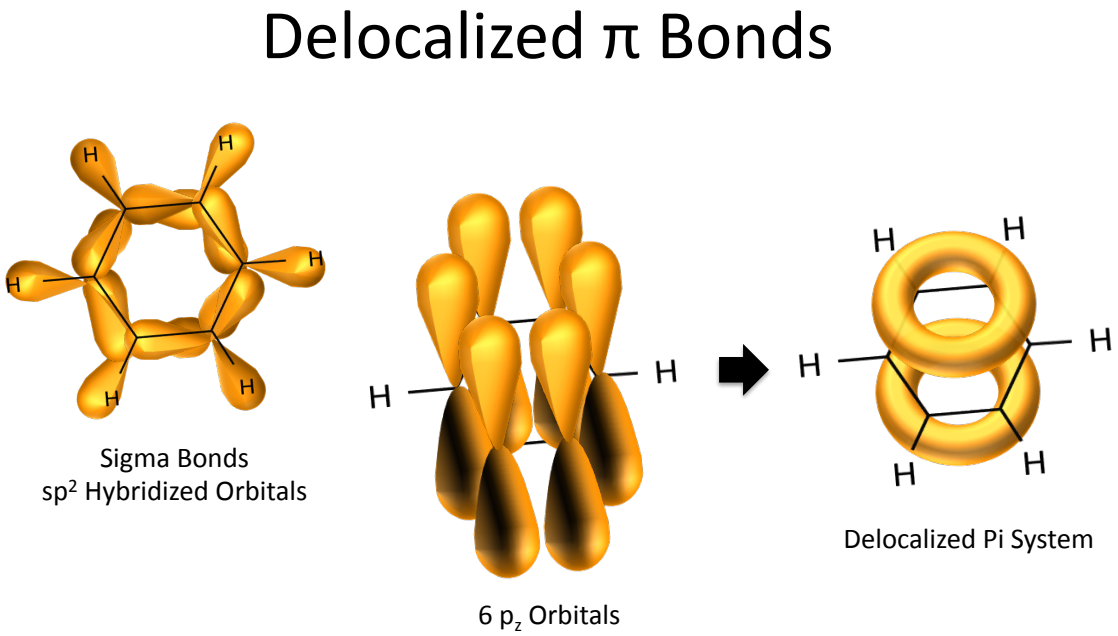

Figure 1.6: The delocalization of π bonds over conjugated organics creates bandlike transport.

1.2 Organic Semiconductors

Several different types of organic semiconductors were used in this work. Their classes and characteristics are described below.

1.2.1 Semiconducting Polymers

Poly-3-hexylthiophene (P3HT) is a sulfur/thiophene-based semiconducting polymer. Because the thiophene ring is planar like benzene, long polythiophene chains exhibit a two-dimensional band structure similar to that of polycyclic aromatic hydrocarbons. The hexane group contributes to solubility in nonpolar liquids and monolayer assembly during solution processing.

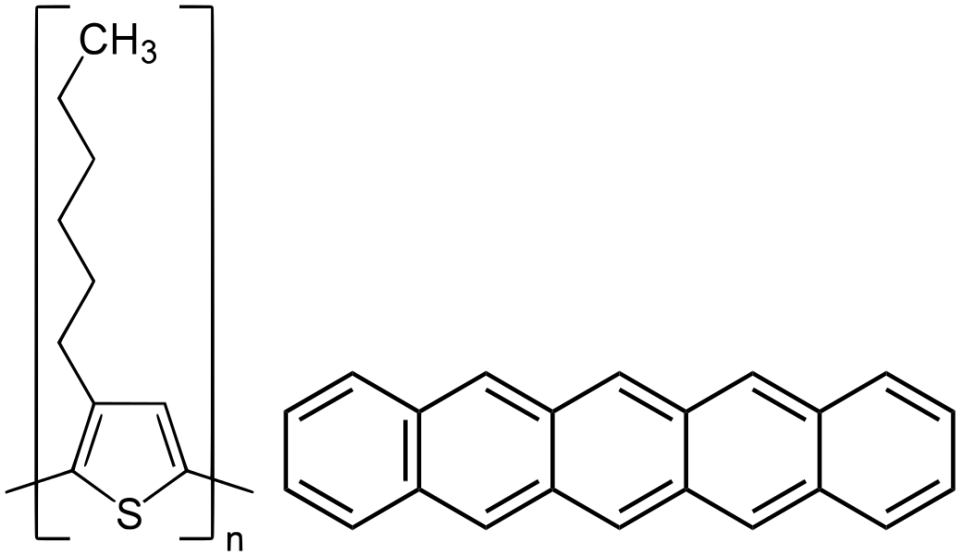

Figure 1.7: The chemical structures of poly-3-hexylthiophene and pentacene.

1.2.2 Small Molecule Organic Semiconductors

Polyacetylene is a long-chain semiconducting polymer, but small molecule organic semiconductors also exist—most with the same alternating double and single carbon bond backbone. Pentacene ($C_{22}H_{14}$) is a well-understood semiconductor in this category. Pentacene is a small organic molecule consisting of five fused benzene rings in a flat, linear arrangement. The π bonds are delocalized in molecular orbitals over the top and bottom of the two-dimensional molecular plane.

Copper phthalocyanine (CuPc) ($C_{32}H_{16}CuN_8$) consists of the phthalocyanine molecule coordinated to a central copper (II) atom. Phthalocyanine is a cyclic structure consisting of four isoindoles joined by amines. The molecule is, like pentacene, primarily two-dimensional in structure. Copper phthalocyanine is deposited in a manner identical to pentacene.

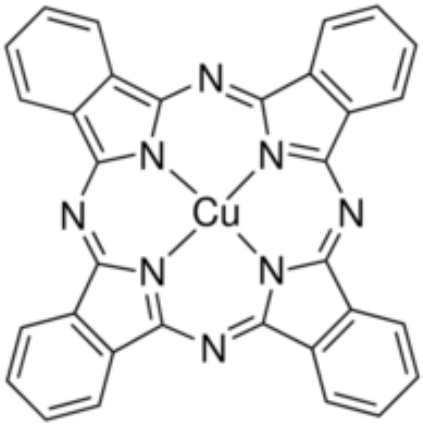

Figure 1.8: The chemical structure of copper phthalocyanine.

1.2.3 Deposition and Layer Structure

Pentacene and copper phthalocyanine are small molecule organics that form semi-crystalline structures. In pentacene, the molecules grow in a herringbone pattern, eventually forming terraces with additional monolayers [6]. In copper phthalocyanine, the individual atoms also form well-ordered monolayers [7]. Poly-3-hexylthiophene, however, forms disordered films due to its polymeric behavior.

Pentacene, copper phthalocyanine, and poly-3-hexylthiophene are primarily hole-transporting materials, or p-type semiconductors. Pentacene is one of the better-characterized organic semiconductors, with a reported hole mobility as high as 0.1 $cm^2/V*s$ [8]. As reported by Tanese *et al*., majority carrier (hole) mobility is highest in pentacene, followed by copper phthalocyanine and then poly-3-hexythiophene. A copper phthalocyanine derivative, hexa-deca-fluoro copper phthalocyanine, is a commonly used electron-transporting material, or n-type semiconductor, particularly for organic CMOS devices [9].

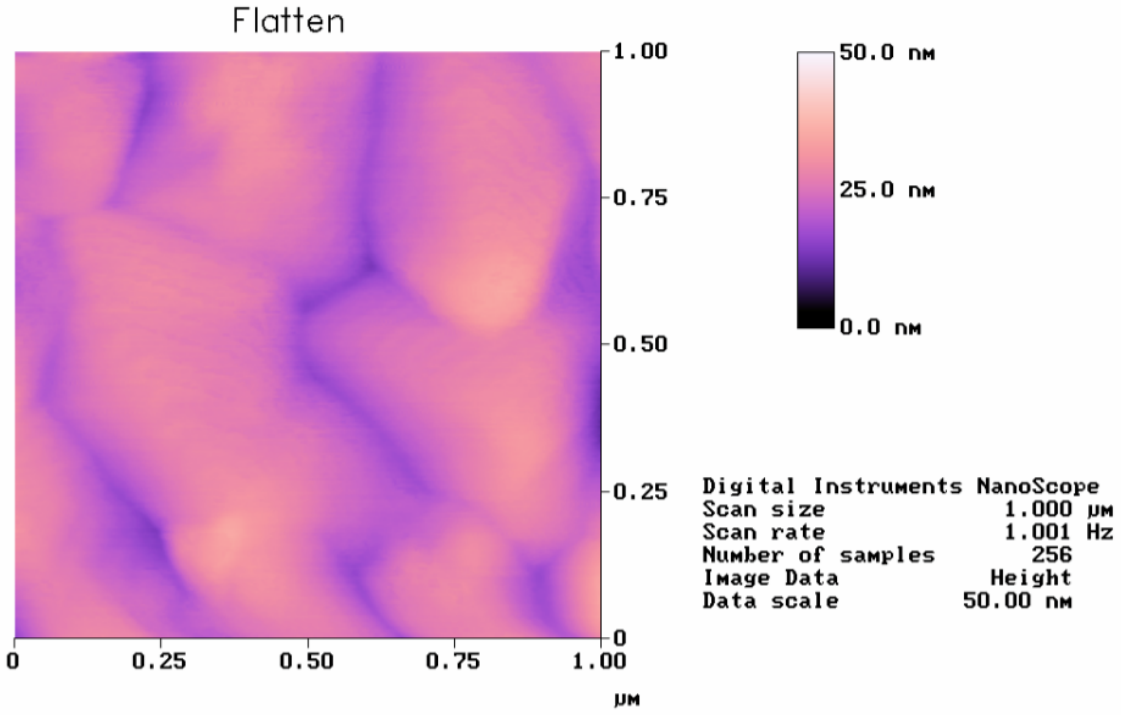

Figure 1.9: Atomic force microscopy image of deposited pentacene organic semiconductors, from S. Nadkarni "*Organic transistor based circuits as drivers for planar microfluidic devices,*" p. 5, [10].

1.3 Charge Transport in Organic Polymers

Within organic semiconductor molecules, charges travel along delocalized π bonds. Several models describe the delocalized transport of holes and electrons through organic polymers. Because both hole and electron mobilities are much lower in organics than in crystalline inorganic semiconductors, the charges cannot be viewed as delocalized and travelling in a band. Rather, charges are so localized that they deform the electronic structures around their physical locations and consequently deform the electronic bands at those locations.

In a crystal lattice, the excited vibration of atoms or molecules out of their proscribed lattice spacing is represented by a phonon. The phonon is a quantum

mechanical description of the vibrational wave energy in a solid. The allowed states of phonons in any given solid give rise to that solid's macroscopic properties, such as electrical and thermal conductivity, heat capacity, and optical permissivity.

Electrons in a solid interact with phonons. For ionic and polarizable crystals, the location of a charge carrier deforms the crystal, giving rise to electron-phonon coupling.

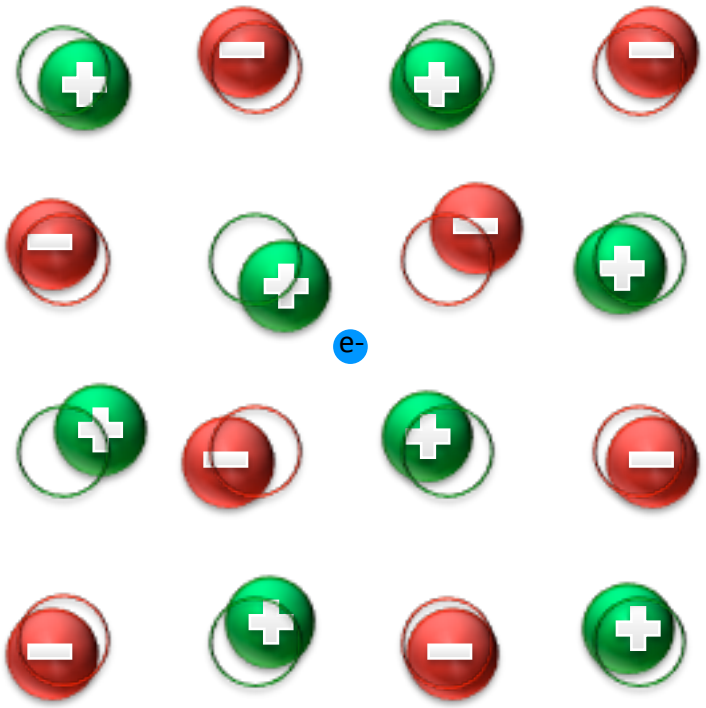

Figure 1.10: A charge causing lattice deformation. A polaron is the charge carrier taken together with the physical distortion it causes.

The combination of a charge carrier and its accompanying structural deformation is known as a polaron.

1.3.1 Multiple Trap and Release

For well-ordered organic materials, the most complete model of charge transport is the multiple trap and release model [11]. In this model, the trap states are divided into deep traps (that cannot be thermally excited) and shallow traps (within a few k_BT of the

mobility band edge). For a charge carrier caught in a shallow trap, there is a relaxation time—some average time the charge is trapped. The presence of these shallow traps reduces the effective mobility via the equation:

$$\mu_{eff} = \mu_0(T)\frac{\tau(T)}{\tau(T)+\tau_{tr}(T)}$$

This relationship assumes that all induced charge carriers contribute to current flow. Otherwise, only untrapped charges are assumed to contribute to current flow, and they are given by the relationship

$$n_{eff} = n\frac{\tau(T)}{\tau(T)+\tau_{tr}(T)}$$

There are thus two major modes of transport. For small numbers of traps or vanishingly small trapping times, the effective mobility is the mobility of band transport. In this case, the mobility is inversely temperature-dependent. When trapping phenomena dominate, the mobility increases with temperature, because the hopping between states is thermally activated. If the carrier concentration is high enough that all the trap states are filled, then the Fermi energy level is pushed into the band. For this case, the mobility is given by

$$\mu_{eff} = \mu_0 \alpha e^{-\frac{(E_C - E_t)}{kT}}$$

where E_c is the energy of the conduction band edge, E_t is the trap energy level, and α is the ratio of the trap density of states to effective density of states at the band edge.

1.3.2 Phonon-Assisted Hopping

If each trap state is considered to be a separate energy well, then quantum tunneling between such states by localized carriers must be accounted for [12]. According to this model, we get mobility

$$\mu = \mu_{tun} + \mu_{hop}$$

where the total mobility is a function of both the tunneling and hopping mobilities. The temperature dependence of the hopping mobility is given by

$$\mu_{hop} = \frac{ea^2t^2}{k_B T\hbar}\left[\frac{\pi}{2E_{pol}k_B T}\right]^{1/2} \exp\left(-\frac{E_{pol}}{2k_B T}\right)$$

In the classical limit the mobility dependence on temperature becomes

$$\mu_{hop} \propto \left[\frac{1}{T}\right]^{3/2}$$

when $E_{pol} \ll k_B T$, which is the high temperature limit.

For wide conduction bands, the tunneling mobility is given by

$$\mu_{tun} = \frac{e\tau}{m_{eff}} = \frac{\hbar^2}{2ta^2} \ (in\ the\ 1D\ limit)$$

where the charge moves as a wave but experiences phonon-scattering, causing the charge to move to different states.

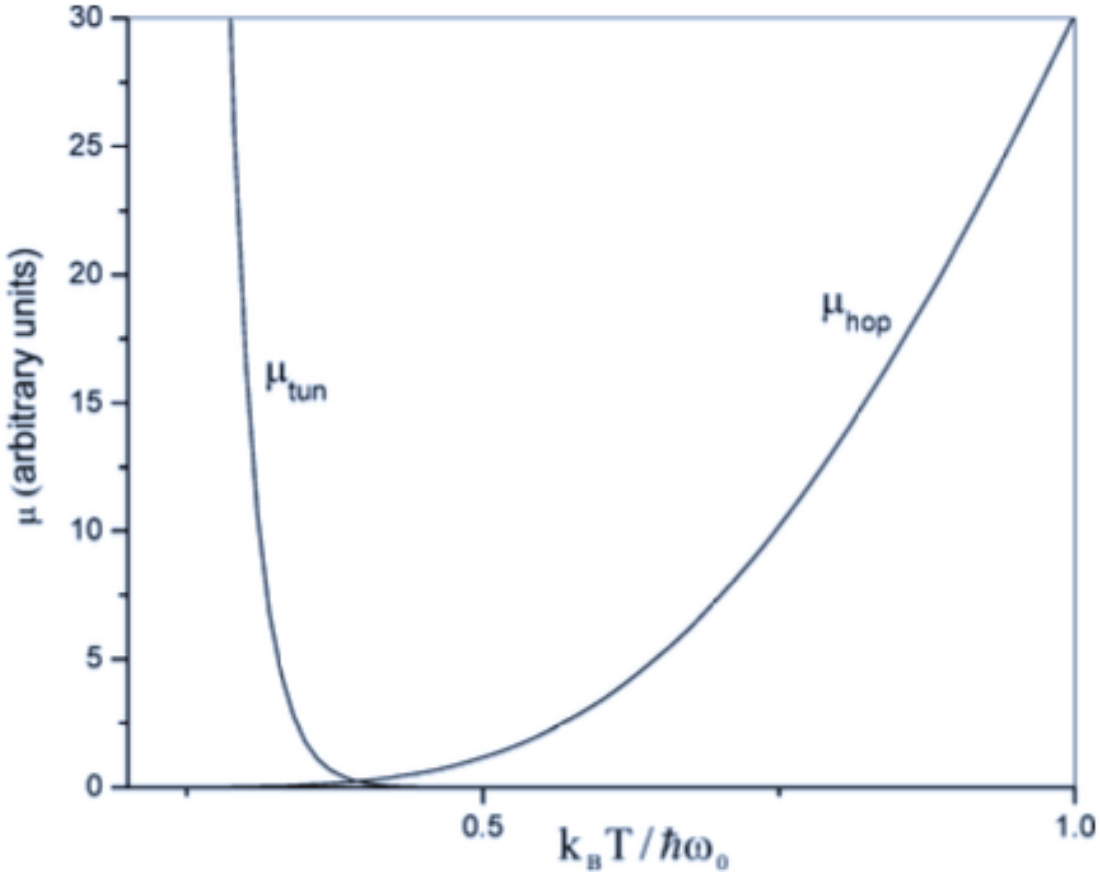

Figure 1.11: Theoretical graph of the relationship between hopping and scattering mobilities at as a function of temperature with g^2=10 and $t = \hbar\omega_0$. From Coropceanu *et al*, Figure 19, p. 947 , [12].

1.3.3 Low Temperature Band-like Transfer

At low temperature in high-mobility organics, such as single-crystal pentacene, the charges can travel in bands. This condition gives an Arrhenius relationship between mobility and temperature such as

$$\mu = \mu_0 e^{-\frac{E_A}{k_B T}}$$

Sakanoue and Sirringhaus show that for low-temperature and moderate electric fields, single crystal organic semiconductors follow this linear relationship with temperature [13]:

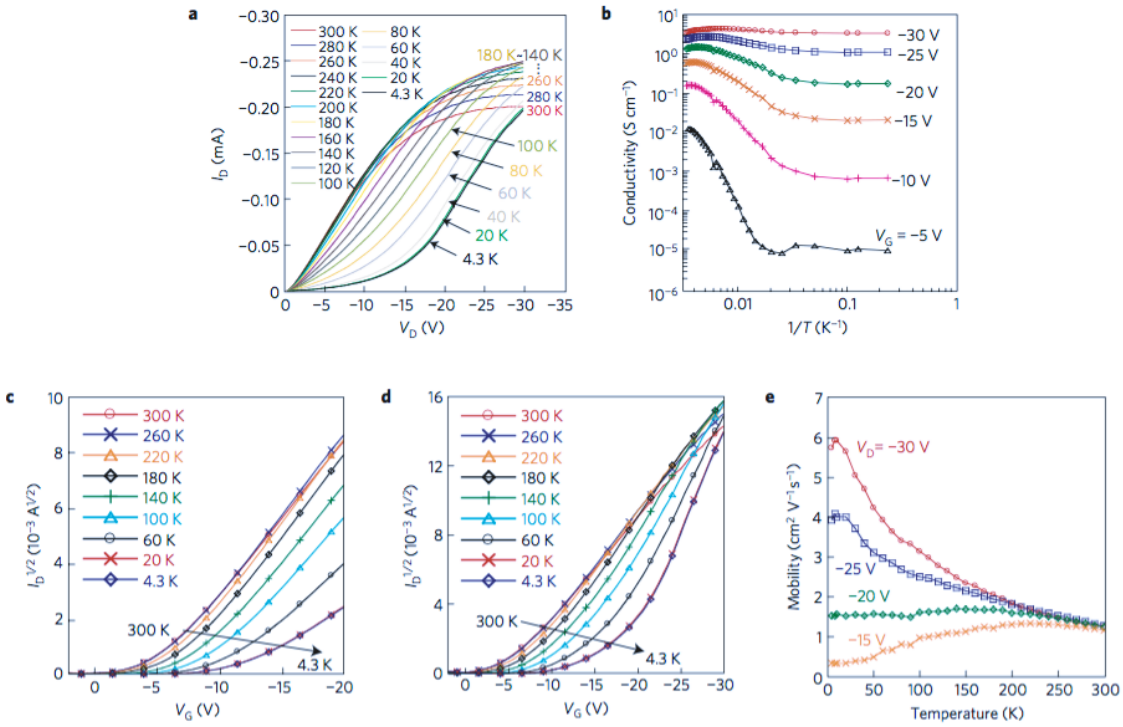

Figure 1.12: Experimental graph of the relationship temperature and mobility, showing Arrhenius relationship at low temperature and high field. From Sakanoue and Sirringhaus, Figure 2, p. 737, [13].

For low electric fields, charges are localized onto individual molecules in shallow traps. The lateral source-drain voltage frees the carriers and raises their energy into the conduction band.

1.3.4 Inter-Molecular Hopping

For multi-crystal semiconductors, charge trapping at the grain boundaries is the major limit on charge transport. Larger crystals will therefore have higher mobilities. Single crystals with mobilities as large as 100 $cm^2\ V^{-1}\ sec^{-1}$ have been reported [14].

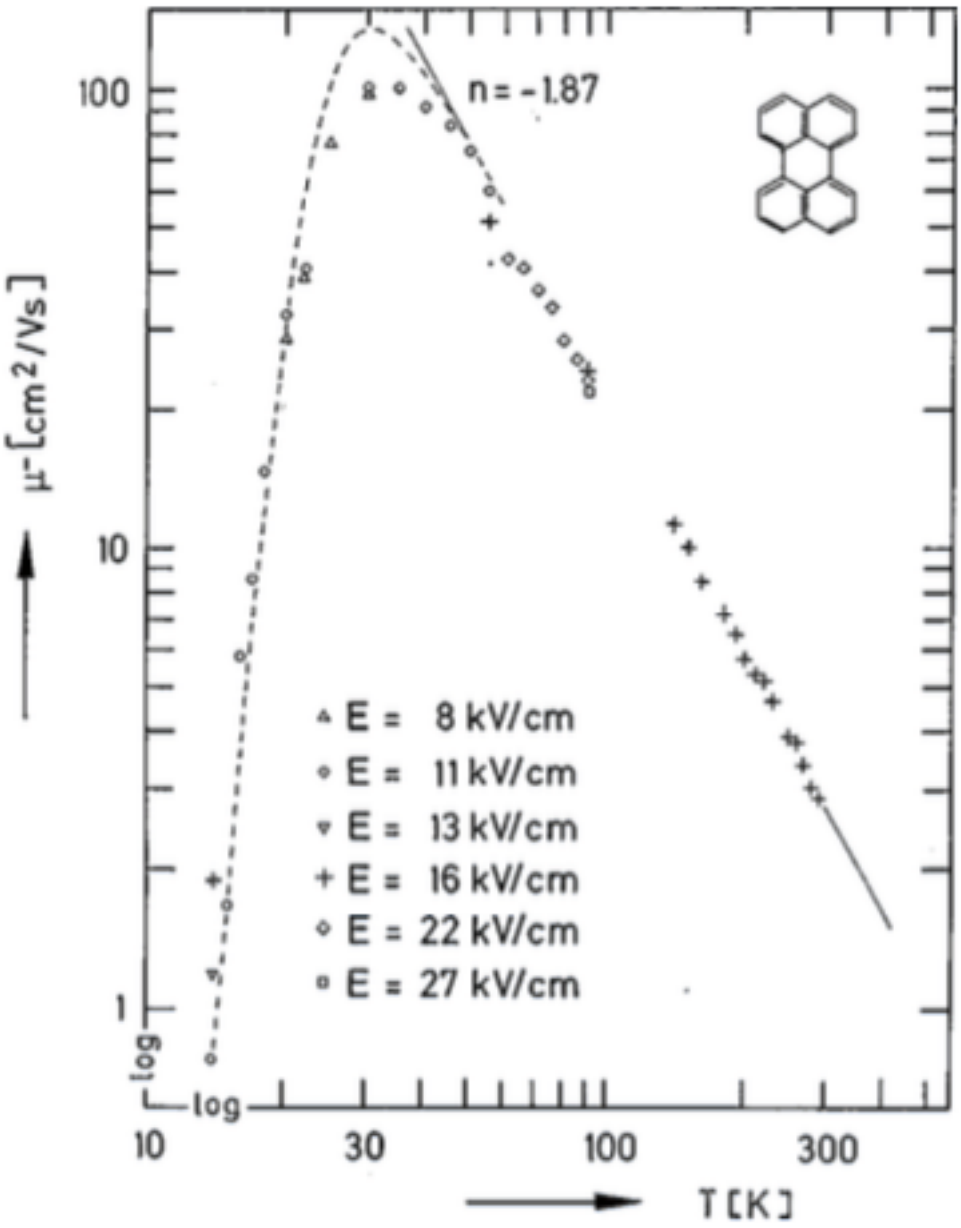

Figure 1.13: Experimental graph of the relationship between temperature and mobility for single crystal α-perylene. From Karl *et al*, Figure 4, p. 2321 [14]

Because the mobility of polymer and poly-crystalline organics is much smaller, a common assumption is that grain boundary scattering significantly limits mobility. Furthermore, the anisotropy of mobility in single-crystal organics proves that crystalline

structure and directionality are important in charge transport. Most organic semiconductor deposition concludes with a moderate temperature anneal around 200 °C in order to minimize the number of grain boundaries and increase the crystal grain size. Charge injection at the source and drain electrodes is limited by a Schottky barrier, which can be minimized by the correct choice of electrode metals and work functions.

1.4 Organic Electronics

There are several applications for which organic semiconductors are superior to traditional inorganic semiconductors. Organic semiconductors can be deposited and processed at far lower temperatures (less than 120°C) and higher pressures (near atmosphere), allowing for the use of substrates, such as glass, that cannot withstand the high temperatures necessary to process silicon [15]. The major deposition methods for organic semiconductors are spin coating from solution and vacuum evaporation. Furthermore, some semiconducting molecules can be screen-printed, ink-jet printed, and even micro contact printed as detailed by Bao *et al* [16]. Today, these organic semiconductors are used in wearable electronics, flexible electronics, and e-readers—a variety of applications for which silicon-level mobility is not necessary.

1.4.1 Organic Field Effect Transistors

State-of-the-art organic field effect transistors (OFETs) are currently available as small display screens, displacing liquid crystal displays (LCDs) in smart phone applications [17]. However, organic radio frequency identification (RFID) tags that will meet the Electronic Product Coding (EPC) standards for data rates are still some years away from being developed [18]. Optoelectronic applications are currently the major commercial avenue for organic semiconductors. Most organic semiconductors have a direct, optical bandgap in the 2 eV range. They are therefore useful for transparent

applications such as backside circuitry on glass or plastic substrates, e-readers, light emitting diodes, and solar cells.

1.4.2 Light Emitting Diodes

Electroluminescence in organics was first discovered in anthracene single crystals in the 1960s. For the emission of a photon from an organic, holes injected from one electrode and electrons from another must recombine to form an exciton, which decays to produce a photon. For this process to be possible on the large scale necessary for commercially successful organic light emitting diodes (OLEDs), two organic semiconductors in close proximity are required: one hole-transporting and one electron-transporting. The first organic semiconductors were all hole-transporting *p*-type semiconductors. OLEDs were not commercially viable until the development of compatible *n*-type semiconductors, such as copper hexadecafluorophthalocyanine (F_{16}CuPc) which was developed in 1995 [19].

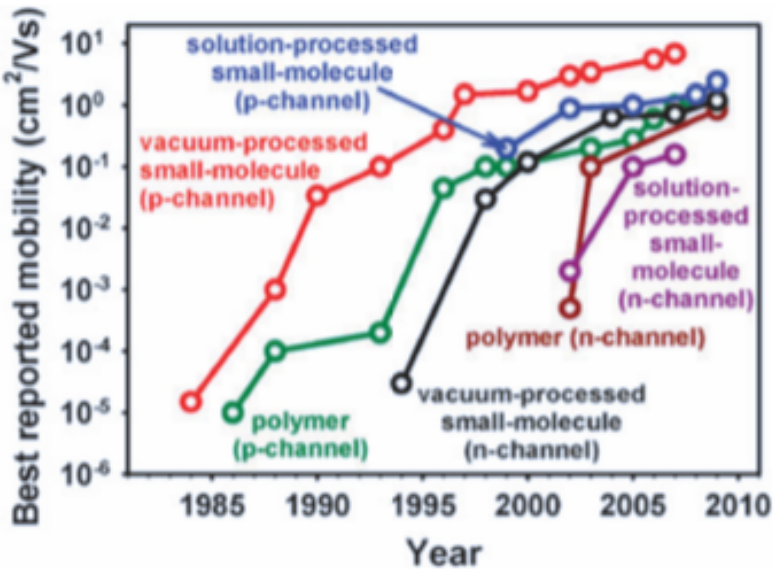

Figure 1.14: Timeline of the development of *n* and *p*-type semiconductors showing highest reported carrier field-effect mobility. From Klauk, Figure 21, p. 2653, [19].

Organic semiconductors are also important for use in solar cells. The formation of an exciton after photon absorption and its subsequent dissociation into hole and electron creates an electrical current. Organic semiconductors have low mobilities, but they also have high absorption coefficients and small exciton diffusion lengths [20]. These efficiencies are not as high as those of inorganic solar cells, but the low cost of these organic materials drives further development.

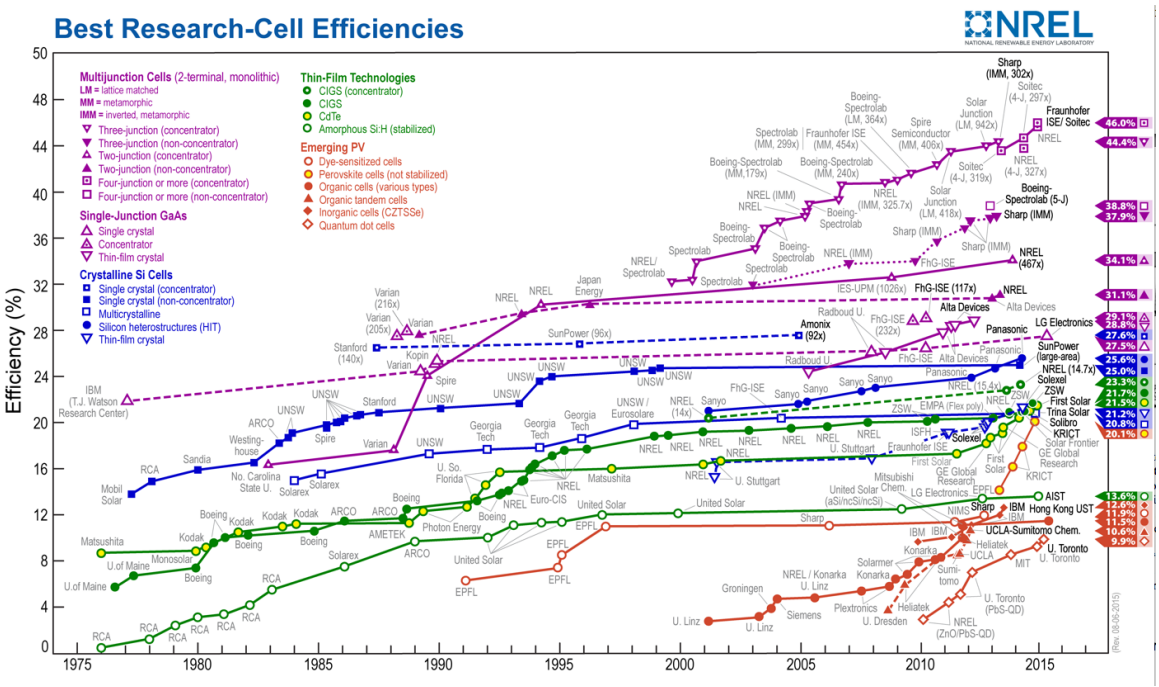

Figure 1.15: Timeline of the development of efficient solar cells, including organic cells. This plot is courtesy of the National Renewable Energies Laboratory, Golden, CO [21].

1.5 Bias Stress Effect

In organic semiconductors exposed to the atmosphere, the channel current will continually degrade due to the bias stress effect. The bias stress effect is due to charge trapping in the organic semiconductor channel that causes a threshold voltage shift [22]. The charge carriers created by the gate voltage in the channel become trapped in

localized states as these carriers interact with defects in the organic semiconductor [23]. These localized states are lower in energy than the band-like density of states, and charges that lack the activation energy to delocalize and participate in the channel current become trapped. In a *p*-channel device, the threshold voltage becomes more negative over time, while in an *n*-channel device the threshold voltage becomes more positive. A greater magnitude of voltage is needed to turn on the field-effect transistor in order to compensate for the trapped charge.

The physically trapped charges can be located in the bulk of the organic semiconductor, at the semiconductor-dielectric interface, or within the gate dielectric. Localized charges at the semiconductor-dielectric interface or in the dielectric screen the gate voltage, reducing the effective gate voltage applied to the channel. Charges trapped in the organic semiconductor disrupt the charge in the channel and the local density of states.

This bias stress effect can be reversed by reverse biasing the gate and driving out trapped charges. In a deeply off state—when the gate is very positive in a *p*-channel device, or very negative in an *n*-channel device—more-mobile trapped charges can be removed. However, some charges are so deeply trapped that only thermal annealing can remove them. In order to reduce the current fall due to bias stress, most organic semiconductors are coated and protected from atmosphere when used in consumer products.

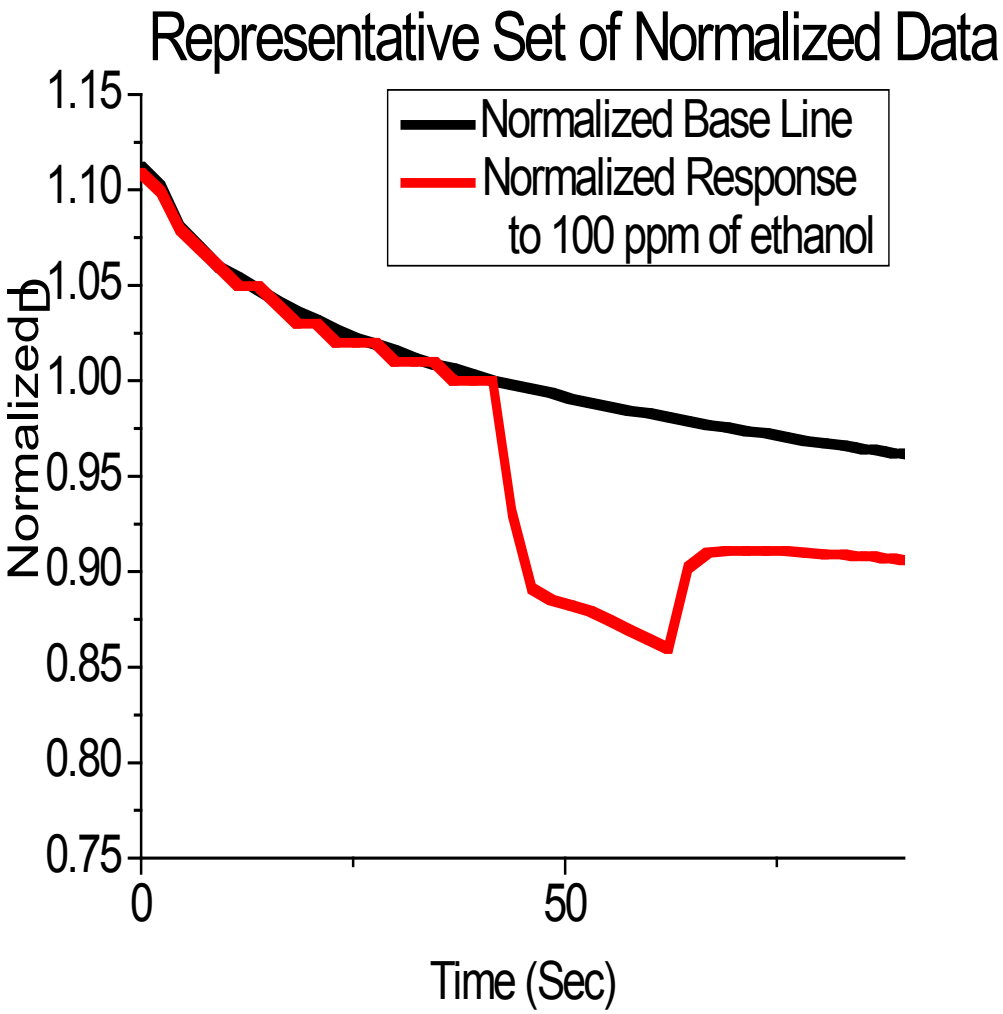

Figure 1.16: The drain current falls as a function of time due to the bias stress effect. From Someya *et al*. Figure 1, p. 3800, [24].

The bias stress shift in the threshold voltage as a function of time is given by

$$\Delta V_{th} = [V_{th}(\infty) - V_{th}(0)]\left[1 - e^{-(\frac{t}{\tau})\beta}\right]$$

which is a stretched exponential fitting function where $V_{th}(\infty)$ is the threshold voltage at equilibrium as $t \to \infty$, β is the stretching parameter $(0 < \beta \leq 1)$, and τ is the time constant.

Chapter 2: Inorganic Oxide Semiconductors

While organic semiconductors have advantages in sensing applications, there are valid reasons for using or incorporating inorganic semiconductors. The two major inorganic semiconductors discussed in this work are crystalline silicon and oxides such as zinc and zinc tin oxides.

2.1 SILICON

Silicon is the most commonly used semiconductor. The maximum electron mobility of silicon is nearly 1500 $cm^2\ V^{-1}\ sec^{-1}$, while the slower hole mobility is up to 450 $cm^2\ V^{-1}\ sec^{-1}$. This charge carrier mobility is much larger than the mobilities in organic semiconductors. Other crystalline semiconductors such as germanium and gallium arsenide have larger intrinsic mobilities and better electronic properties, but silicon is the dominant material used in semiconductor production today. Silicon semiconductors have proliferated because the insulator silicon dioxide is easily grown on bulk silicon in an oxygen-rich furnace. Because insulators are an important part of field effect transistor (FET) fabrication, silicon quickly became the industry standard.

Silicon semiconductor manufacturing is established and robust—approximately 3 billion square inches of patterned silicon wafers were sold in the second quarter of 2015 alone [25], and $10 billion (US) was spent on silicon fabrication equipment during the same period. Because so many resources have been expended perfecting silicon processing, the techniques used to create silicon transistors and wafers are robust and scalable.

Unlike organic semiconductors, silicon is not degraded by exposure to atmospheric pressure or a temperature under about 600° C. These properties are advantageous in many applications, but sensing applications require a different material

that interacts with volatile organics. The four-terminal device described in the next chapter was developed in order to combine the advantages of a silicon electronic platform with an organic semiconductor sensing material so that the strengths of both materials could be maximized.

2.2 INORGANIC OXIDE SEMICONDUCTORS

Several types of inorganic semiconductors provide the same physical flexibility for large area devices that organic semiconductors provide. Amorphous silicon (α-Si) is currently the state of the art and the second most economically significant semiconductor, behind crystalline silicon [26]. Additionally, inorganic oxide semiconductors that possess mobilities higher than those of the best organic semiconductors are available. In particular, inorganic oxides such as Indium Tin Oxide (ITO) are even used for large area, conductive electrodes. The mobilities of these oxides are so large that they can be used effectively as metals. The scarcity and expense of indium has led to the development of other metallic oxides such as zinc oxide and doped zinc oxides such as zinc tin oxide [27]. For many transparent applications, the direct bandgap of these materials makes them superior to amorphous silicon with its indirect bandgap.

Crystalline silicon has mobilities in excess of 200 $cm^2\ V^{-1}\ sec^{-1}$, whereas amorphous silicon is limited to about 1 $cm^2\ V^{-1}\ sec^{-1}$. However, inorganic oxides can have large mobilities in excess of 10 $cm^2\ V^{-1}\ sec^{-1}$. These large mobilities are due to the overlap of the metal cations' symmetrical *s*-orbitals. Both amorphous and crystalline structures exhibit this large overlap in orbitals, which produces bandlike transport as shown in Figure 2.1. These overlapping orbitals make amorphous oxide semiconductors electronically superior for certain applications [28].

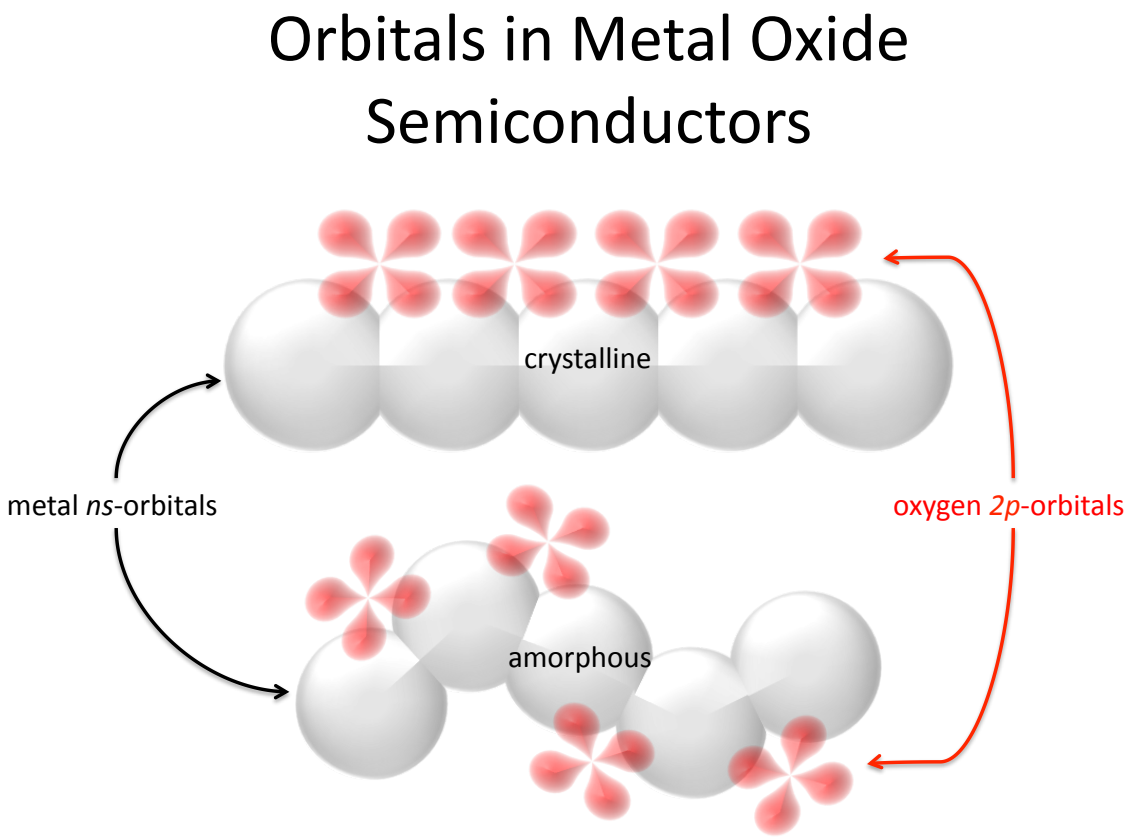

Figure 2.1: Electronic orbitals in post-transition metal oxide inorganic semiconductors. The overlap between metal *ns*-orbitals is large, while the oxygen 2*p*-orbital overlap is small. The overlap of the metal s orbitals is not significantly affected by deviations in structure in amorphous materials.

Metal oxides are very temperature stable in the range below 500°C. Above this temperature, ionic charge transport occurs when the oxygen ions become liable. At room temperature, charge transport is thermally activated along surface states [29].

2.2.1 Tin Oxide

Tin oxide, in both resistive and semiconducting forms, has been used in noxious gas sensors for over twenty years. In 1993 Suehle, Cavicchi, Gaitan, and Semancik described a self-heating resistive tin oxide sensor sensitive to both reducing and oxidizing

gasses [30]. Because tin oxide operating at 100°C to 200°C is known to be sensitive to gasses, this oxide will be used as a complement to organic semiconductors.

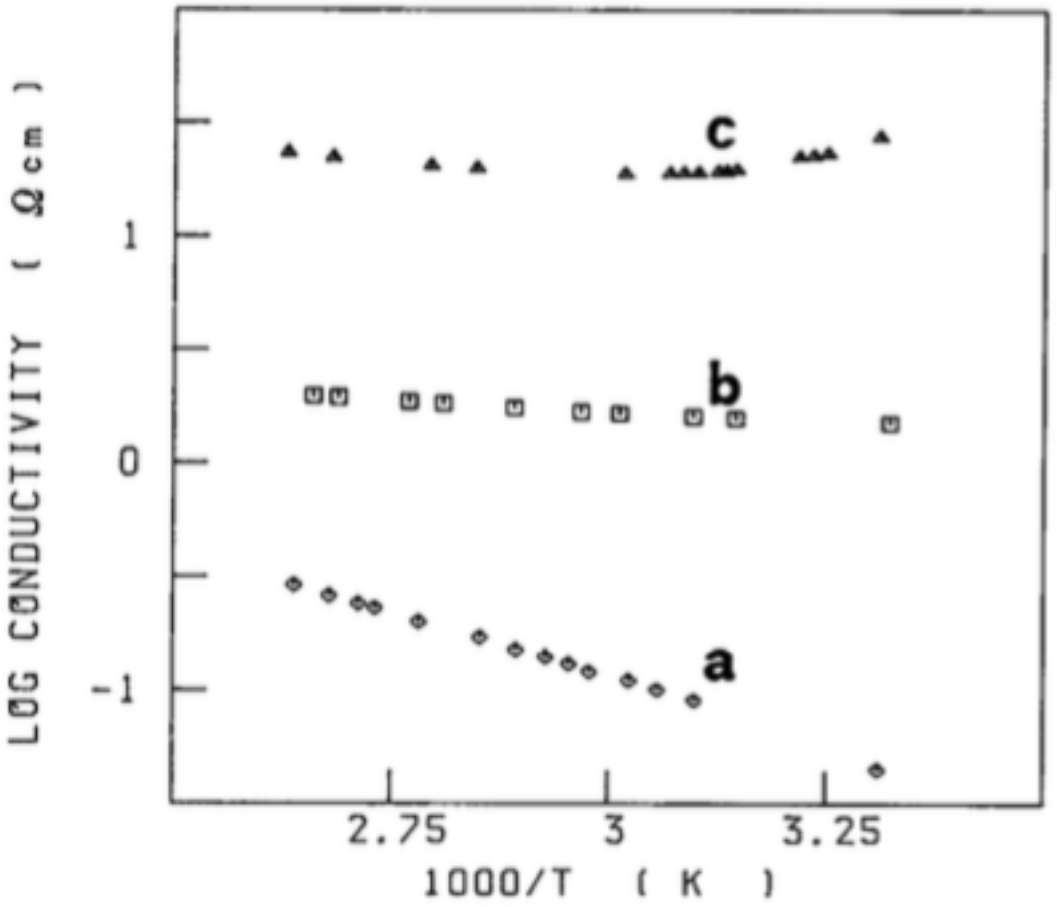

Figure 2.2: Conductivity as a function of temperature for tin oxide films prepared by the gel-sol method: (a) undoped, (b) zirconium oxide doped, and (c) titanium oxide doped. From A. Maddalena *et al*, Figure 4, p. 368, [31].

The tin oxide sensing mechanism is due to the two major valence states of tin. Sn^{2+} and Sn^{4+} are both found in bulk tin oxide. Reducing or oxidizing gasses can affect the relative concentration of these two cations. However, the sensing capabilities of thin films are predominantly due to surface chemisorption and ion sorption. The presence of charged surface states, both ionic and simply highly polar, causes band bending and

changes the mobility of the charges of the semiconductor [32]. Shih-Chia Chang [33] found that the bulk donor level of Sn^{2+} lies very close to the conduction band; the activation energy is calculated as $E_\alpha = 0.06\ eV$ for oxygen chemisorption.

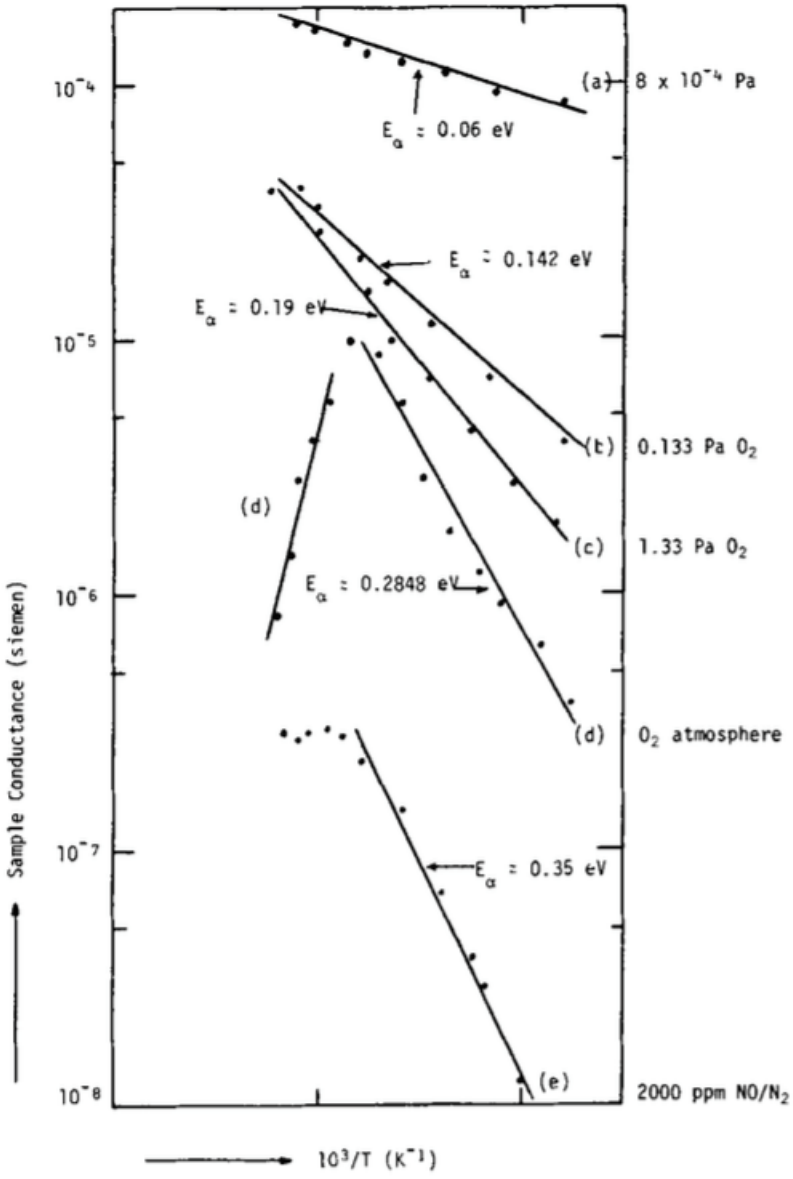

Figure 2.3: Equilibrium conduction of thin film tin oxide in different ambient conditions. From S. Chang, Figure 1, p. 367, [33].

Tin oxide can be highly conductive, with channel mobilities of up to 100 $cm^2\ V^{-1}\ sec^{-1}$ [34] and a direct band gap of 3.6 eV. Dependent on doping, tin oxide can be both hole and electron transporting.

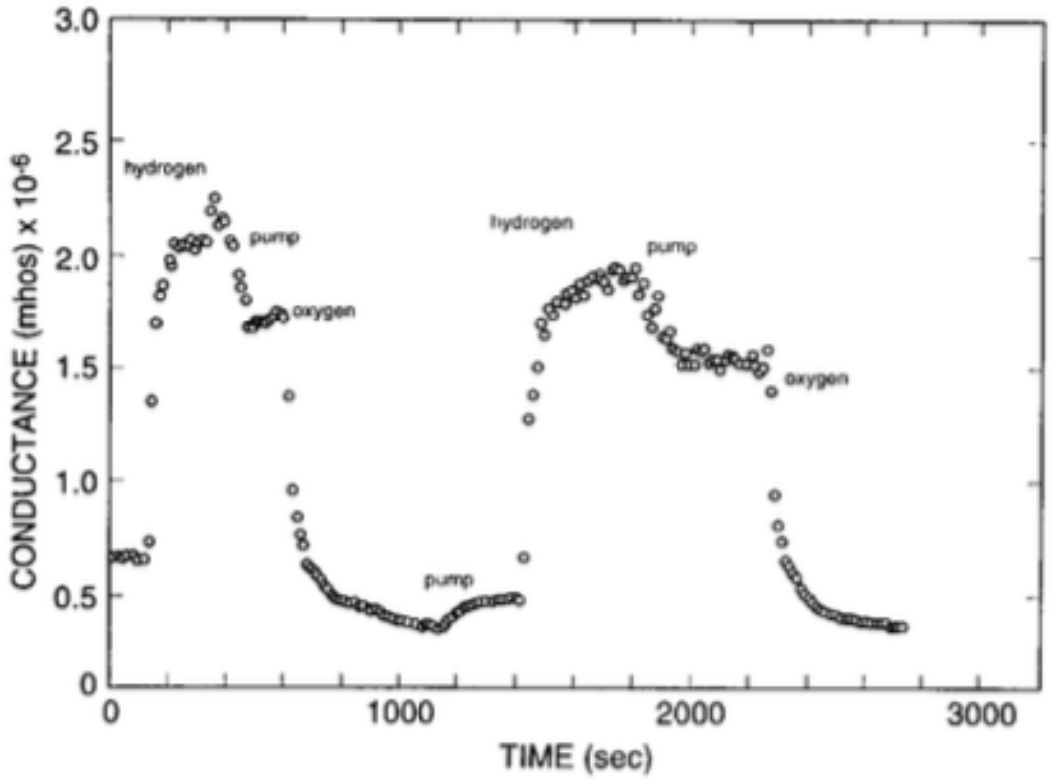

Figure 2.4: The conductance of SnO_2 film versus time when exposed to reducing gas H_2 and oxidizing gas O_2 for two cycles. From Suehle *et al*, Figure 3, p. 120, [30].

2.2.1.1 Adsorption

Tin oxide behaves like an extrinsic *n*-type semiconductor. Its electrical conductivity is directly related to oxygen vacancies. The equilibrium between ionized oxygen vacancies in tin oxide and gaseous oxygen in ambient atmosphere is given by

$$\left(\frac{1}{2}O_2\right)_g + 2e^- + 2V_0^{2+} \leftrightarrow 2O_0^x$$

Where V_0^{2+} is a doubly ionized oxygen vacancy and O_0^x is an adsorped oxygen atom on the surface of the oxide [35].

The chemisorbed species create localized electronic states that act as traps for holes or electrons (acceptor-like or donor-like, respectively) [36]. These localized electronic states create band-bending and charge-scattering centers, necessarily affecting the transport of charge carriers through the bulk tin oxide.

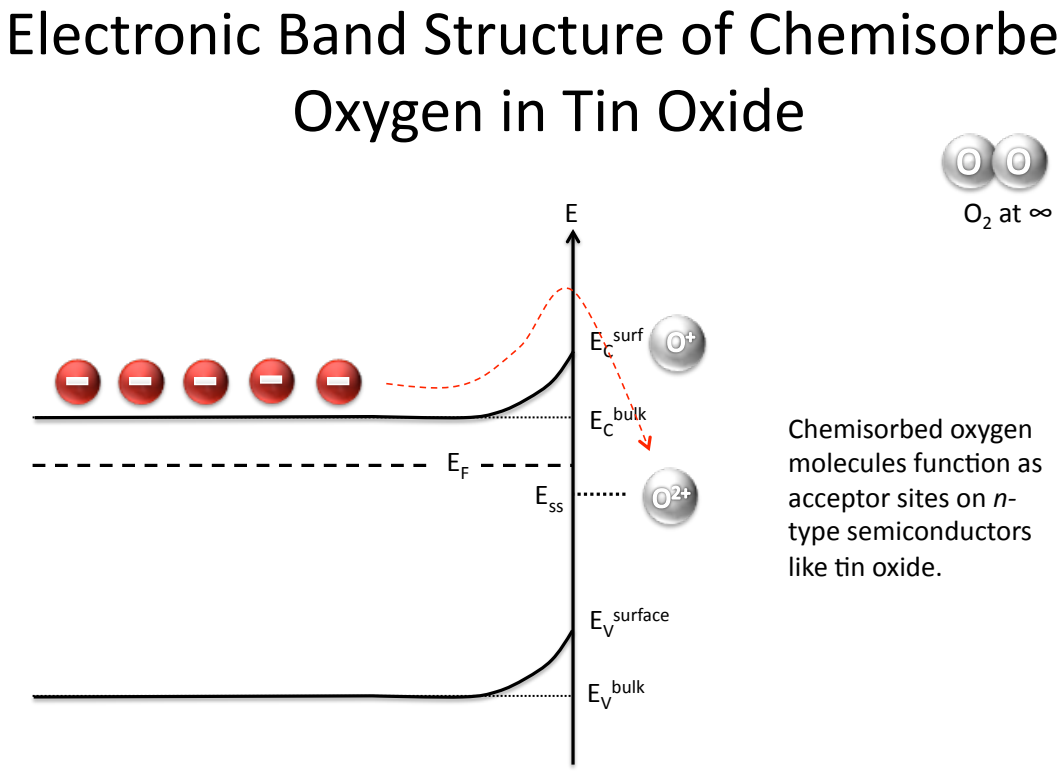

Figure 2.5: Chemisorbed oxygen causes band bending in *n*-type tin oxide.

For temperatures below 150° C, oxygen chemisorbs non-dissociatively on tin oxide in its molecular form. For higher temperatures, the oxygen molecule disassociates to atom $O_{(s)}^{0/-}$. This high temperature dissociation affects the adsorption rate (increasing the power exponent from 1 to 2) because each impinging molecule dissociates into two adsorped atoms which each need an empty adsorption site in order to chemisorb. The

high temperature dissociation also increases the total surface coverage and therefore increases the amount of occupied surface states, because there are now two atoms adsorped, rather than one molecule. The rate of adsorption for oxygen is less important than the total amount of adsorbed species and the total amount of surface states causing band bending and charge carrier scattering. The rate of analyte adsorption must be fast enough to cause a sensing event that is distinguishable from the bias stress effect, but otherwise has minimal importance if the adsorption reaction reaches a quasi-equilibrium state.

2.2.1.2 Scattering

Surface scattering occurs in all semiconductors of non-infinite size. The interactions of free charge carriers with the surface can be modeled as diffuse (random) scattering and specular (perfect) reflection. In a diffuse scattering event, the collision with the surface completely erases all previous velocity. This inelastic collision therefore reduces the mobility of all charge carriers within a mean free path length of the surface. In a specular reflection event, the momentum normal to the surface changes, but the parallel momentum component and the total energy remain constant. Because all real scattering events are not completely specular, surface layers will decrease the conductance of any semiconductor. This decrease is non-negligible when the sample length is not orders of magnitude longer than the mean free path of the charge carriers. In this case, all free charge carriers can be expected to interact with the surface and therefore lose momentum.

From Gomri *et al*. provide the following equations for electron mobility in the depletion layer if we define ω as the probability of diffuse scattering:

$$\mu = \mu_b \left(1 - \frac{\alpha}{2}\omega\left(1 + e^{\psi_s/2}\right)\right)$$

and accumulation layer

$$\mu = \mu_b \frac{1}{1 + \omega\left(a\frac{F_s}{\psi_s}\right)\sqrt{1+\psi_s}}$$

where $\psi_s = eV_s/kT$ and V_s is the potential barrier caused by a surface adsorbate, and $a = \lambda/L_D$ where L_D is the Debye length and λ is the mean free path for charge carriers. The equation for α is given as

$$\alpha = \frac{\left(E_F - E_i^b\right)}{kT} = ln\left(\frac{n_b}{n_i}\right)$$

Where E_i^b is the instrinsic Fermi level in the bulk, n_b is the concentration of free electrons in the bulk, and $n_i$is the intrinsic charge density. The equation for F_s is as follows:

$$F_s = \sqrt{2}\left[\frac{cosh(\alpha + \psi_s)\cosh}{cosh(\alpha)} - \psi_s tg(\alpha) - 1\right]^{1/2}$$

2.2.2 Zinc Tin Oxide

Zinc tin oxide (ZTO) is a wide-bandgap, hole-transporting semiconductor with the general form $(ZnO)_x(SnO_2)_{1-x}$ where (0<x<1). This oxide has a large, direct optical band gap in the range of 3.3-3.9 eV and is therefore very useful in transparent conductor applications [37]. ZTO has two crystalline phases: trigonal perovskite or ilmenite, with a chemical formula of $ZnSnO_3$, and cubic spinel, with a chemical formula of Zn_2SnO_4. The $ZnSnO_3$ structure is temperature stable to 600°C, but then decomposes to $ZnSnO_4$ and SnO_2. This structure is also more useful as a gas sensor because of a mean grain size that promotes analyte diffusion and analyte-semiconductor interactions [38]. The exact electrical properties of ZTO are highly dependent upon stoichiometry and deposition/anneal conditions, as shown in Figure 2.6.

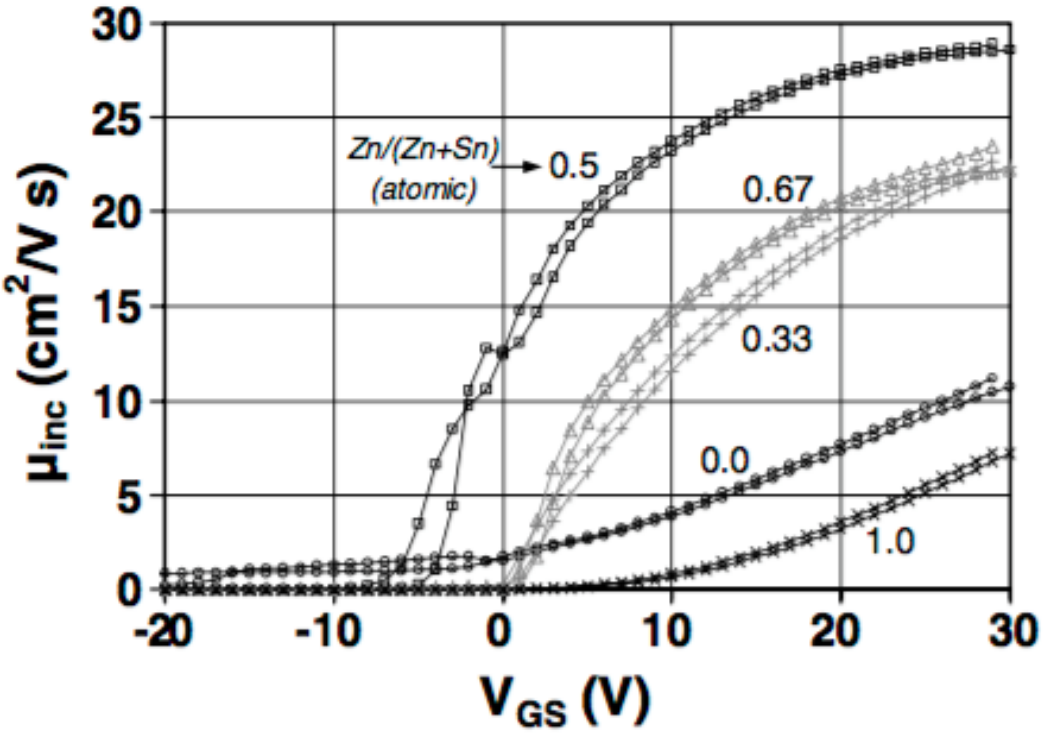

Figure 2.6: The incremental channel mobility for a zinc tin oxide TFT as a function of V_{GS} with various stoichiometry ratios of Zn to Sn. From Hoffman, Figure 2, p. 786, [39].

The stoichiometric ration of 1:1 Zn to Sn corresponds to both the most sensitive chemical vapor sensing and to the highest charge carrier mobility.

Zinc tin oxide combines the advantages of both zinc oxide and tin oxide. Zinc oxide is more transparent than indium tin oxide (ITO)—the gold standard for transparent conducting electrodes—and less susceptible to hydrogen-activated degradation than ITO and SnO_2. SnO_2 is very stable in acidic and basic solutions and in oxidizing environments at higher temperatures than ITO [40]. There are several methods of ZTO deposition, including RF magnetron sputtering, electron-beam deposition, ink jet printing [41], and the sol-gel method described in the following section 2.2.2.1.

Conductive zinc tin oxide is used as a sensor for reducing gasses such as oxides of nitrogen. The desorption of chemisorbed oxygen from the surface and at grain boundaries increases the electron concentration at the surface and thereby increases conductance. The reaction is given by

$$O_{ads} + NO \rightarrow e^- + NO_2$$

However, for an oxidizing gas, electrons are consumed in the adsorption reaction, which for nitrogen oxide is given by [42]

$$NO_2 + e^- \rightarrow NO + O_{ads}^-$$

The conductance of the film is directly affected by the addition or removal of a hole charge carrier. This theory of oxidation and reduction of adsorbates attributes changes in electrical characteristics to changes in the carrier concentration. This can be true if the adsorped species do not contribute to localized trap states in the electronic bands.

2.2.2.1 Sol-Gel Method

Zinc tin oxide can be deposited via a sol-gel based spin coating process, which is an extremely low cost deposition method. Zinc chloride ($ZnCl_2$)—or another zinc precursor such as zinc acetate ($Zn(CH_3COO)_2$)—and tin chloride ($SnCl_2$) powders are first dissolved in a polar organic solvent such as acetonitrile (CH_3CN) or acetyleacetone ($CH_3COCH_2COCH_3$). The concentration and molar ratio in solution determine the stoichiometry of the final ZTO layer. The solution is then filtered and deposited via spin coating. A final annealing around 500°C in air converts the precursor materials into ZTO [43], [44].

2.2.2.2 Thin Film Transistor Sensors

Previous work by Dutta and Dodabalapur [38] has demonstrated that ZTO thin film transistors are sensitive to ethanol vapor. The sensitivity of such sensors deposited

via the sol-gel method is dependent upon the annealing temperature in oxygen. The sensitivity of such thin films is highly dependent upon the grain sizes of ZTO.

2.2.3 Zinc Oxide

Zinc oxide has a large direct band gap of 3.4 eV in the near-UV spectral range and a large exciton binding energy of 60 meV. Because of the large free-exciton binding energy, exciton emission processes can occur even at or above room temperature, making zinc oxide an ideal material for optoelectronic applications. ZnO crystallizes in a wurtzite structure and can be purchased as large single crystals [45], [46], giving it an advantage over GaN (to which it is otherwise very similar). However, ZnO is an *n*-type semiconductor and is resistant to doping to produce *p*-type material. Some incidences of acceptor doping have been reported, but stability and reproducibility remain challenges. Janotti and Van de Walle propose that the difficulty of producing *p*-type ZnO is not due to native point defects and oxygen vacancies (which are deep donors), but rather to the incorporation of impurities during growth and annealing. In particular, they theorize that hydrogen always acts as a donor in ZnO, instead of operating amphoterically as it does in other semiconductors [46].

2.2.3.1 Resistive Sensors

Zinc oxide is used to detect humidity [47], ketones [48], and ammonia [49]. However, these existing sensor applications are based on resistive ceramic sensors—not semiconducting zinc oxide. Zinc oxide resistive sensors are often functionalized with additional ceramic additives (such as MoO_3 and WO_3 for acetone and RuO_2 for ammonia) in order to increase specificity to vapor phase analytes. For such resistive sensors, sensitivity is given as dimensionless number S as

$$S = \frac{R_a - R_g}{R_a} = \frac{\Delta R}{R_a}$$

where R_a is the resistance in air and R_g is the resistance measured in the analyte gas. A plot of sensitivity versus temperature for such a resistive sensory is shown in Figure 2.7.

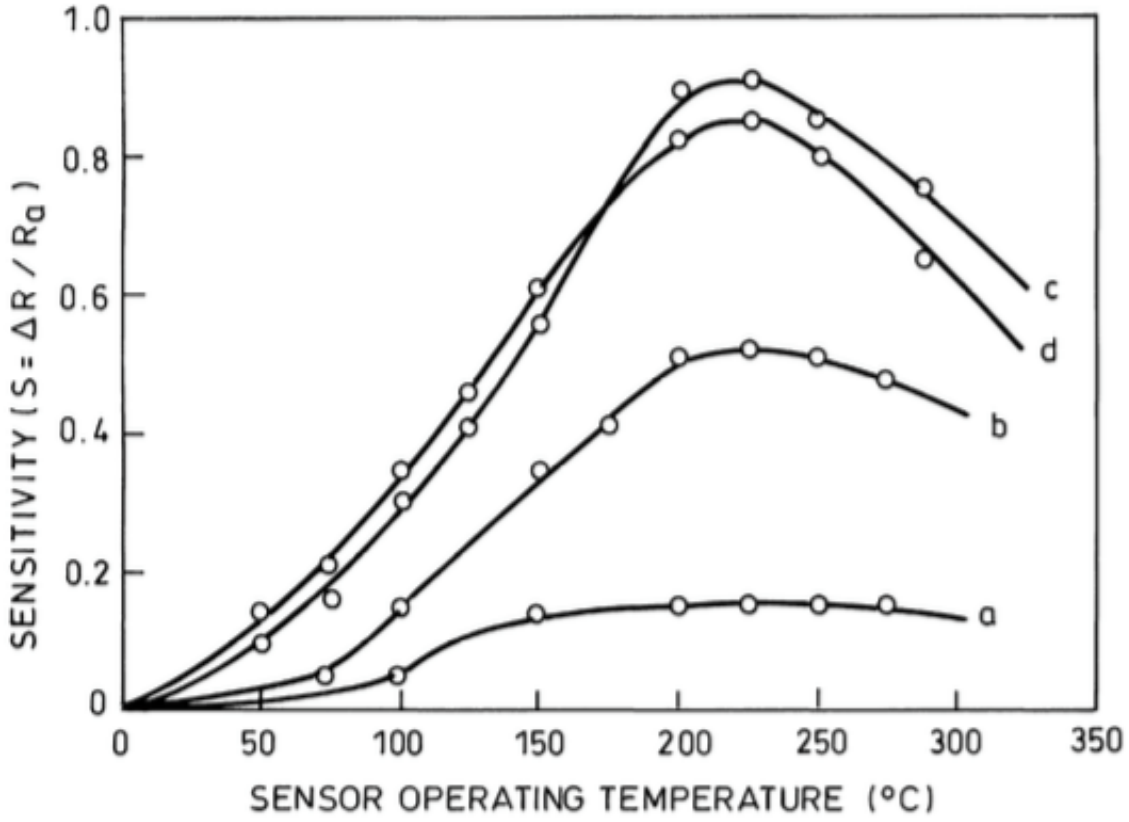

Figure 2.7: Sensitivity to ethanol vapor as a function of operating temperature for a resistive ZnO sensor, from B. B. Rao, Figure 3, p. 63, [50]. This work contains (a) ZnO, (b) ZnO+2La_2O_3, (c) ZnO+4La_2O_3, and (d) ZnO+6La_2O_3, indicating that lanthanum oxide can promote the sensitivity of ZnO to ethanol vapor.

Resistive sensors display different sensitivity levels based on the location of functionalization groups. Surface modification increases sensitivity versus bulk co-deposition for the same dopant as described by Wagh *et al.* [49]. This indicates that the surface adsorption is the step catalyzed by dopant in zinc oxide.

2.2.3.2 Semiconducting Zinc Oxide

If zinc oxide can be used as a resistive sensor, and is also an *n*-type semiconductor, it stands to reason that it can also be used as a semiconductor in a thin film transistor (TFT) chemical vapor sensor. Use of zinc oxide as a semiconductor sensor instead of a chemi-resistive sensor should increase its sensitivity. ZTO semiconducting TFT sensors were produced and reported by Dutta and Dodabalapur in 2009, so it is logical to try to produce sensing results with zinc oxide [38].

Chapter 3: Chemical Vapor Sensing

Organic semiconductors are useful as chemical vapor sensors because they display electronic changes in response to certain analyte vapors. The specific nature of the detection/change is dependent on the interaction between each specific analyte and semiconductor. The presence of a detectable analyte can cause changes in FET channel current due to shifts in threshold voltage, changes in mobility, and/or charge carrier concentration changes. These changes are caused by both reversible and irreversible interactions of the semiconductor and analyte at the surface of the semiconductor, at the boundaries between semiconductor grains, at the dielectric surface, and at the metal-semiconductor interface. The direction and magnitude of each parameter change depend upon the specific chemistry of both semiconductor and vapor phase analyte. In order to definitively identify an analyte using organic semiconductors, it may be necessary to construct a detection array using many organic semiconductors to create a chemical "fingerprint" for a specific vapor. Crone *et al* [51] described the change in source-drain voltage for single thin film transistors (TFTs) exposed to various vapors, as shown below.

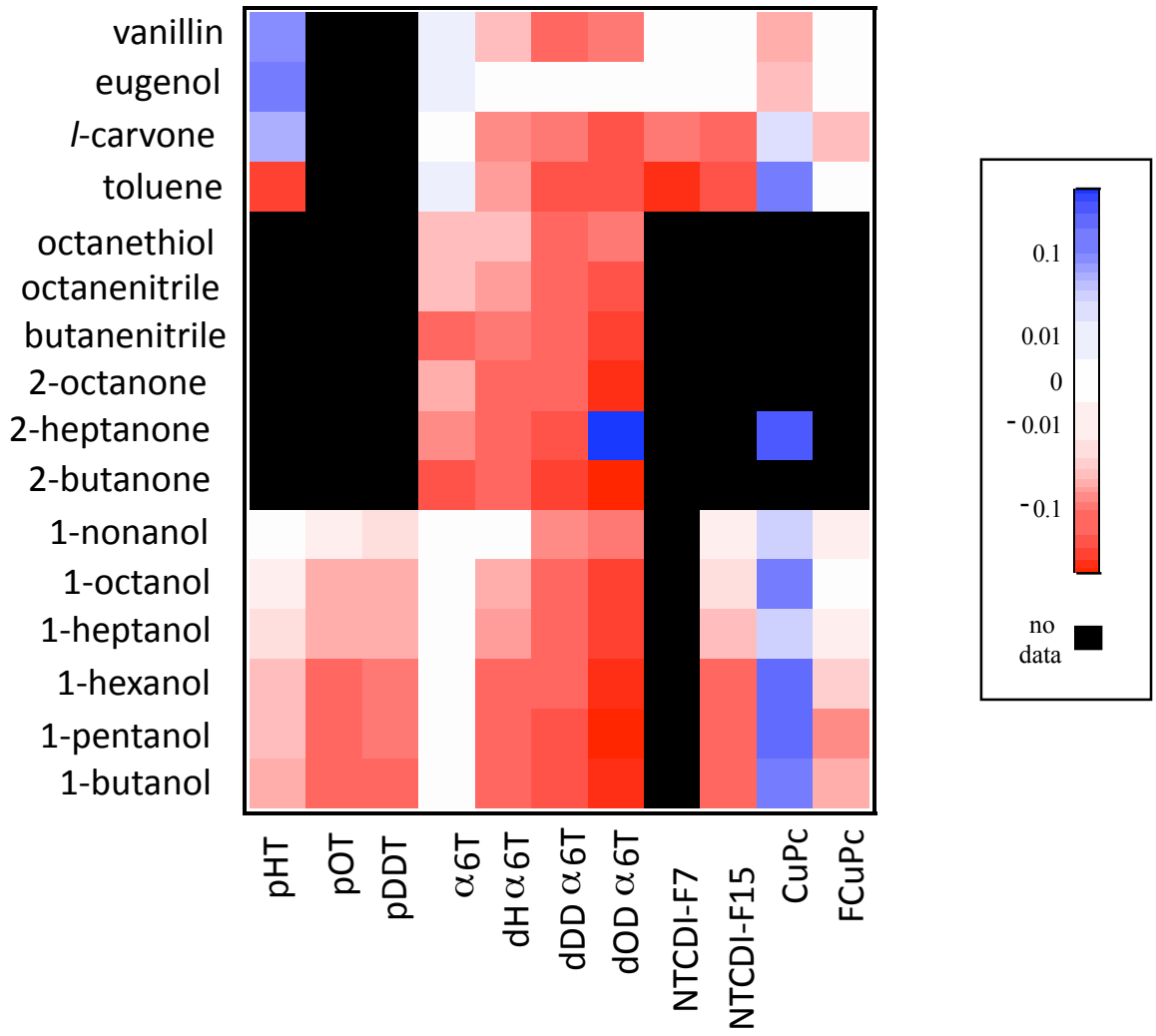

Figure 3.1: Various organic semiconductors as OFETs, plotted versus their response to several small polar organic molecules. From Crone *et al,* Figure 2, p. 2230, [51].

Electronic nose arrays currently exist, but are too expensive to produce or operate commercially [52]. Gas chromatography/mass spectroscopy remains the gold standard in odor detection, but it is too expensive for continual environmental monitoring or detection of a broad array of vapors. An electronic nose combines a multitude of sensors with a pattern recognition method (PARC) [53], which is still in development. The major

barrier to electronic nose development is the cost of the sensory array necessary to map the odor space. For the human sense of smell, there are seven primary odors: musk, putrid, pungent, camphor, ether, floral, and mint. So far, chemical vapor sensors are only sensitive to specific odor vapors based on chemical group detection and do not map onto the full human smelling experience [53], [54].

Organic semiconductors and inorganic oxide semiconductors have cost and production advantages for flexible sensors and low-cost sensor arrays. Both organic semiconductors and inorganic oxide semiconductors have large area deposition advantages. They don't require high-temperature processing like amorphous silicon or crystalline semiconductors—save for some mid-temperature annealing steps. Poly-crystallinity and small grain sizes are actually necessary for sensing response in these materials, as long as mobility is not too severely impaired. These materials were developed first as semiconductors for use in large area arrays for display technology. Many are printable or spin-coat-able. Furthermore, small molecule organics are susceptible to chemical functionalization to increase specificity. Inorganic oxide semiconductors can also be made more receptive to certain analytes using small molecule organic receptors as a topcoat, as will be shown in the following chapters.

Not every analyte produces an electrical response. Chang *et al*. [55] showed that completely nonpolar molecules such as alkanes produce no electrical response. This is because the nonpolar molecules interact with the organic semiconductors via Van der Waals forces, which are relatively weak. Two separate interactions are necessary for sensing. Vapor molecules must interact with the surface of the semiconductor or adsorp. They must also cause electrical response in the channel current by trapping or creating charges. Alkanes surface adsorp well onto organic semiconductors but fail to influence electrical characteristics. The vapor molecules that do cause sensing events are polar and

influence charge via dipole interactions. The sensing capabilities of organic semiconductors are therefore maximized for organic molecules with strong dipole moments such as alcohols, ketones, and hydroxyl groups. Organic semiconductor sensors also show great potential for chemical or biological modification leading to increased sensitivity [56], [57].

3.1 Polarization Effects

For small molecule organic semiconductors like pentacene, there is no existing polar moment. The pentacene molecule is completely nonpolar, as is undoped polyacetylene. These semiconductors can exhibit sensing properties, however. This is due to an adsorped polar analyte inducing a dipole in the charge-transporting channel. Analytes with a large organic portion are able to adsorp onto the semiconductor's surface via Van der Waals interaction. The smaller dipole is then close enough to the semiconductor's electron cloud to induce charge in the channel. The interaction strength is modulated by the surface attraction the semiconductor holds for the analyte and the strength of the dipole moment.

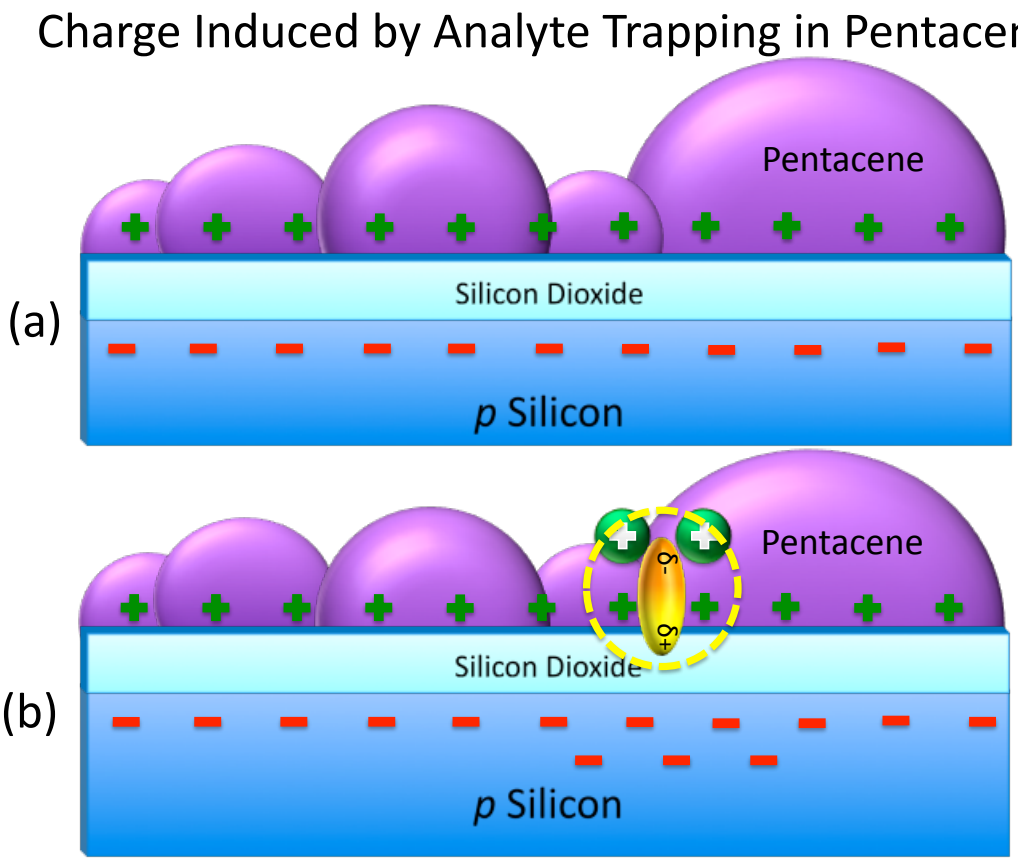

Figure 3.2: (a) Charges in a pentacene TFT on silicon for use as a chemical sensor FET. (b) Additional charges induced in silicon and pentacene by trapped polar analyte after exposure.

Non-polar molecules do not cause a sensing response [24], This indicates that adsorption via Van der Waals attraction is not enough by itself to cause an electronic reaction. Only polar molecules can cause changes in either charge carrier mobility or charge carrier concentration and thereby produce electronic changes. Someya *et al*. theorized that polar molecules could produce a sensing response if they were sufficiently absorped into the organic semiconductor to change its physical characteristics.

3.2 Dipole-Dipole Interactions

Other organic semiconductors such as P3HT have a pre-existing dipole moment, which facilitates the interaction of polar analytes with the charge-transporting material. For these semiconductors, the polar analyte is electrically attracted to adsorp to the surface. These analytes can then function either as dopants, attracting charge to the channel, or as traps, removing charge from the channel by holding it in a trapped state on the surface boundary of the semiconductor.

3.3 Analyte Charge Injection Mediation in Organic Oxides

Inorganic oxide semiconductors (such as the tin oxide, zinc tin oxide, and zinc oxide described in this work) are ionic metallic oxides with large electronegativity differences between anion and cation. For these materials, chemical vapor sensing is due to charge injection mediation effects at electrodes and gain boundaries [58]. This effect will be explored further in the following chapters.

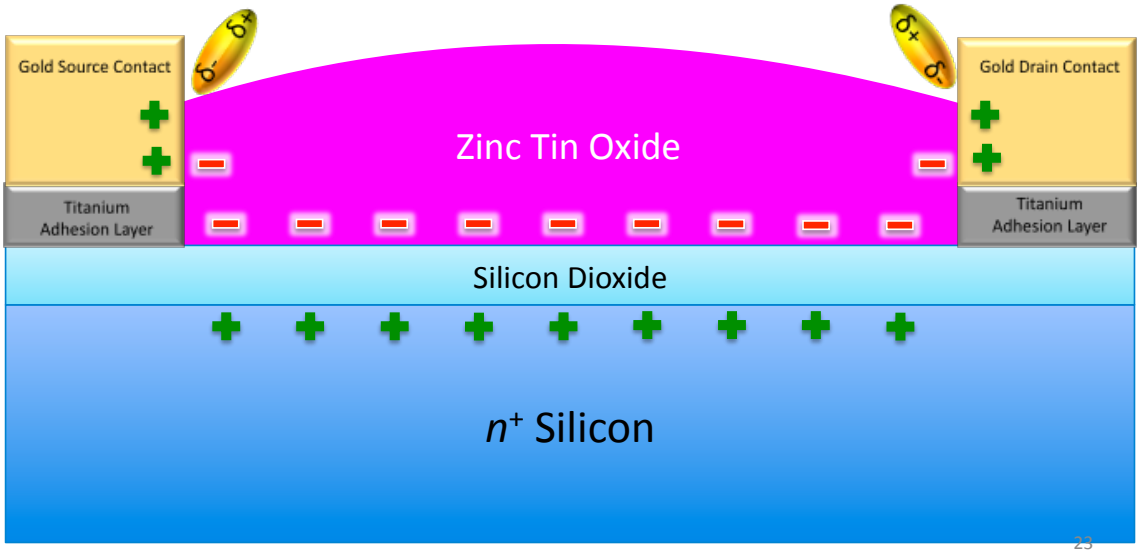

Figure 3.3: Analyte charge doping in inorganic oxide semiconductors.

Further sensing in inorganic oxides, particularly in oxides containing tin, is due to reduction and oxidation of the chemical constituents. Tin oxide forms both stannous tin(II) oxide and stannic tin(IV) oxide. In strong oxidizing and reducing gases, the chemical reaction between the two forms of tin produces or consumes enough electrons to entirely account for any sensing response. These are high-temperature effects occurring in a highly reactive environment. Any gases strong enough to cause these electronic changes must be contained to an unreactive environment that is necessarily an expensive proposition. Sensors that operate at high temperature are not further explored in this work, because they are expensive and less useful for low-cost sensing arrays.

3.4 Grain Boundary Effects

One of the major limitations in charge transport in an organic semiconductor is transport through grain boundaries. When organic semiconductors are deposited by vacuum deposition, the small molecules self-assemble into areas consisting of similarly oriented molecules bound by in a semi-crystalline structure. Grain boundaries are the areas between well-organized crystals where the orientation of the molecules can shift. Because these semiconductors are anisotropic, so is charge transport. When two different orientations of molecules meet at a grain boundary, charge transport is limited by the ease with which a polaron can jump from one area to another. Grain boundaries are also regions with large number of localized states due to crystal defects, disorder, and other forms of inhomogeneity.

Someya *et al*. described how the presence of an analyte can facilitate charge transport at grain boundaries and other imperfections in the macromolecular structure. When grain size is many times smaller than the length of the channel, small increases in the speed with which a polaron travels from grain to grain can produce a large net change in the conductivity of the channel. In this model, grain boundary defects dominate charge transport; charge transport can be modeled by hopping between localized states deep in the tail end of the density of states distribution. Analyte exposure can lead to increased channel current if analyte molecules induce more charge carrier in the channel, or to decresed mobility if the polar molecules are trapped at grain boundaries and function as scattering centers.

Analyte Mediation of Charge Carrier Transport

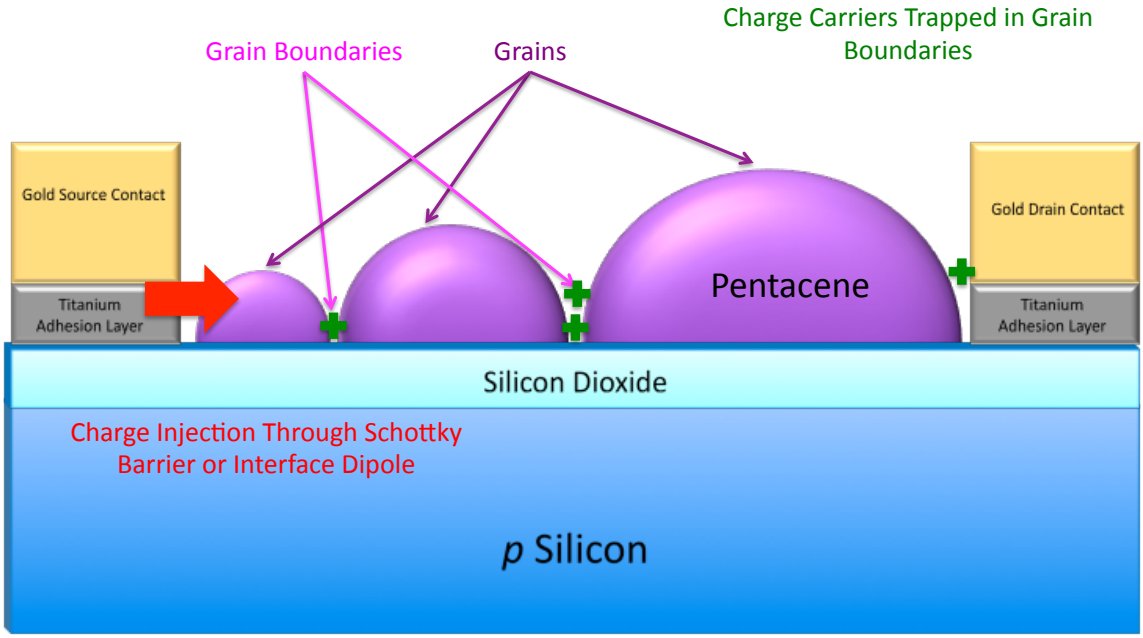

Figure 3.4: Analyte vapor mediation of charge injection from electrodes and between organic semiconductor grains.

3.5 Charge Injection Moderation

For organic semiconductor FETs, the charge injection barrier of the source and drain electrodes remains significant. For gold electrodes, the work function is 5.1 eV. Silver electrodes have a work function of 4.5 eV, while aluminum electrodes have a work function of 4.08 eV. Titanium, often used as an adhesion layer before e-beam metal deposition, has a work function of 4.33 eV. For the devices described in this dissertation, the metals aluminum, gold, and silver are the most important for use as contacts. Extrapolating from a single molecule of pentacene, Endres *et al*. have calculated a theoretical large band gap (>1.0 eV) with a bandwidth of 260 meV for electron transport and a bandwidth of 145 meV for hole transport for a pentacene solid [59]. Gold

electrodes are the best choice for charge injection into pentacene and similar organic semiconductors, but gold and aluminum interact unfavorably. Electrodes made of silver, aluminum, or titanium in combination with either of these, will present Schottky barriers to charge injection into organic semiconductors. The presence of dipole analyte vapor can mediate the charge injection barrier and therefore increase current through the device. This effect is especially strong in short channel devices where charge injection at the electrodes has a large effect and dominates over the fewer grain boundaries functioning as charge trapping centers.

Contact geometry is also important. For bottom contacts (i.e. metal contacts that are deposited on the substrate first, then coated with organic material), the surface morphology and grain size of the deposited organic semiconductor determine charge injection limits. For contacts patterned with photolithography, like those used in the four-terminal device described in Chapter Four, the method of exposure matters. For most metal layers, photoresist with liftoff is the preferred method, because the undercut sides of the photoresist ensure that the unwanted metal is washed away. Because the organic semiconductor is granular and only subjected to a low-temperature annealing step, it is important that its metal contacts have smooth sidewalls with no undercut. These metal contact layers are in-plane with the materials they must contact.

For top contact devices (i.e. when metal contacts are shadow-masked onto organic semiconductors), the existing topography of the organic semiconductor plays a pivotal role. These metal layers must be thick enough to cover the granular surface and remain contiguous.

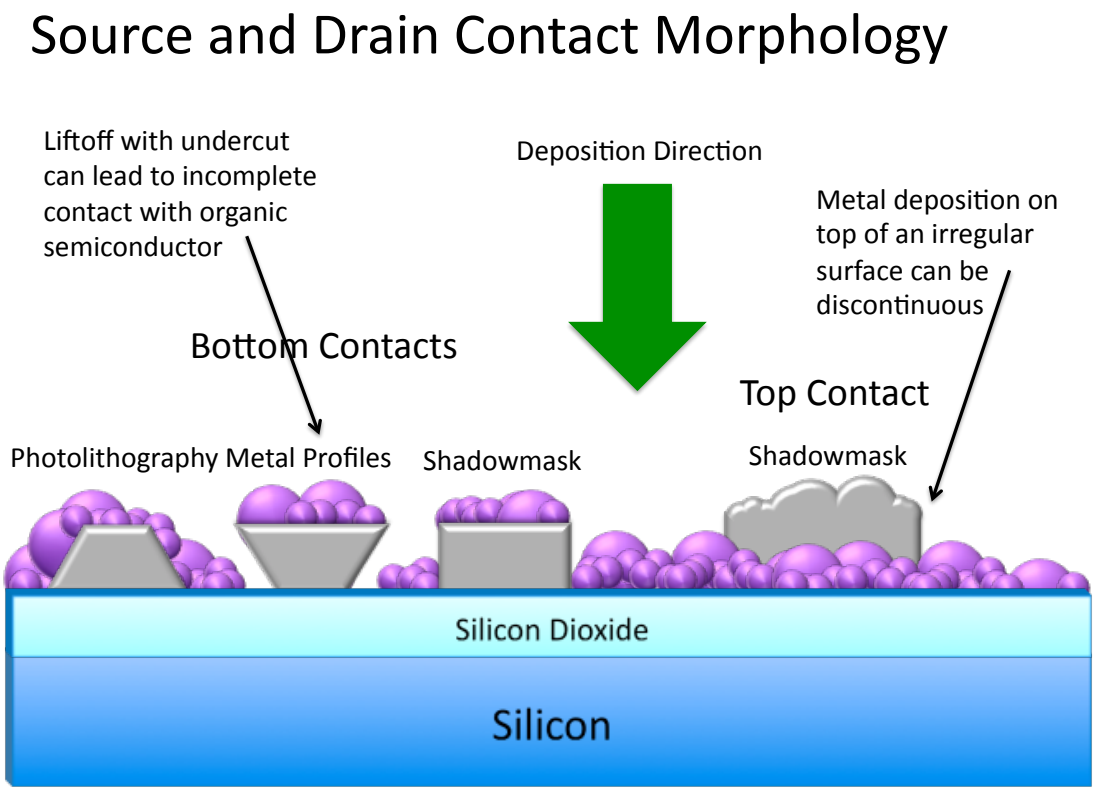

Figure 3.5: The method of deposition for source and drain contact deposition can have a large effect on the barrier for charge injection.

Additionally, for the testing discussed in this work, a HP 4155 Semiconductor Parameter Analyzer was used. This machine makes contact using needle-sharp electrical probes that can tear or puncture a thin or rough top contact pad. For a fully processed, commercially packaged hybrid device, this would not be a problem, because electrical contacts would be made to metal leads at the edge, not metal in contact with the organic semiconductor.

Chapter 4: The Four Terminal Device

The four-terminal dual-channel sensing device was first developed and demonstrated by Deepak Sharma in order to combine the advantages of silicon with the sensitivity of organic semiconductors [60]. Silicon devices do not experience the bias-stress effect, which is a steady decrease in current due to the dynamics of charge trapping. Mobility and currents in silicon FET devices are constant for long periods if the bias conditions are unchanged. Silicon processing techniques are well-established. Organic semiconductors are effective chemical vapor sensors, as previously shown. By combining organic semiconductors with a silicon FET device structure, it is possible to combine the sensitivity of organic material with the reliability of silicon in a single sensor device.

4.1 Hybrid Organic/Inorganic Devices

There has been considerable recent progress in the synthesis and device characterization of numerous organic and polymeric semiconductors for transistor applications. Some of these materials have also been evaluated as chemical sensors [61]. The fabrication of the four-terminal sensing device involved the development of four specific photoresist mask layers and a mechanical shadowmask. The designs reported in this chapter represent improvements over those used by Sharma in earlier work, including patterning the organic semiconductor layers and additional materials used for both organic semiconductors and sensing analytes.

4.2 Coupled-Channel Device Design

The four-terminal device was designed to include two capacitively-coupled charge-transporting channels. The silicon and organic semiconductor channel are separated by a 400 Å SiO_2 gate oxide layer. The physical proximity of the two channels

and the capacitive coupling allows charge concentrations in one channel to easily influence corresponding charges in the opposite channel. The contacts to the silicon nFET are configured conventionally with implanted source and drain regions and metal contacts. A bottom-contact configuration is employed for the organic pFET channel.

Top contact devices have electrical contacts that are applied on top of the source and drain regions. The contacts are geometrically placed on top of the charge transporting regions. Bottom contact devices, common in organic semiconductors, have electrical contacts underneath and adjacent to the semiconducting material. The semiconductor is physically deposited on top of the metallic electrical contacts. This architecture is commonly employed for semiconductors that are cast from solution (such as spin-coated polymers) or sensitive to photolithographic processing. Many steps in photolithography can potentially damage delicate organic semiconductors that are designed to be chemically sensitive. By combining these structures as shown below, it is possible to create a coupled channel device that exploits the strengths of both silicon and organic semiconductors.

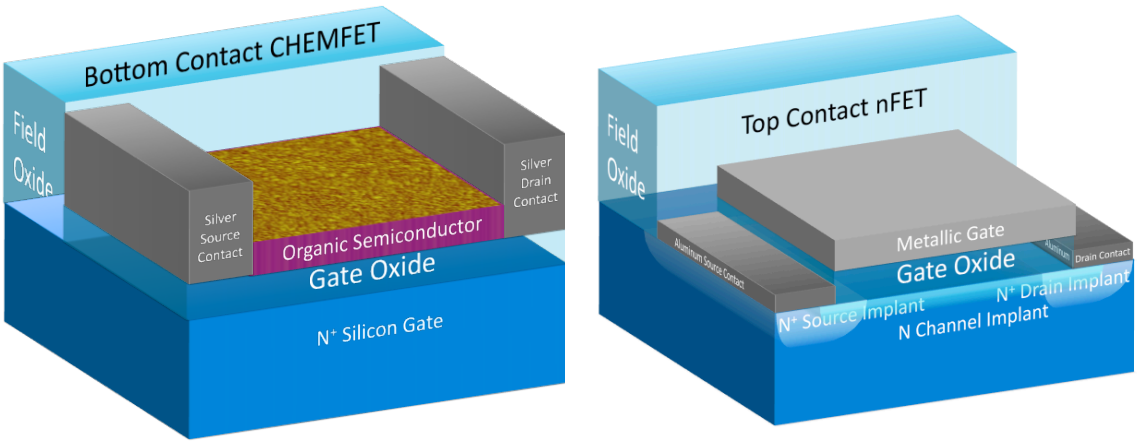

Figure 4.1: The similar layer geometry of a bottom contact OFET and a top contact MOSFET allows the FETs to be placed on top of one another, leading to the development of the four-terminal device.

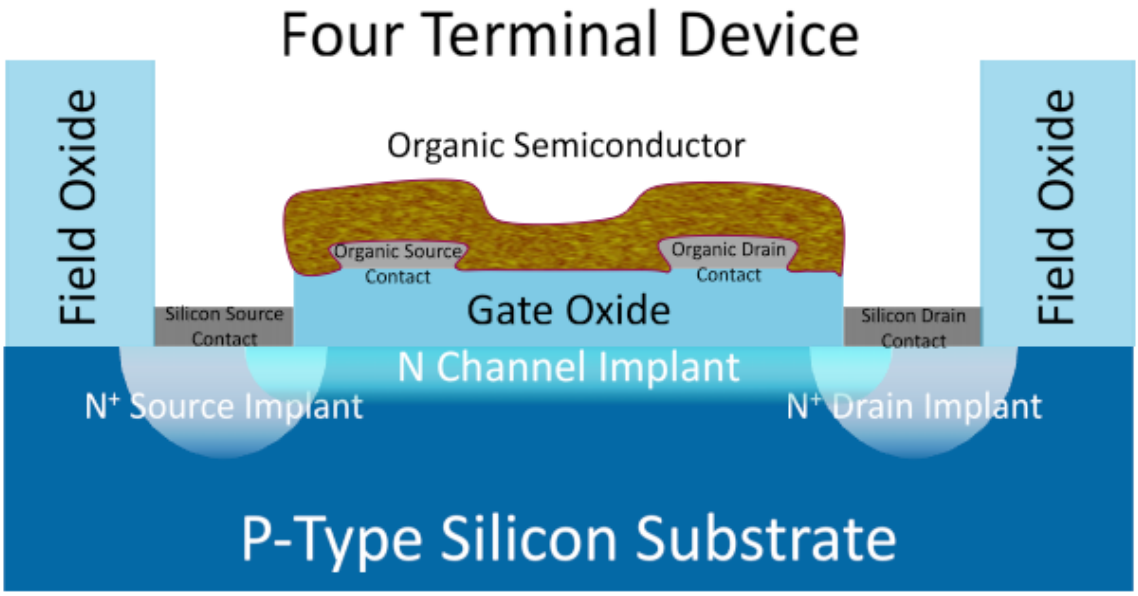

Figure 4.2: In the final four-terminal device, the silicon nFET and bottom contact organic pFET share a gate dielectric (thermal oxide), allowing the two semiconducting channels to function as gates for one another. The silicon nFET is designed to be a depletion mode device.

4.3 FABRICATION

The development of the four-terminal device at the University of Texas at Austin required several simulations to optimize the device design and several layers of mask design. The fabrication itself was done mostly at the Microelectronics Research Center on the J. J. Pickle Research Campus at the University of Texas at Austin. Ion implantation was outsourced to a commercial vendor.

In some cases, for simpler three-terminal sensors, the Si wafers with thermal oxide coatings as provided by wafer manufacturers were the starting point in fabrication. This thermal oxide was used as the gate insulator, and the doped silicon was used as the gate. All processing was conducted at the Microelectronics Research Center.

4.3.1 Mask Design

Organic semiconductors are low-mobility charge transporters, with hole mobilities typically below 1 cm^2/V-s [62]. Because of this, they are produced with relatively high channel width to length (W/L) ratios so that the total current across the device is significant. For the four-terminal device pFET, the W/L ratios of 5, 10, and 20 were used. The channel lengths were 20 μm, 30 μm, and 40 μm with widths of 100 μm, 150 μm, 200 μm, 300 μm, 400 μm, 600 μm, and 800 μm.

Because the device is directly probed, the source and drain contact pads are also macroscopic. The silicon source and drain pads are 1000 Å thick aluminum and 500 μm by 500 μm in cross-sectional area so that a probe tip can be lowered into physical and electrical contact. The organic semiconductor source and drain are 20 Å titanium followed by 350 Å silver and at least 500 μm by 500 μm in area. Because the organic semiconductor has the lower mobility, the organic source and drain contacts are closer together than the silicon source and drain contacts. The source and drain contacts extend

beyond the device and connect to large pads away from the channels so that the device current can be measured using a HP 4155 Semiconductor Parameter Analyzer.

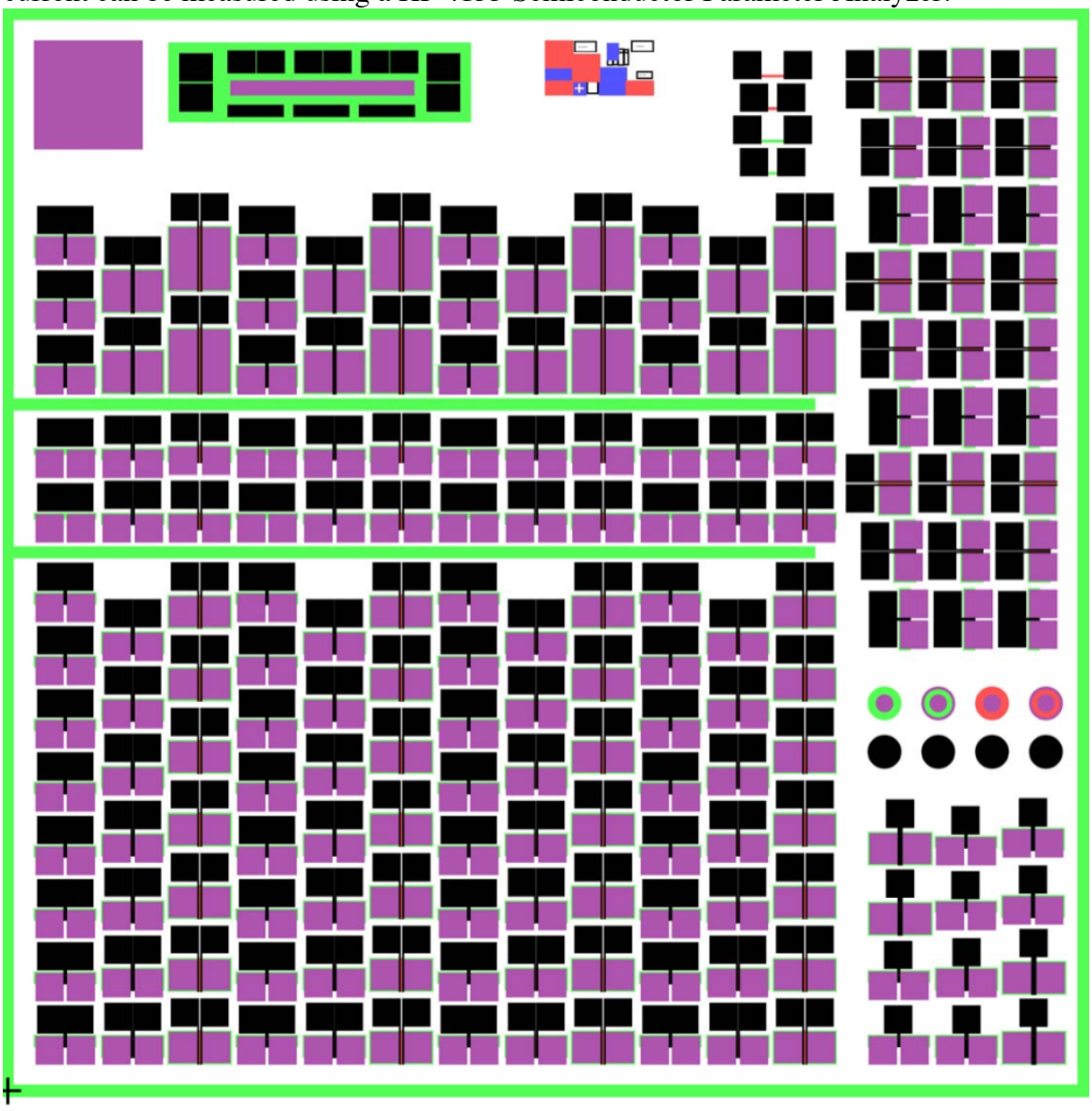

Figure 4.3: View of the 1” chip containing the four-terminal devices. The first layer (green) is the source and drain implant layer. The second layer (red) is the channel implantation layer. The third layer (purple) contains the silicon source and drain contacts, while the fourth layer (black) makes the organic semiconductor source and drain contacts.

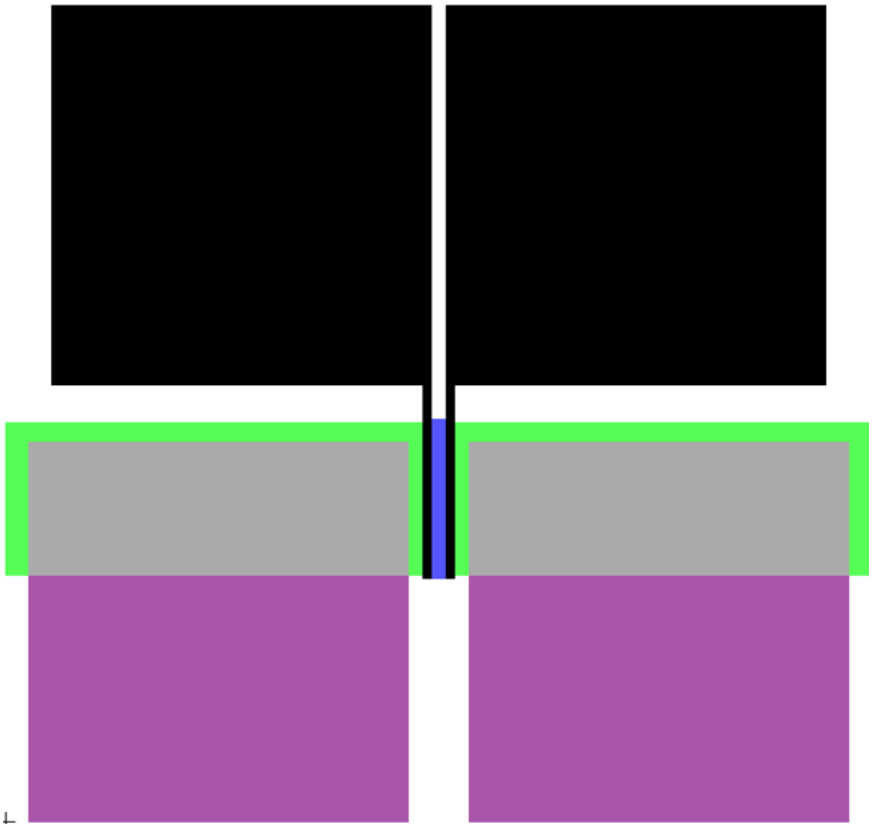

Figure 4.4: View of single four-terminal device, with two source/drain pads for the silicon channel (purple and gray) and two source/drain pads for the organic semiconductor (black).

4.3.2 Doping Simulation

The doping profiles for the four-terminal device were determined by doping simulations in MEDICI and T-SUPREME in order to produce a threshold voltage of close to zero but also slightly negative [60]. The device will therefore operate in the depletion region and be normally on. The phosphorus channel doping level of $1*10^{12}$ cm^{-2} and 30 keV ion energy was therefore chosen to optimize threshold voltage, subthreshold swing, and I_{on}/I_{off} ratio. The projected ion implantation range is 0.0371 micrometers and the projected longitudinal straggle is 0.0158 micrometers. The simulation results are shown in Figure 4.5.

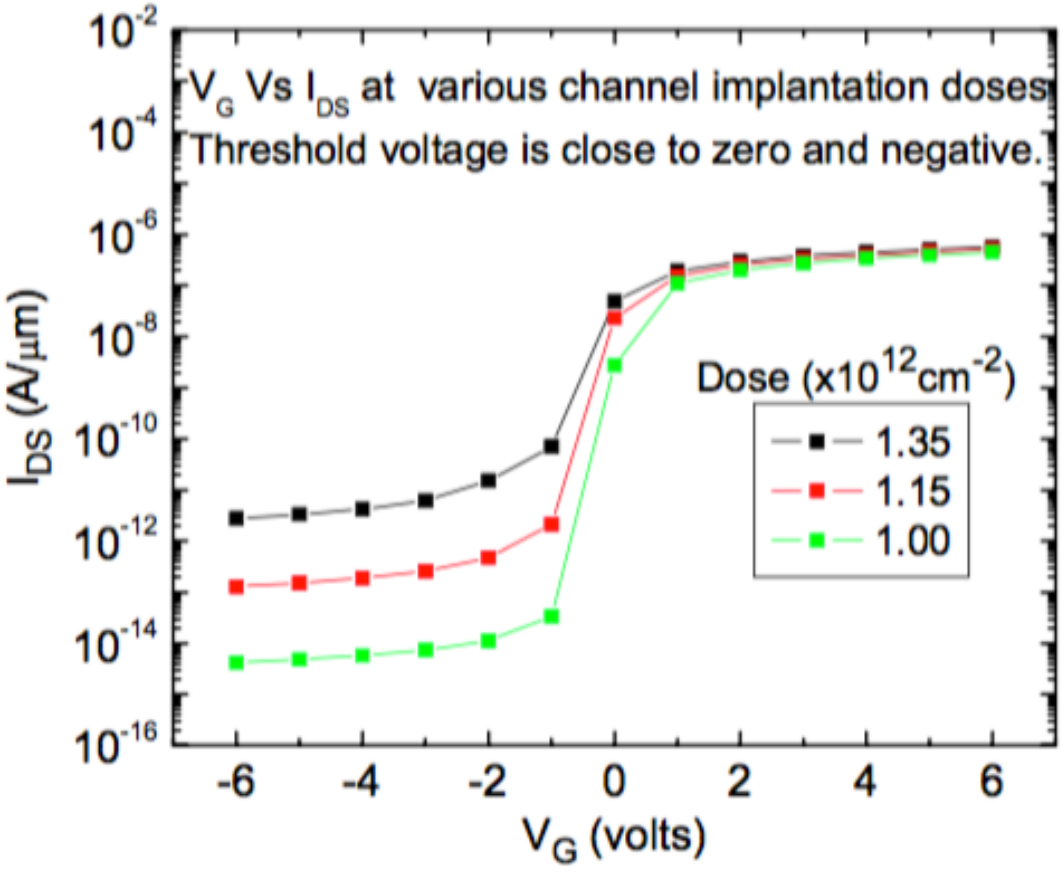

Figure 4.5: MEDICI simulation nFET current graphs from Sharma [60].

The doping concentrations were developed to be high enough that the channels would gate each other even with a certain amount of alignment error. The contacts for the organic semiconductor lay within the arms of the contacts for the silicon source and drain, as shown in Figure 4.4 above. The source and drain phosphorus implant (at $5*10^{15}$ cm^{-2} and 60 keV ion energy) creates a very high and shallow doping concentration in the source and drain region. The ion implantation range is 0.0729 micrometers with a projected longitudinal straggle of 0.0288 micrometers.

When the gate oxide is grown, the furnace activates the source, drain, and channel implants and also reduces the damage caused by the ion implantations. The gate oxide is grown in a two-step process: wet oxide growth for six minutes at 950C and dry oxide growth at 1000C for ten minutes. The maximum phosphorus dopant concentration is $2.07*10^{20}$ cm^{-3} at a substrate depth of 0.07 micrometers. The dopant profile after annealing is shown in Figure 4.6 below.

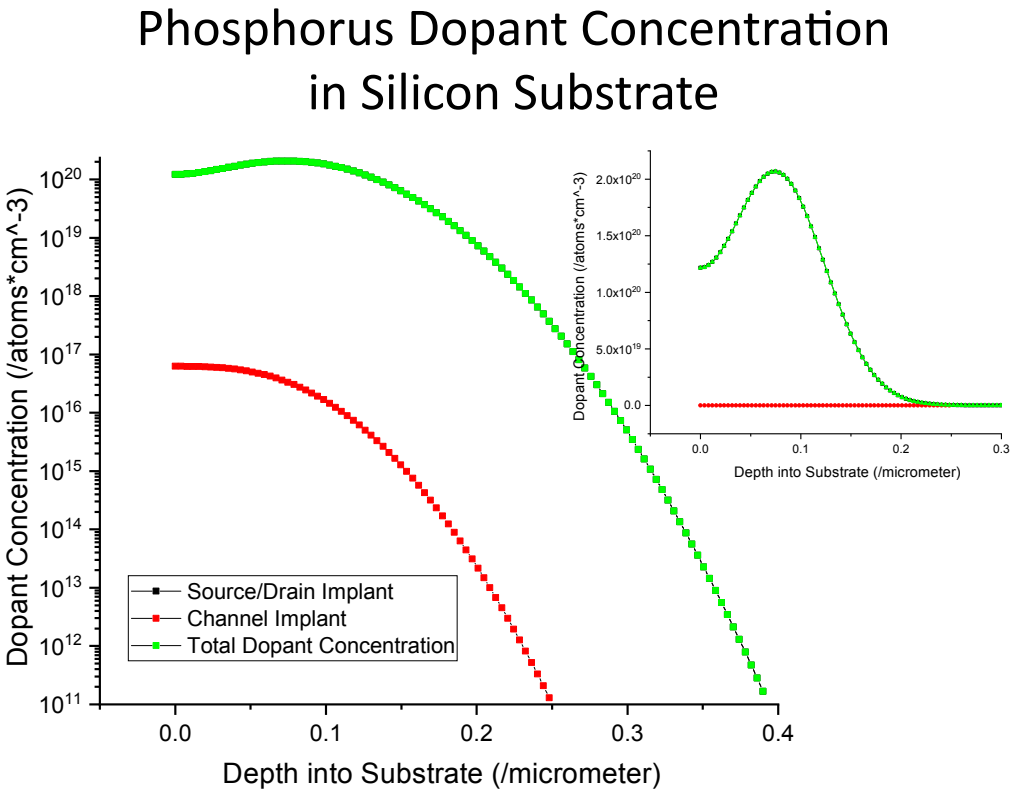

Figure 4.6: Implantation and annealing simulation showing silicon channel threshold adjustment and silicon source/drain implant concentrations as a function of depth in silicon wafer [63] after the gate oxide growth.

As fabricated, the channel lengths of the silicon nFETs are 35 μm, 54 μm, and 0.1 mm.

4.3.3 Silicon Platform Processing

The four-terminal sensing device is fabricated on a silicon platform. The substrate is a p-type <100> silicon wafer with resistivity in the range 1-10 Ω*cm. The fabrication begins with the stripping of native oxide using HF and cleaning with a 33% H_2O_2 66% H_2SO_4 piranha clean. This is followed by the thermal growth of SiO_2 field oxide at 900C in 5% H_2 in O_2 for approximately 55 minutes, yielding 1500 Å of field oxide. The wafers are again cleaned by the piranha method and primed for sixty seconds at 150C with a hexamethyldisilizane (HMDS) adhesion layer. A positive photoresist (AZ 5209) is spin-coated on at 4000 rpm for forty seconds and cured at 90C for 2 minutes. The first mask is aligned and exposed for twenty seconds to UV light. The photoresist is developed for sixty seconds and hard-baked at 120C for ten minutes. The first photoresist mask defines the source and drain implant regions of the symmetric silicon channel, so a buffered oxide etch (BOE) dip is used to strip the field oxide before the wafers are sent out for the source-drain implant of phosphorus with a dose of $5*10^{15}$ cm^{-2} and 60 keV ion energy.

When the wafers return from the first implant, the photoresist is stripped via a fifteen-minute ozone clean followed by a piranha clean. The HMDS layer and AZ 5209 are reapplied following the same procedure detailed above, and the second mask layer is aligned, exposed, and developed. This mask outlines the channel implant region. The channel implant is used to adjust the silicon nFET threshold voltage upwards to zero volts. The channel implant region is designed to overlap the source and drain implant regions by one to five microns in order to reduce the severity of alignment errors. The wafers are again sent out for ion implant—this time for phosphorus implant with a dose of $1*10^{12}$ cm^{-2} and energy of 30 keV.

When the lot returns from implant a second time, a ten-minute ozone clean and a piranha clean remove the photoresist. The wafers are then cleaned via RCA clean, which consists of an organic clean of 2000 mL H_2O, 400 mL H_2O_2, and 400 mL NH_4OH; an oxide strip of 2400 mL H_2O and 60 mL HF; an ionic clean of 1750 mL H_2O, 300 mL H_2O_2, and 300 mL HCl; and a final oxide strip. Following this rigorous cleaning, the wafers are loaded into the gate oxide furnace. Gate oxide is grown at 950C with 5% H_2 in O_2 for six minutes and at 1000C in O_2 for 10 minutes. This combination of wet and dry oxide growth results in 400 Å of gate oxide and the activation of the implanted ions.

After gate oxide growth, the batch is cleaned by the piranha method and primed with HMDS, as described above. The wafers are coated with AZ 5209 for 50 seconds at 4000 rpm and prebaked at 90C for two minutes. The third mask is then aligned and exposed for 13 seconds. AZ 5209 is then converted to negative resist by a one-minute heat treatment at 120C and a 45-second direct UV exposure. The resist is developed for 30 seconds and hard-baked at 125C for ten minutes. The third mask layer defines the silicon source and drain metal contacts. In order to expose the N^+ source and drain regions, the field oxide is stripped using BOE. The wafers are then immediately loaded into the high vacuum of a Varian aluminum sputterer. Approximately 1000 Å of Al are deposited, and the unwanted aluminum is removed by the acetone dissolution of the remaining photoresist. The aluminum is then sintered in forming gas for 20 minutes at 300C in order to form ohmic contacts. At this point the fabrication of the shared silicon nFET platform is complete.

4.3.4 Organic Semiconductor Processing

The four-terminal vapor-sensing pFET is a bottom-contact, bottom-gate device. The nFET device is coated with HMDS and photoresist following the same procedure,

and the fourth mask is aligned and exposed using the image reversal procedure used to fabricate the aluminum contacts. The organic semiconductor source and drain contacts are deposited on top of the oxide layers using e-beam deposition. The usual contacts consist of 20 Å of Ti and 350 Å of Ag, even though silver is not an ideal hole injection contact for organic semiconductors. Some devices have been fabricated using contacts of 20 Å of Ti and 350 Å of Au, but gold and aluminum can react corrosively. A titanium and silver contact source/drain contact layer is used for the 4T device because device stability is more important than charge injection. Following deposition of the last metal layer, the 4" wafers are diced with a wafer-dicing saw into nine identical 2" square chips and the photoresist and extraneous metal are removed by dissolution in acetone. Each chip contains over 100 dual-channel FETs divided into nine sets. There are three groups of devices with varying W/L ratios: 5,10, and 20. Each of these groups further contains devices with three channel lengths: 20 μm, 30 μm, and 40 μm.

From this step onwards, the smaller chips are processed individually. For pentacene (and other small molecule organic semiconductors such as copper phthalocyanine) devices, a macroscopic shadowmask is aligned in order to separate the organic semiconductor devices and reduce pFET gate leakage. 350 Å of semiconductor are deposited by vacuum sublimation. Shadowmasking cannot be used for polymer organics such as poly-3-hexylthiophene (P3HT) as these are deposited from solution. The high molecular weight makes it impossible to sublime such polymers. For these materials, the semiconductor is spin-coated onto the chip, where optimal speed and time is material-dependent.

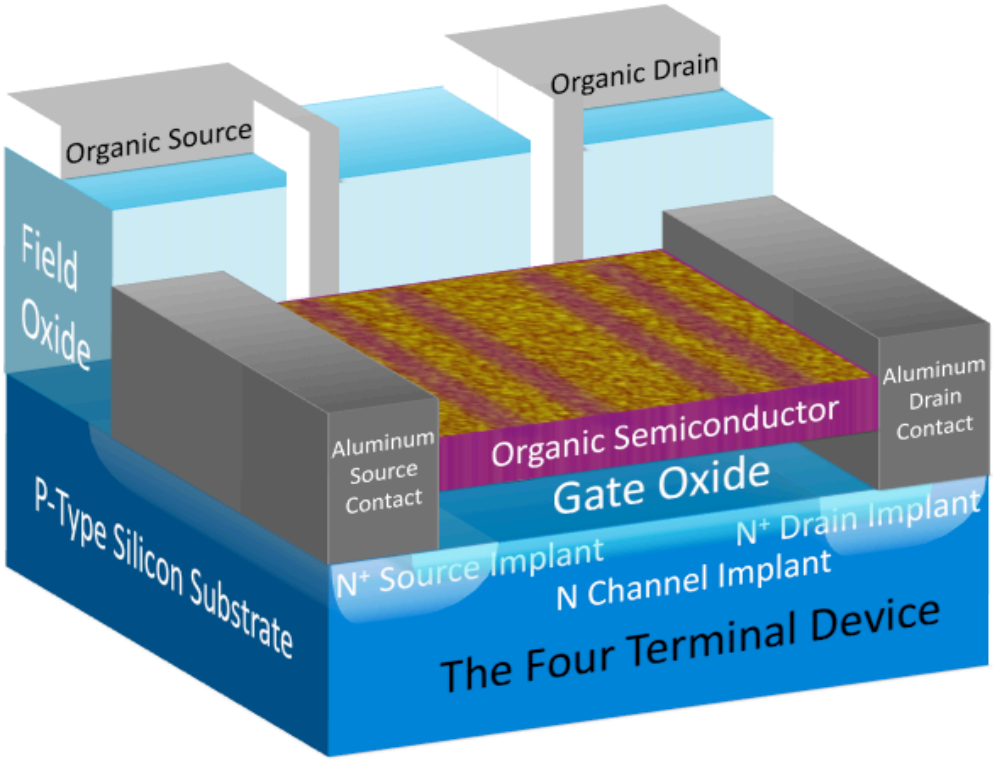

Figure 4.7: The four-terminal device after all fabrication is complete.

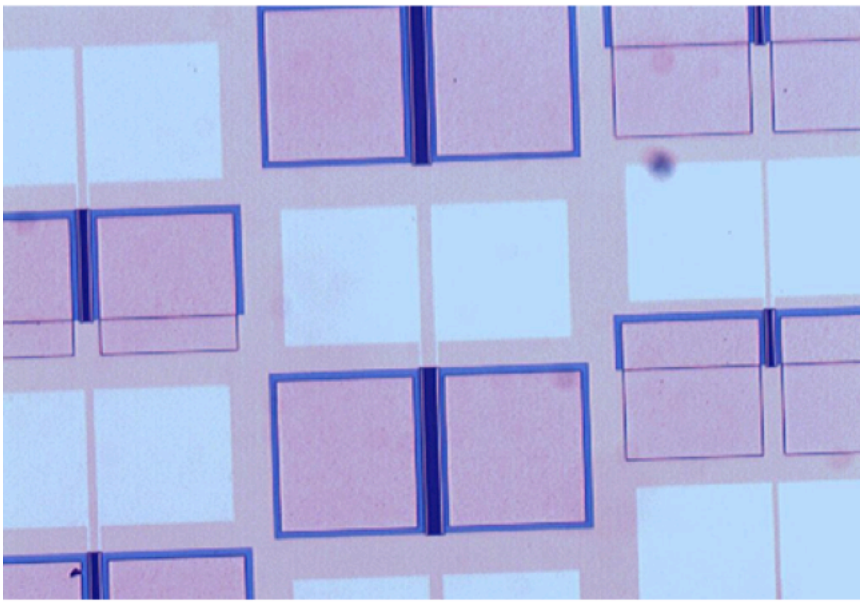

Figure 4.8: Photograph of the finished four-terminal device.

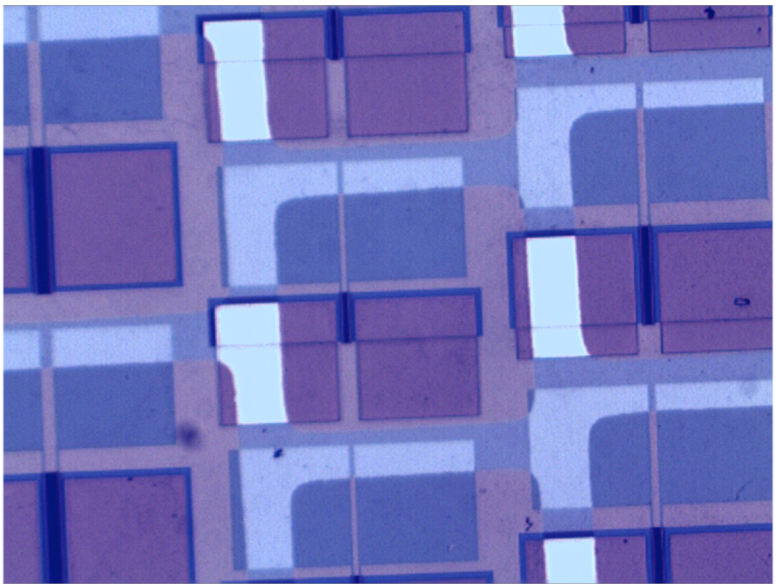

Figure 4.9: Photograph of the four-terminal device with a CuPc organic semiconductor layer deposited using the shadowmask.

4.4 OPERATION

The four-terminal device can function in four different sensing modes. Each channel may be biased independently because of the four contact points. The modes are described below, and representative responses are shown for ethanol delivered as a saturated vapor via peristaltic pump onto a copper phthalocyanine (CuPc)-based four-terminal device.

The experimentally calculated threshold voltage for the silicon nFET is ~0.6V, which is very close to the desired threshold voltage.

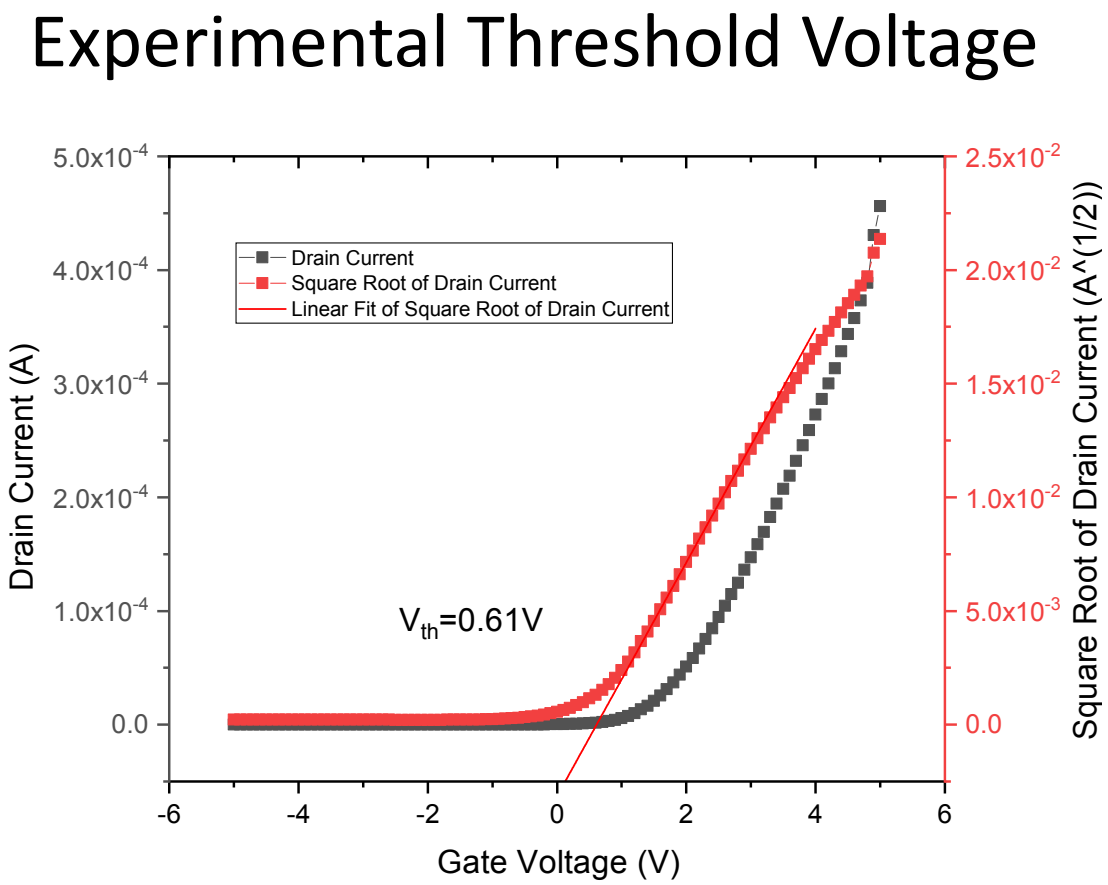

Figure 4.10: Threshold voltage calculation for the silicon nFET in the 4T device using extrapolation in the saturation region method [64].

4.4.1 CHEMFET Mode

In CHEMFET mode, the organic semiconductor functions as a FET gate for the silicon nFET channel. The source and drain of organic semiconductor are equally biased so that the entire organic semiconductor channel functions as one gate for the silicon channel.

The increase in silicon channel current is due to additional charge attracted to the silicon channel by the charged analyte molecules trapped in the organic semiconductor.

These molecules have a permanent dipole moment. The trapped dipoles shift the threshold voltage of the silicon nFET. Because the threshold voltage becomes more negative, the channel is effectively more turned on for the same gate voltage. For a FET device in the linear regime, a small shift in threshold voltage produces a large shift in channel current as can be seen in Figures 4.11 and 4.12.

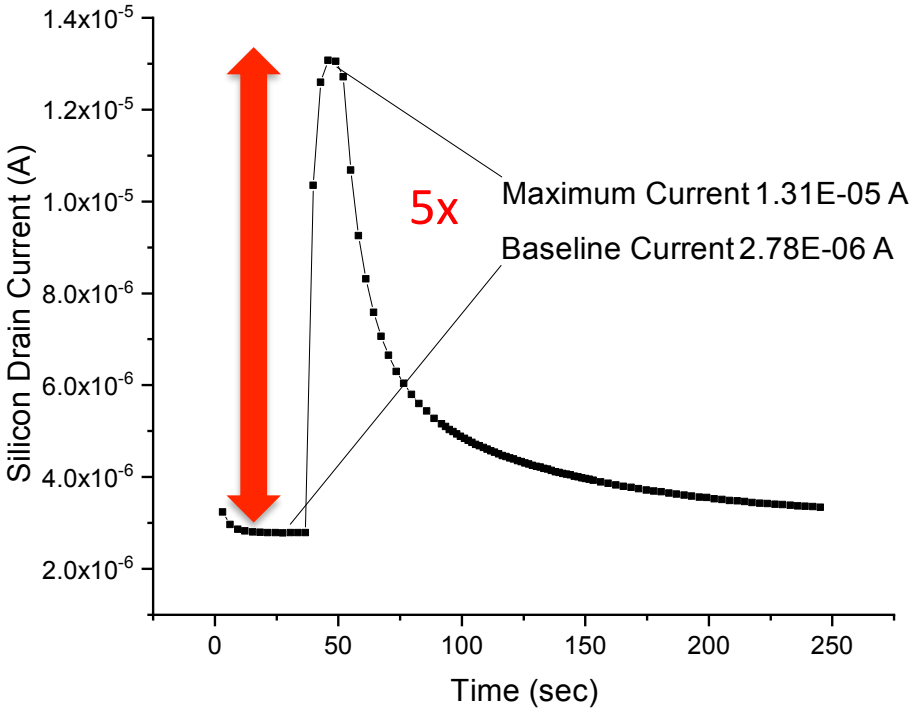

Figure 4.11: CuPc 4T silicon drain current response to ethanol analyte in CHEMFET mode with V_{ds}=1V, a floating CuPc gate and ethanol vapor delivered via peristaltic pump for 10 seconds starting at t=40 sec.

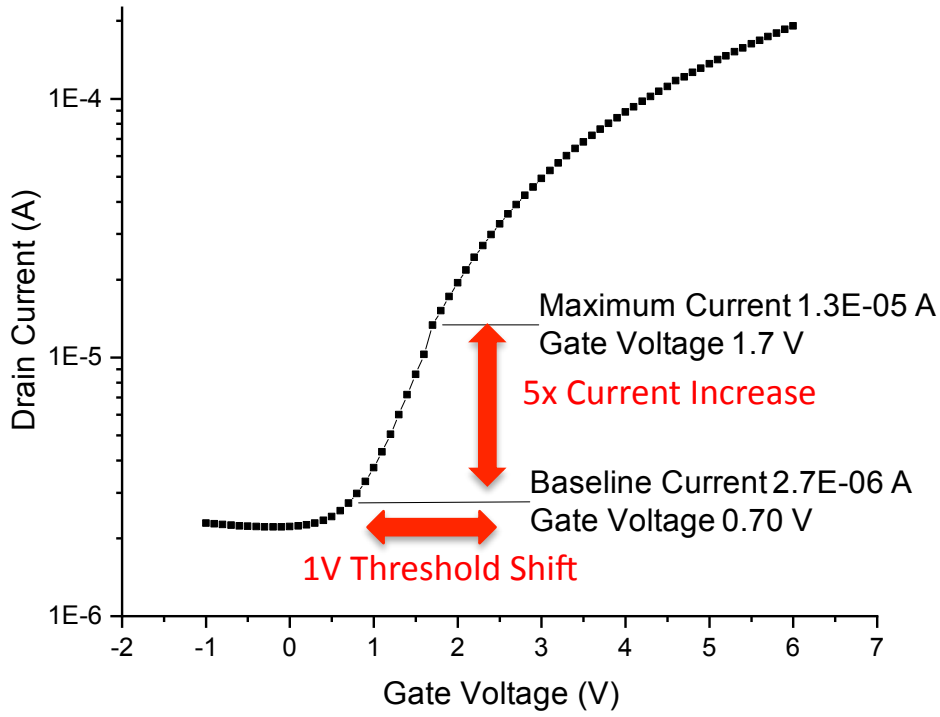

Figure 4.12: CuPc 4T silicon nFET transfer characteristics when V_{ds}=1V. A fivefold increase in drain current corresponds to a 1V threshold voltage shift, all other parameters being equal.

4.4.2 TFT Mode

When operated in the thin film transistor mode, the silicon functions as a gate for the pFET organic semiconductor. In this mode of operation, the silicon source and drain contacts are at the same voltage so that the silicon channel gates the entire organic semiconductor channel. The silicon channel dimensions are larger than that of the organic channel, greatly facilitating the operation of the TFT mode sensor.

The current decreases in the organic due to dipole-mediated charge trapping. The hole mobility in the organic semiconductor falls due to charge scattering caused by trapped analytes. Such decreases in current upon exposure to polar analytes have been

previously observed in organic TFT chemical sensors [65], [66]. Large changes in sensor current upon exposure to the analyte are observed in Fig. 4.13.

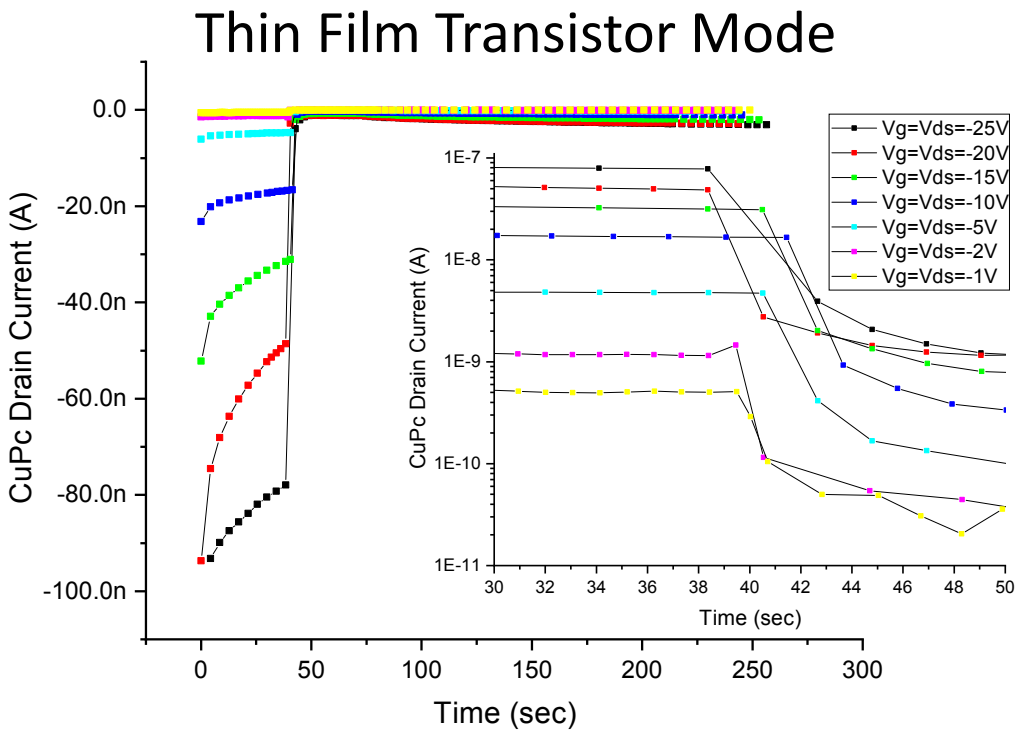

Figure 4.13: CuPc drain current in TFT sensor mode with V_{ds}=V_g for various voltages in linear and semilog plots. The current after analyte delivery decreases by as much as 98%.

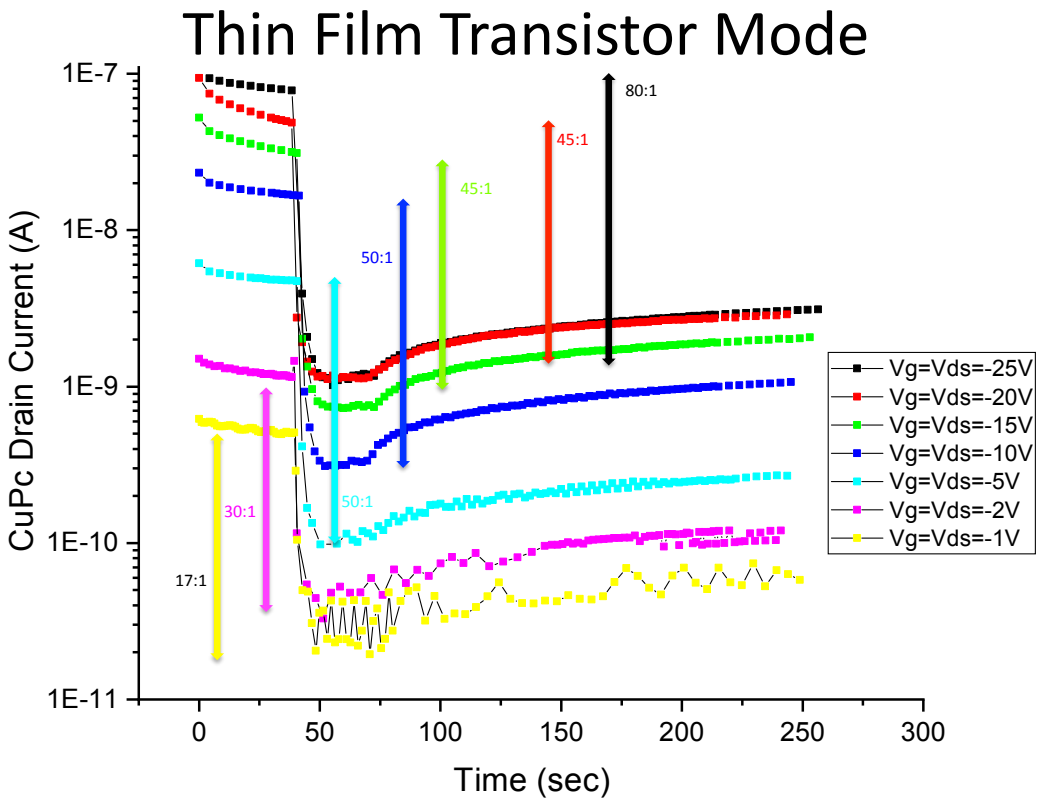

Figure 4.14: Semilog CuPc drain current in TFT mode with-25V < V_{DS}=V_{GS}<-1V. The ratios of baseline current to current after analyte delivery are shown.

4.4.3 Both Channels On

If both channels are biased on, it is possible to see the total effect a dipole has on the organic semiconductor and the corresponding silicon nFET. The electron population in the silicon channel increases as additional charge centers are created in the analyte/gate, shifting the threshold voltage more negatively and increasing the corresponding channel current. The organic hole mobility falls as charges are trapped within the channel, leading to a decrease in current. This mode was explored by Sharma *et al*. using pentacene 4T devices, with the results shown below.

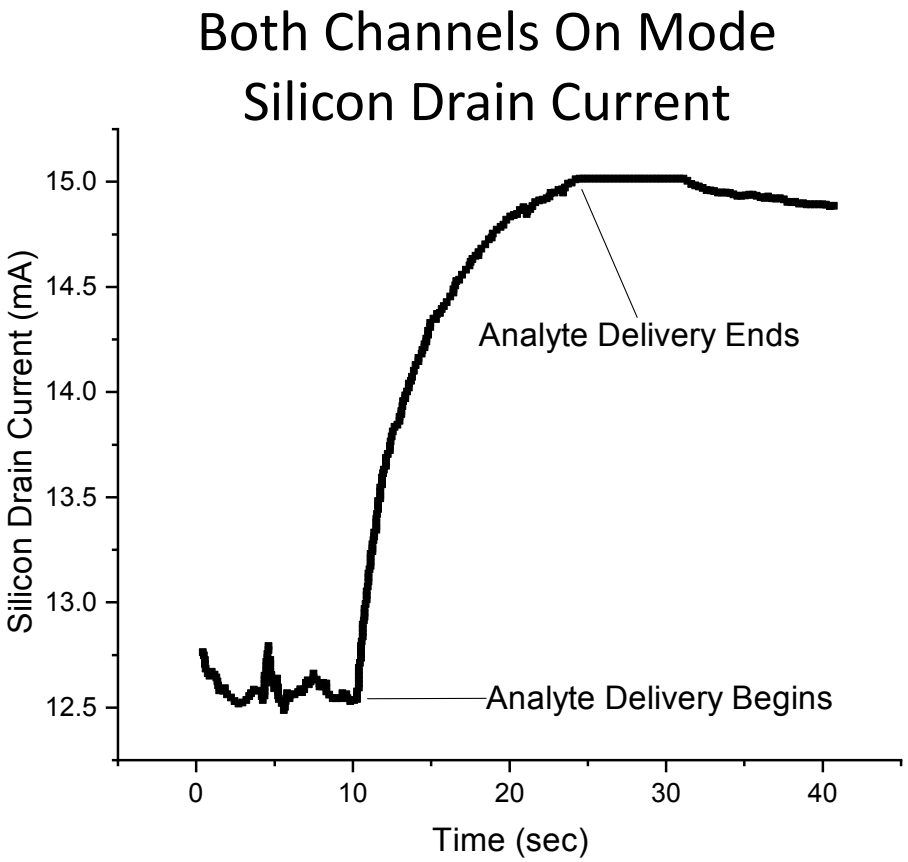

Figure 4.15: Silicon electron current for a pentacene 4T device exposed to ethanol when both channels are on, with V_S= 0V and V_D= 5V. Based on Sharma [60].

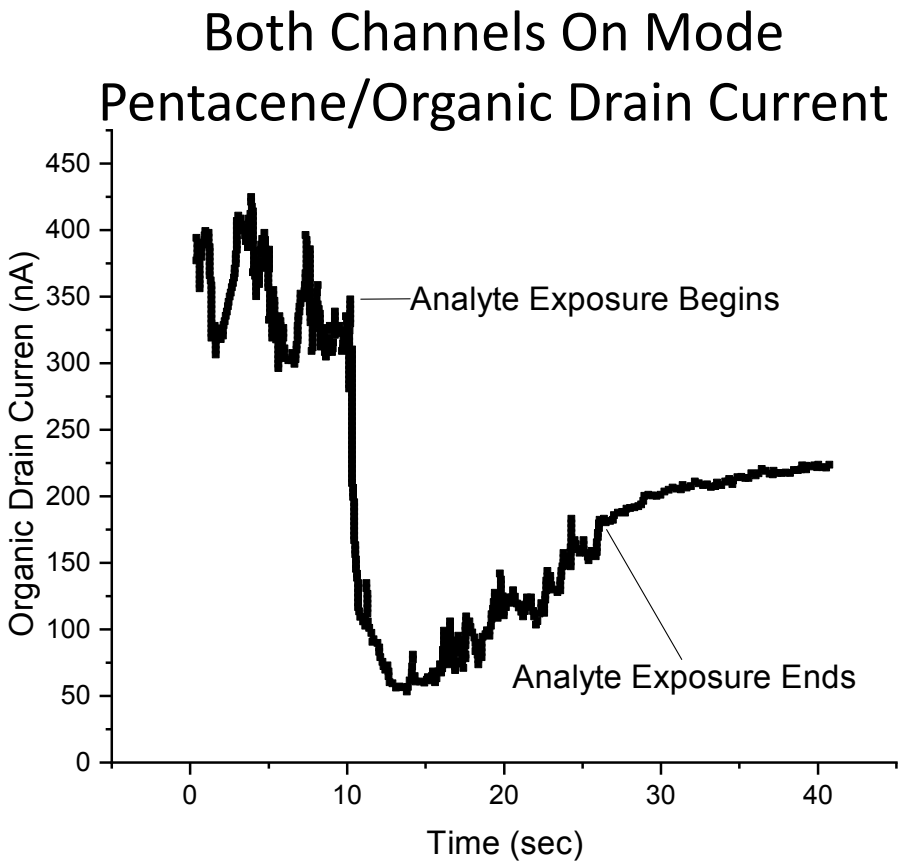

Figure 4.16: Pentacene hole current in both on mode for the same device when both channels are on, with V_D=15V and V_S=25V during ethanol exposure. Based on Sharma [60].

This mode is not well-suited to chemical vapor sensing at this time. The contribution of various effects combine to limit the specificity of detection. The analyte trapped in the organic layer causes a negative threshold shift in silicon, which leads to increased silicon current. These trapped charges, however, decrease the hole mobility in the organic layer, leading to a decrease in pFET current which effectively decreases the gate voltage applied to the silicon nFET. These two effects work against each other,

making each contribution hard to determine. For those reasons, this mode is not explored further in this work.

4.4.4 Chemical Memory Mode

For organic semiconductors, the dipole trapping effect can be used to create a more sensitive response in chemical memory mode. In the mode, the four-terminal device is cycled through a series of biases. Initially, the device is biased as a CHEMFET, and the silicon source-drain current is measured under a floating gate. Then, both channels are biased on, and the vapor or analyte is delivered. Under these conditions, any dipoles present are attracted to the dielectric-organic interface and trapped. Next, the biases are removed, and the device is once again measured in the CHEMFET arrangement. If any charges have been trapped in the organic semiconductor, the silicon source-drain current is altered. The final step of the cycle is a reverse biasing of the silicon n-channel in order to remove any trapped charges in the organic layer.

The main expected advantage of the Chemical memory mode is that the analyte dipoles in the organic semiconductor trap unipolar charges in the organic semiconductor for long enough periods to get a larger shift in the silicon current than is possible in the CHEMFET mode. This has been observed in some 4T devices, such as those reported by Sharma *et al* [67].

4.4.2.1 Reverse Bias

The first step for chemical memory mode measurements is a reverse biasing of the pFET to detrap all the charges in the organic semiconductor. A negative gate voltage is applied over the organic source and drain. A positive drain voltage is applied to the silicon for 1-2 minutes to drive out any charges trapped in the organic semiconductor layer.

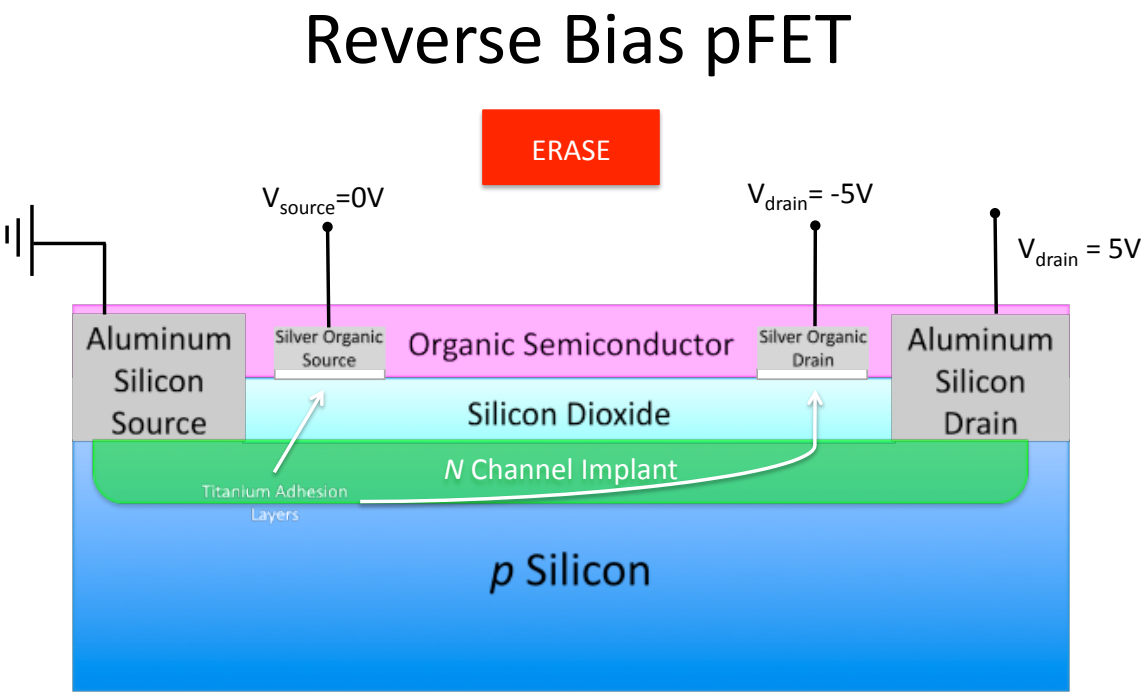

Figure 4.17: The 4T device with the organic channel under reverse bias. The silicon channel is held at V_{ds}=5V in order to drive any charges out of the organic semiconductor layer.

4.4.2.2 Remove Mobile Charges

Next, all of the source and drain contacts for both the pFET and nFET are set to 0V for 30 seconds in order to allow any mobile charges to escape. This is done between each active step to remove extraneous charges.

4.4.2.3 nFET Turned On

Now the pFET source and drain probes are lifted away from the contacts, producing a floating gate for the nFET. The nFET is then subjected to a slightly negative source/drain voltage, turning the nFET on and producing measurable drain current.

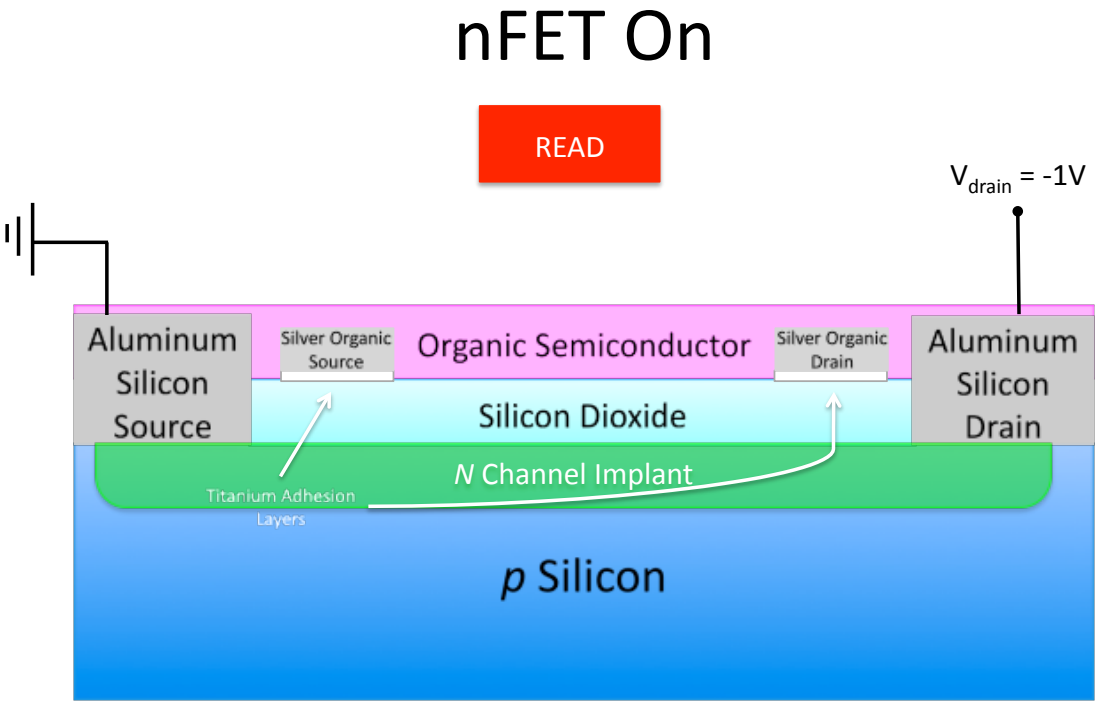

Figure 4.18: The 4T device with silicon channel biased at V_{ds}=-1V. The organic layer functions as a floating gate.

4.4.2.4 Reverse Bias

Then the pFET is reverse biased again, as shown in Figure 4.15, in order to remove any trapped charges in the organic semiconductor layer.

4.4.2.5 Chemical Vapor Delivery

The pFET and nFET are now biased so that charges are trapped in the organic layer and the analyte is delivered. The organic semiconductor is under negative and equal source and drain voltage, like that used in CHEMFET mode. The silicon channel is turned on with V_{ds} small and positive in order to expedite charge trapping.

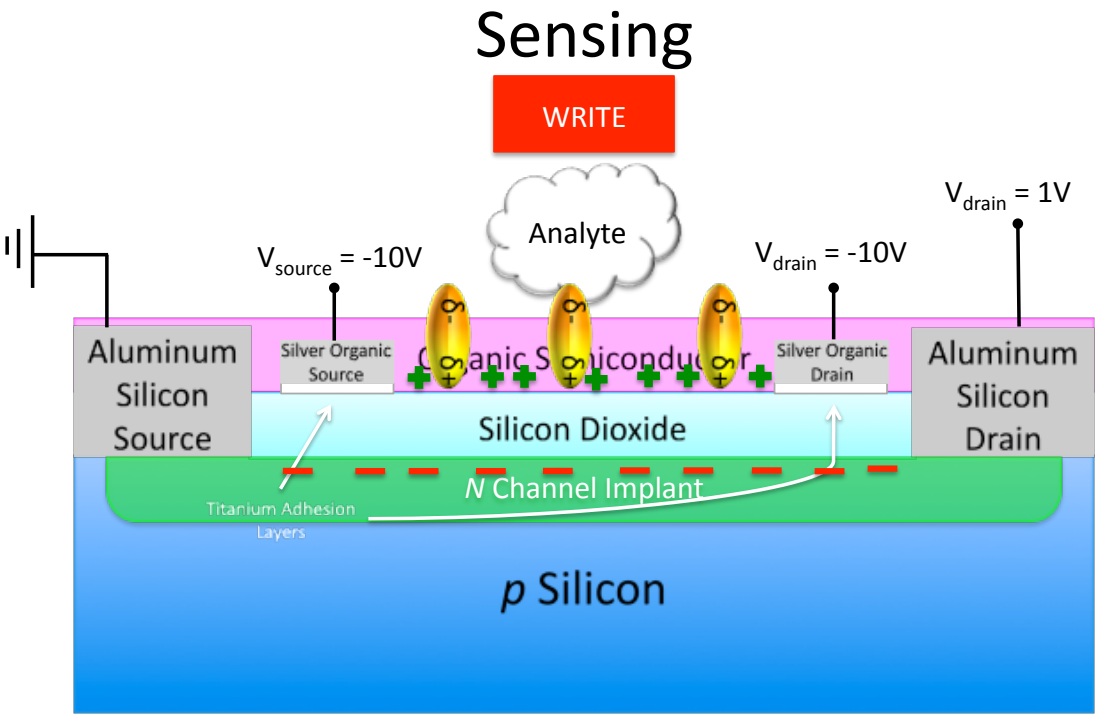

Figure 4.19: The 4T device with the organic semiconductor acting as a CHEMFET with V_{source}=V_{drain}=-10V. The silicon nFET has V_{ds}=1V. The analyte dipoles are actively attracted towards the organic layer and trapped at the dielectric interface.

4.4.2.6 Remove Mobile Charges

Next all of the source and drain contacts for both the pFET and nFET are set to 0V for 30 seconds in order to allow any mobile charges generated during analyte delivery to escape.

4.4.2.7 nFET Turned On

Now the pFET source and drain probes are lifted away from the contacts, producing a floating gate for the nFET. The nFET is then subjected to a slightly negative source/drain voltage, turning the nFET on and producing measurable drain current. This new drain current should be larger than that previously measured because of a negative

change in threshold voltage due to the charges trapped in the organic channel during the analyte delivery.

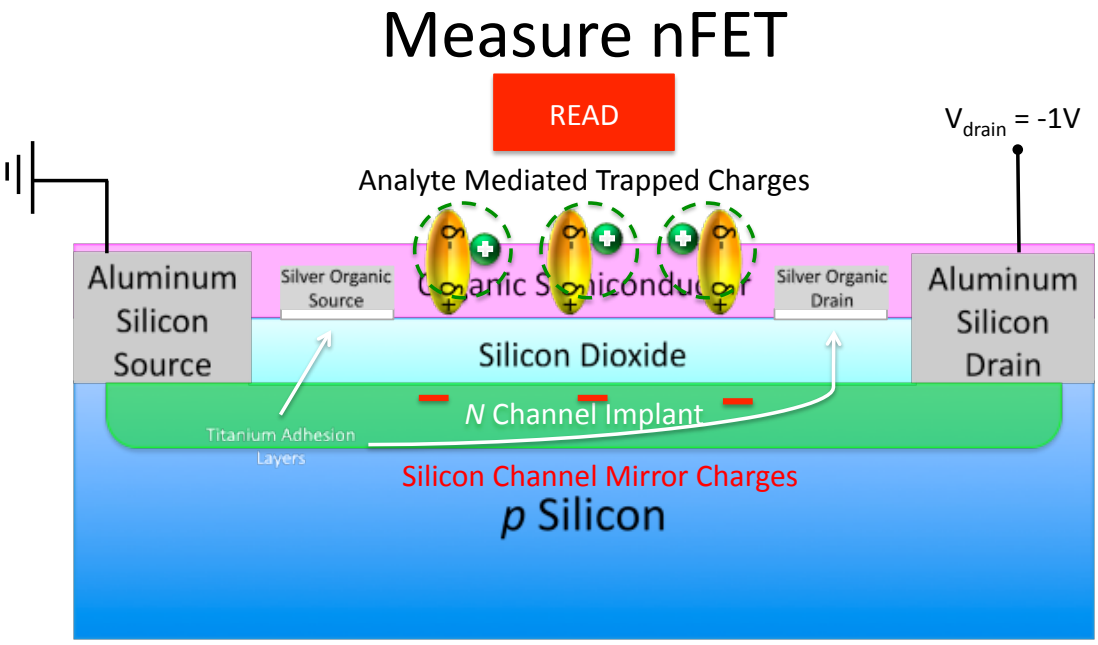

Figure 4.20: The 4T device with the organic layer with trapped analyte charges functioning as a floating gate. The silicon nFET drain current is measured and compared to that detected before the sensing event.

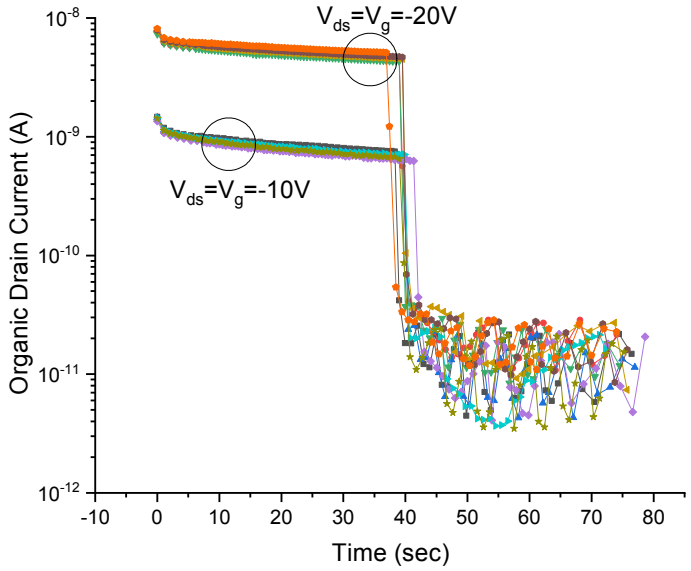

Figure 4.21: The organic drain current for a CuPc 4T device during the OTFT sensor write portion of chemical memory mode. Exposure to ethanol analyte effectively turns the OTFT off.

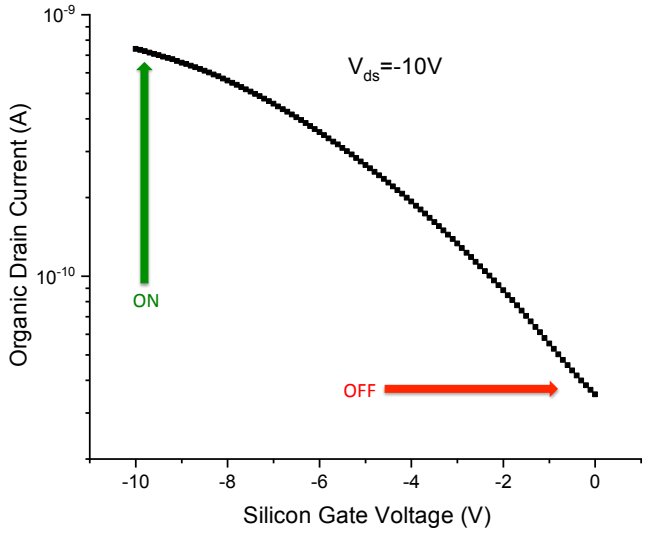

Figure 4.22: CuPc 4T pFET transfer characteristics on a semi-log plot. Analyte delivery effectively turns the OTFT off due to a change in threshold voltage.

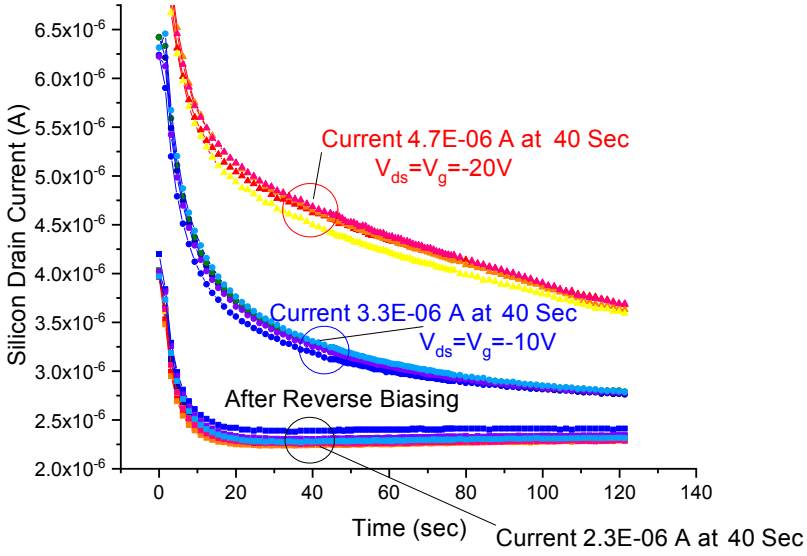

Figure 4.23: Silicon drain current during read portion of chemical memory mode. The displayed voltages are the organic bias conditions during writing, which effect the amount of analyte trapped.

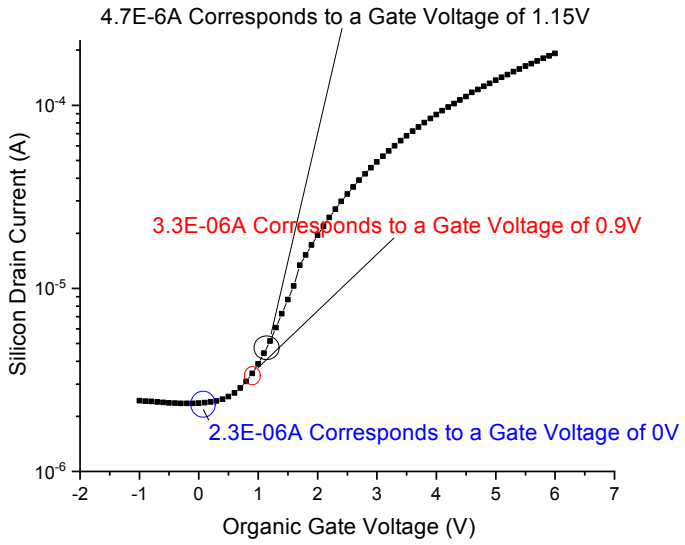

Figure 4.24: CuPc 4T nFET transfer characteristics semi-log plot. Trapped analyte molecules in the organic semiconductor layer effectively gate the silicon channel causing a change in drain current.

Chemical memory mode is the most sensitive of all the described modes—responsive to 100 ppb ethanol in nitrogen as reported by Sharma [60]. This sensitivity is due to the responsivity of high mobility silicon to the analyte charges trapped in the organic semiconductor gate. Chemical memory mode is more sensitive than CHEMFET mode because of in CHEMFET mode external bias voltage is applied to the organic semiconductor during measurement. In chemical memory mode, all of the applied gate voltage is due to trapped analyte.

4.5 TESTING

The four-terminal device was tested as a gas sensor under several different testing regimes.

4.5.1 Filter Paper and Peristaltic Pump

A peristaltic pump was used to deliver saturated vapor. First, a 20-μm pore size filter paper was soaked in the desired liquid. Then the wetted paper was placed into an angled syringe. Finally, nitrogen gas was pushed through the paper creating an analyte vapor. The syringe itself was aimed towards the channel of the device being tested. Because the channels of the organic device are so large, they are easy to visually identify.

The limitations of this method are the uncertainty in the strength of the vapor. On some occasions, the filter paper was beyond saturated, and liquid droplets landed on the surface of the device. The device functions differently with liquid phase analyte contact. If the analyte is in liquid instead of vapor form, it is both much more concentrated and not limited by adsorption. It is also possible for the filter paper to dry inside the syringe. This is hard to detect without ending testing and resetting the testing apparatus.

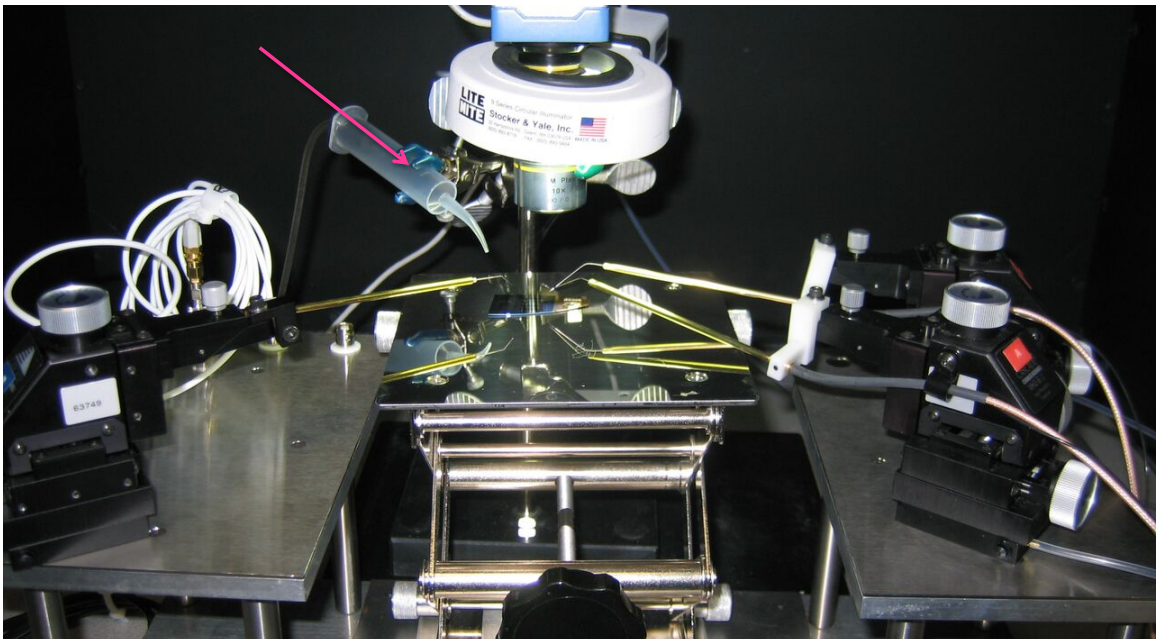

Figure 4.25: The peristaltic pump with analyte delivery syringe and probes as used to test chemical sensitivity. Pink arrow indicates gas delivery direction.

4.5.2 Gas Cylinder

Some analytes were purchased in gas-phase solution. Buying a known concentration of an organic vapor in nitrogen allows the exact part per billion (ppb) response to be calculated. However, most organic analyte vapors of interest are flammable and difficult to purchase. The highest concentration of ethanol vapor purchased was 500 ppm (parts per million) in nitrogen.

4.5.3 Chamber Flooding

In order to test the device in a consistent gas concentration, a Desert Cryogenics probe station was used. This allows the system to be evacuated and then filled with a known concentration of ethanol in nitrogen gas.

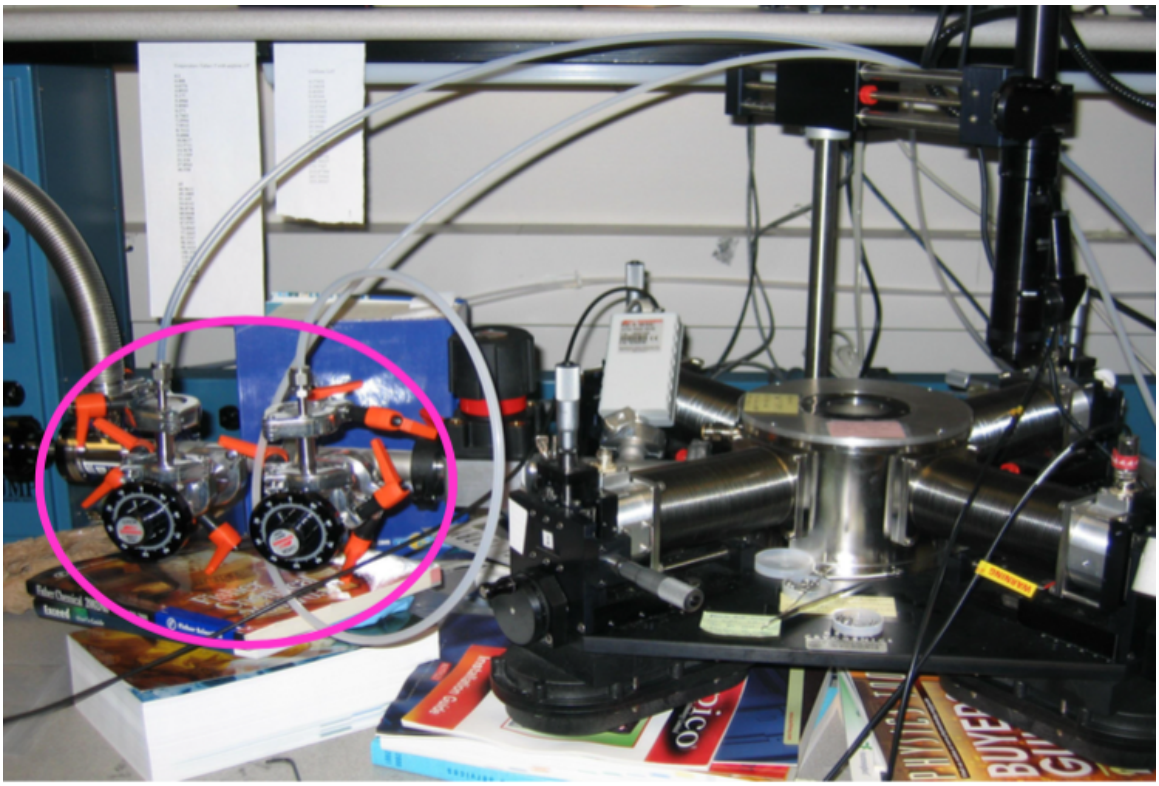

Figure 4.26: The Desert Cryogenics probe station with gas mixing valves (highlighted in pink) as used to test chemical sensitivity. From D. Fine "*Approaches and Evaluation of Architectures for Chemical and Biological Sensing Based on Organic Thin-Film Field-Effect Transistors and Immobilized Ion Channels Integrated with Silicon Solid-State Devices*," Figure 36, p. 74, [68].

Chapter 5: Metal Oxide Thin Film Transistors

As described in Chapter 2, both tin and zinc oxide are electrically sensitive to chemical vapors. Thin film transistors using semiconducting tin and zinc tin oxides were fabricated and tested for sensitivity to organic chemical vapors. Further testing was conducted on tin and zinc tin thin film oxides treated with cavitands in order to increase specificity and responsiveness to organic vapor phase analytes.

5.1 Inorganic Oxide Thin Film Transistors

Inorganic oxides such as SnO_x and ZnO_2 exhibit surface sensing due to chemisorption and surface reduction/oxidation of oxygen states. The surface properties are more important than bulk properties, so most metal oxide sensing research concerns thin films and nanowires [69]. In order to eventually integrate metal oxides into the four-terminal device platform, metal oxide thin film transistors were fabricated. Commercially available metal oxide chemical sensors are not very sensitive and are based on thin films that must be heated. The continual heating consumes a significant amount of power, making these devices inefficient.

SnO_2 Surface

400 A Au / 20A Ti / 500 A SnO_2 / 1325 A SiO_2

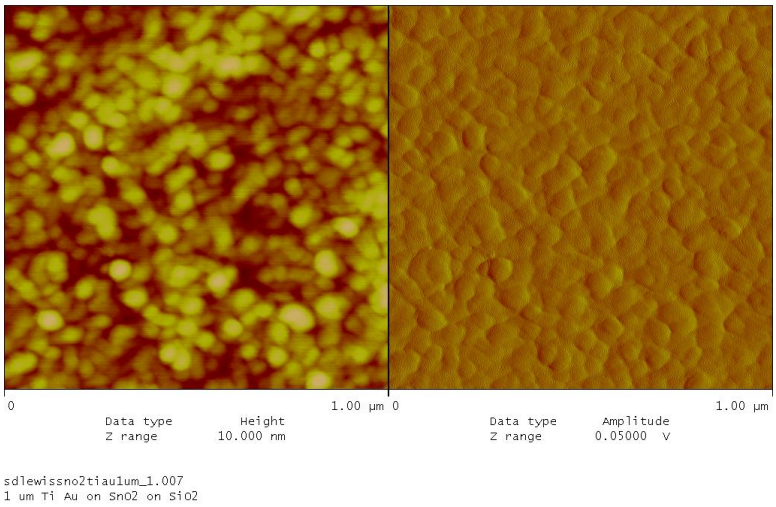

Figure 5.1: Atomic Force Microscopy (AFM) data from SnO_x on SiO_2 TFT device showing the granularity of tin oxide even after annealing. The surface area to bulk volume ratio is high, with many surface states leading to increased sensing sensitivity.

5.2 Tin Oxide Thin Film Transistors

Tin oxide thin film transistors were fabricated as a proof of concept in order to later combine tin oxide into the four-terminal device. The devices were fabricated in-house at the Microelectronics Research Center at the J. J. Pickle Research Campus of the University of Texas at Austin.

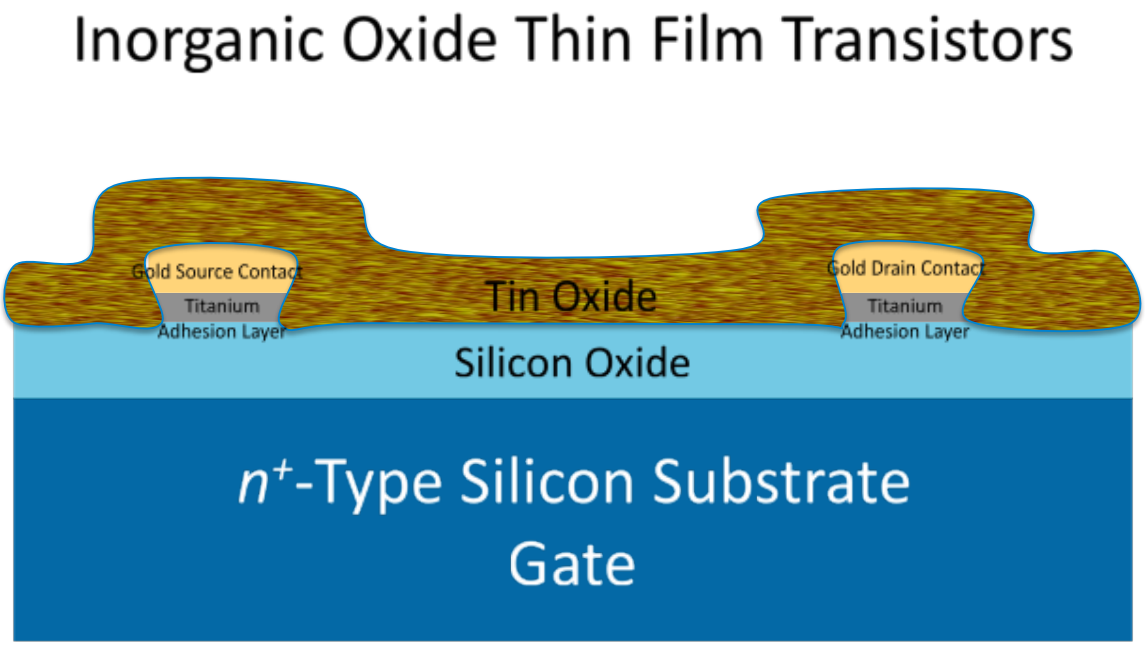

Figure 5.2: Device cross-section for thin film transistor (TFT) with bottom contacts on silicon using SnO_x as the sensing layer.

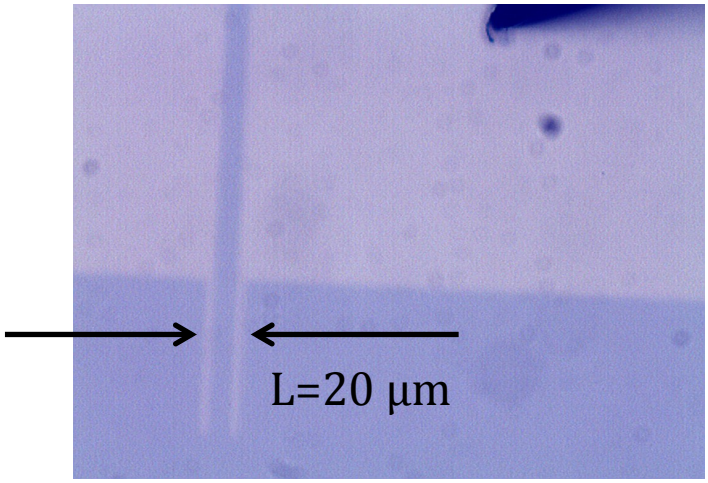

Figure 5.3: Overview of the bottom contacts used to create the SnO_x TFT. The source and drain contacts were created with the same mask used to crease the 4T organic layer bottom contact source and drain. This mask is used with a negative photoresist and image reversal in order to create a smooth sidewall for SnO_x continuity. The channel W/L is 5 and L is 20 µm as marked.

5.2.1 Fabrication

The thin film transistors were fabricated on top of an n^+ doped Si (100) substrate. First 135 nm of SiO_2 was grown in-house via wet oxidation. The substrates were then cleaned of organic contaminates via ultrasonication for five minutes each in acetone, isopropyl alcohol, and de-ionized water. For the bottom contact devices described here, a photolithography mask was used to create gold contacts. The metal contacts were created via image reversal using a negative photoresist in order to create the correct sidewall profile to support a continuous layer of tin oxide. An adhesion layer of 20 **Å** of Ti was followed by 400 **Å** of Au for both source and drain contacts. 50 nm of SnO_x was grown via electron beam deposition on top of the contacts and SiO_2.

5.2.2 Operation

For the SnO_x PFET, the device was tested with the source at ground and with a negative drain voltage. The substrate silicon wafer was gated and stepped from -20 V to 20 V in 5 V increments. The drain current gate current was measured.

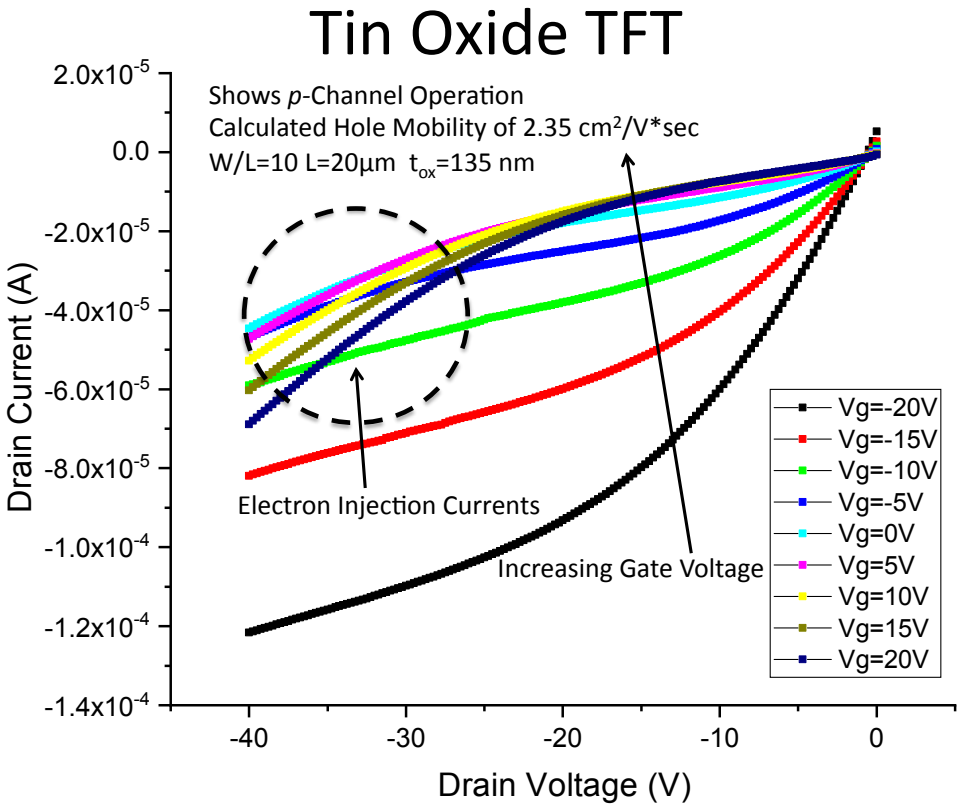

Figure 5.4: Operational characteristics for a SnO_x PFET with W/L=10, L=20µm.

As shown in Figure 5.2, the SnO_x PFET demonstrates some diode like rectifying behavior at the largest negative voltages for positive gate voltages. This indicates that there maybe some *n*-channel activity that is dominating over the expected *p*-type behavior of SnO_x for these bias conditions. This can happen if SnO_x TFTs are ambipolar, as has since been reported by Ogo *et al* [70].

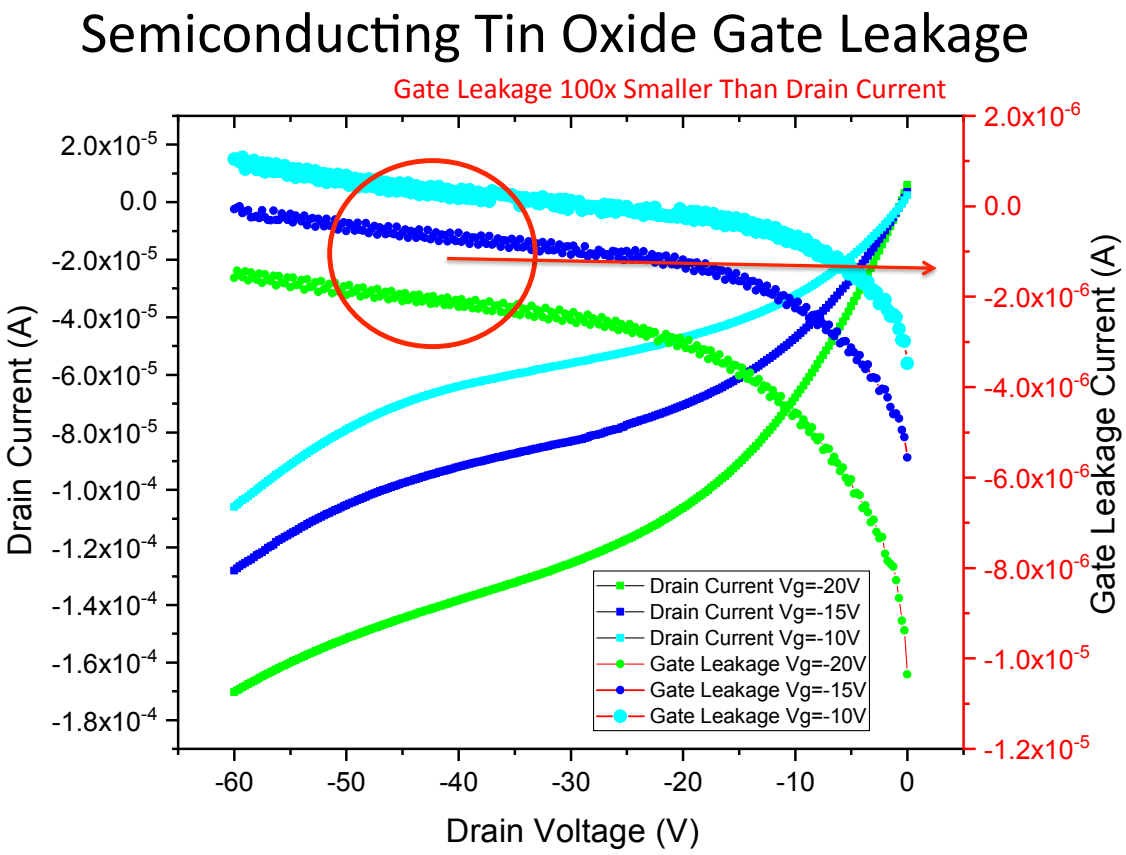

Figure 5.5: Gate leakage current for the same SnO_x PFET is two orders of magnitude smaller than drain current.

As shown in Figure 5.5, the gate leakage current is much smaller than the drain current. The gate current is also at a maximum for the drain voltage of 0 V and decreases as drain voltage gets progressively more negative.

5.2.2.1 Charge Trapping in Ambient

As the SnO_x PFET is operated in atmosphere, without exposure to analyte, the drain current increases in magnitude.

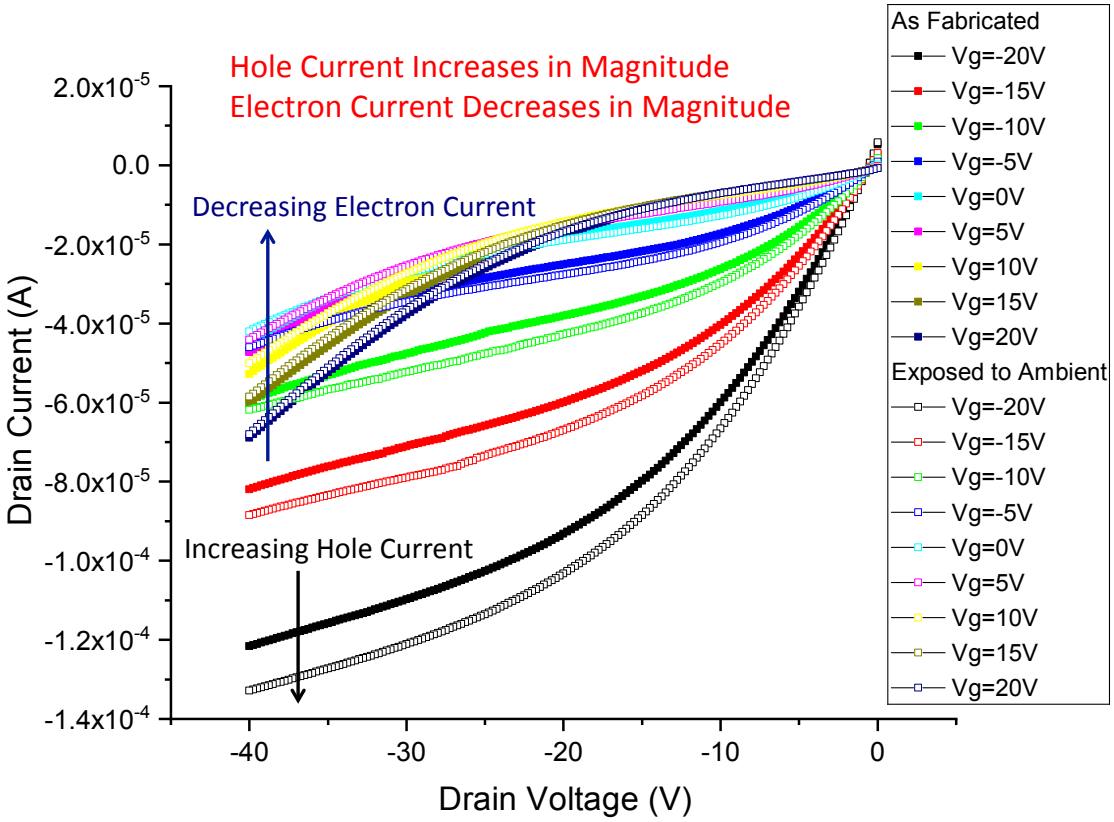

Figure 5.6: The SnO_x PFET experiences an increase in drain current magnitude due to exposure to ambient atmosphere under bias conditions. Empty squares represent output characteristics after exposure to air for the same device from Figures 5.4 and 5.5.

5.2.2.2 Mobility

The mobility for this device was calculated as 2.35 $cm^2/V*sec$. The W/L of 10 applies to the four-terminal device made with this mask. When using the 4T mask as a bottom contact layer for an unpatterned SnO_x TFT, the actual channel width is 755 nm and the channel length is 20 nm, as seen in Figure 5.3. This gives a W/L value of 37.75.

5.2.2.3 Optical Bandgap

One of the reasons SnO_2 is used in thin film transistors is its optical bandgap. SnO has a direct bandgap of ~2.7 eV, but a smaller indirect optical bandgap of ~0.7 eV [70]. The bandgap of rutile crystalline SnO_2 was calculated by Arlinghaus [71] to be 3.68 eV for polarized light perpendicular to the tetragonal axis and 4.07 eV for light polarized parallel to the tetragonal axis. The measured bandgaps of SnO_2 are between 3.57 eV and 3.93 eV. When tested for optical absorbance, the as-grown SnO_x on a prepared glass slide had a transmission cutoff of 300 nm and a corresponding photon energy cutoff of 4.1 eV. This indicates that the stoichiometry of the as-grown tin oxide films is much closer to that of stannic oxide SnO_2.

The tin oxide TFTs were not very reproducible because they depended highly on the dopants present in the e-beam chamber and deposition conditions. For this reason, more TFTs were fabricated using zinc oxide for subsequent sensing experiments.

5.3 ZINC TIN OXIDE THIN FILM TRANSISTORS

Semiconducting zinc tin oxide was also used to create thin film transistors for chemical vapor sensing. Zinc tin oxide is reactive to oxidation from gaseous phase reagents. The devices were fabricated in-house at the Microelectronics Research Center at the J. J. Pickle Research Campus of the University of Texas at Austin.

5.3.1 Fabrication

The thin film transistors were fabricated on top of an n^+ doped Si (100) substrate. First 135 nm of SiO_2 was grown in house via wet oxidation. The substrates were then cleaned of organic contaminates via ultrasonification for 5 minutes each in acetone, isopropyl alcohol, and de-ionized water. For the bottom contact devices described here, a photolithography mask was used to create gold contacts. An adhesion layer of 20 **Å** of Ti

was followed by 400 **Å** of Au for both source and drain contacts. The source and drain contacts were identical to those used for tin oxide and are shown in Figure 5.3.

Zinc tin oxide (ZTO) was deposited directly on top of the metal contacts via a sol-gel based solution process. The precursor solution was prepared by dissolving zinc chloride ($ZnCl_2$) and tin chloride ($SnCl_2$) powders in acetonitrile (CH_3CN). The concentration of the precursor solution is 0.24 M with a 1:1 molar ratio of $ZnCl_2$ to $SnCl_2$. This precursor solution was then filtered through a 0.2 μm pore size polytetrafluoroethylene (PTFE) filter and spin-coated onto the substrate at 6000 rpm for 1 minute in a nitrogen atmosphere. The ZTO precursor film was then converted to ZTO by annealing at 500° C for one hour in air.

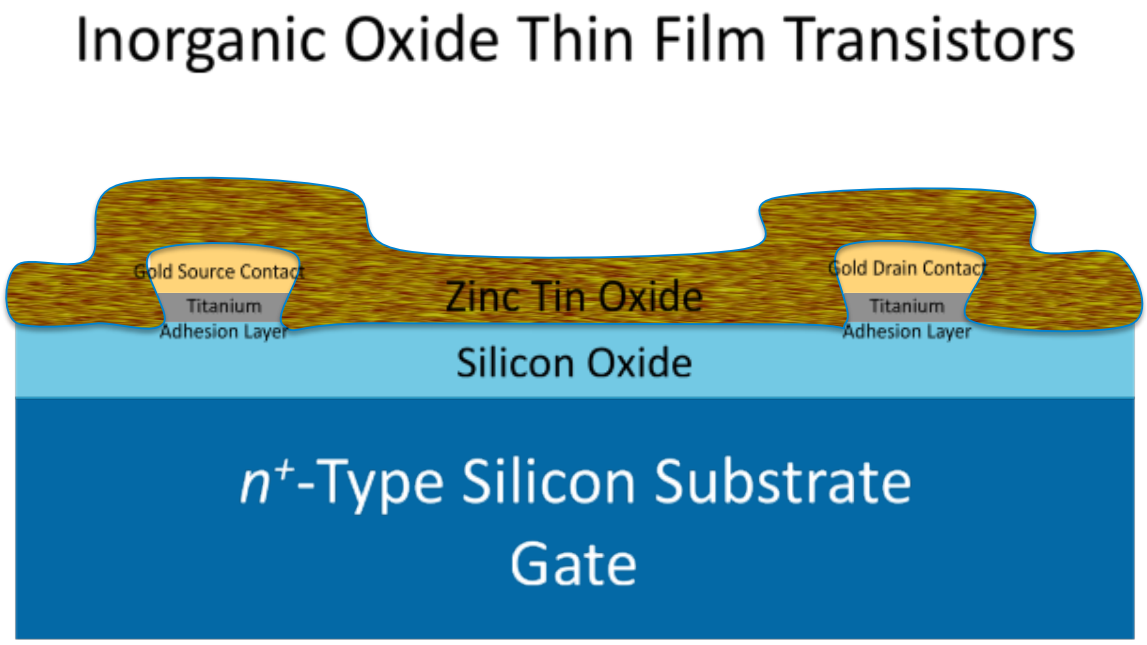

Figure 5.7: Device cross-section for a bottom-contact TFT on a silicon gate substrate using ZTO as the sensing layer.

5.3.2 Operation

As grown, the zinc tin oxide displays *n*-type transport characteristics. The saturation region is flat and well defined when $V_{DS} > V_G$. The linear region exists when $V_G < 0.5*V_{SD}$. The device shows no diode-like behavior—only regular field-effect transistor behavior with well-defined linear and saturation regions. The threshold voltage for this device is 2 V, and the mobility is calculated using $I_{D, sat}$ as 1.14 $cm^2/V*sec$.

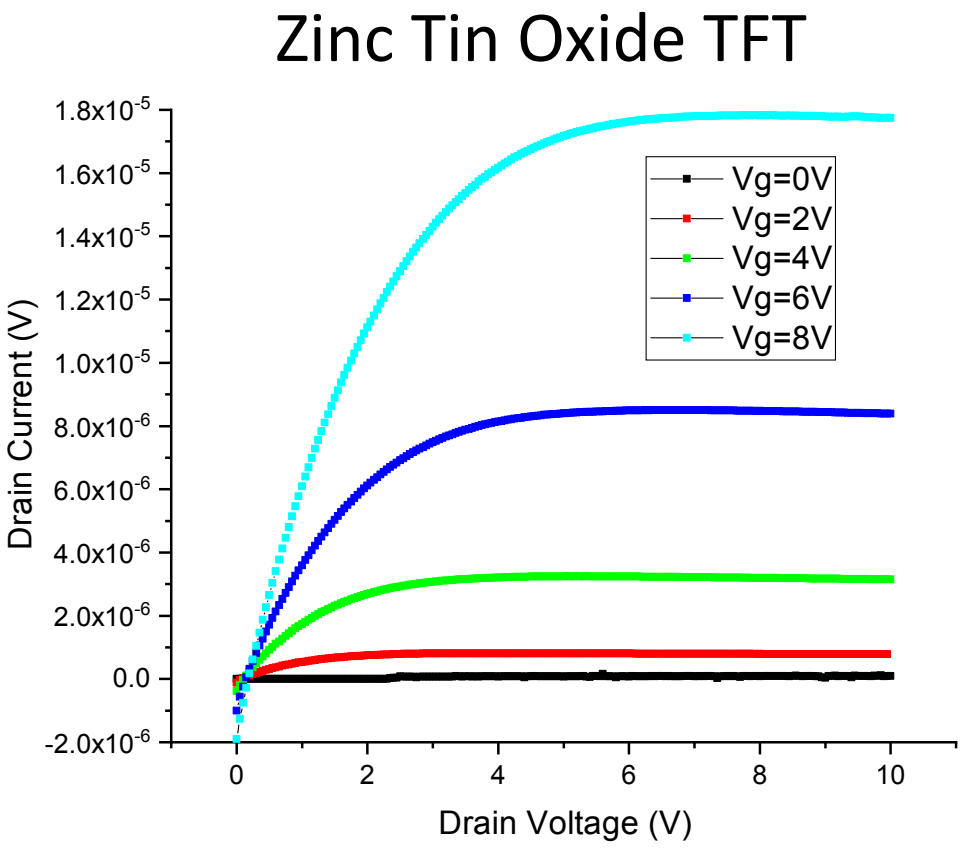

Figure 5.8: Operational characteristics for a ZTO *n*-type TFT in air.

5.3.3 Testing

A peristaltic pump was used to deliver saturated vapor. First a 20 μm pore size filter paper was soaked in the desired liquid. Then the wetted paper was placed into an angled syringe. Finally, nitrogen gas was pushed through the paper, creating an analyte vapor. The syringe itself was aimed towards the channel of the device being tested. Because the channels of the TFT device are so large, they are easy to visually identify.

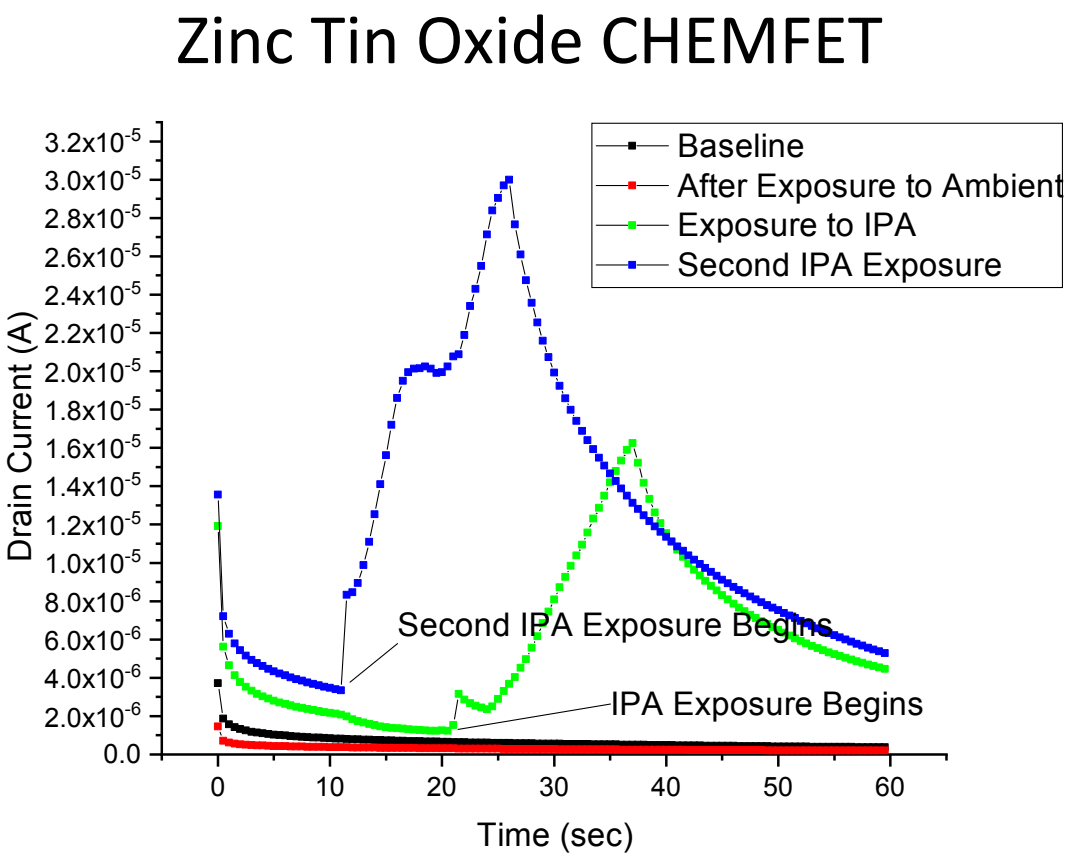

Figure 5.9: ZTO TFT drain current as fabricated, then after exposure to ambient atmosphere, followed by 2 exposures to isopropyl alcohol via peristaltic pump. Ambient charge trapping decreases drain current, while exposure to IPA increases it.

The zinc tin oxide TFT displays an increase in drain current while isopropyl alcohol is being delivered, and then a monotonic decrease in drain current after the sensing event ends. The drain current trends towards the previous baseline but does not return all the way to the pre-sensing level.

The increase in drain current indicates that the analyte increases the amount of charge carriers in the zinc tin oxide sensing layer.

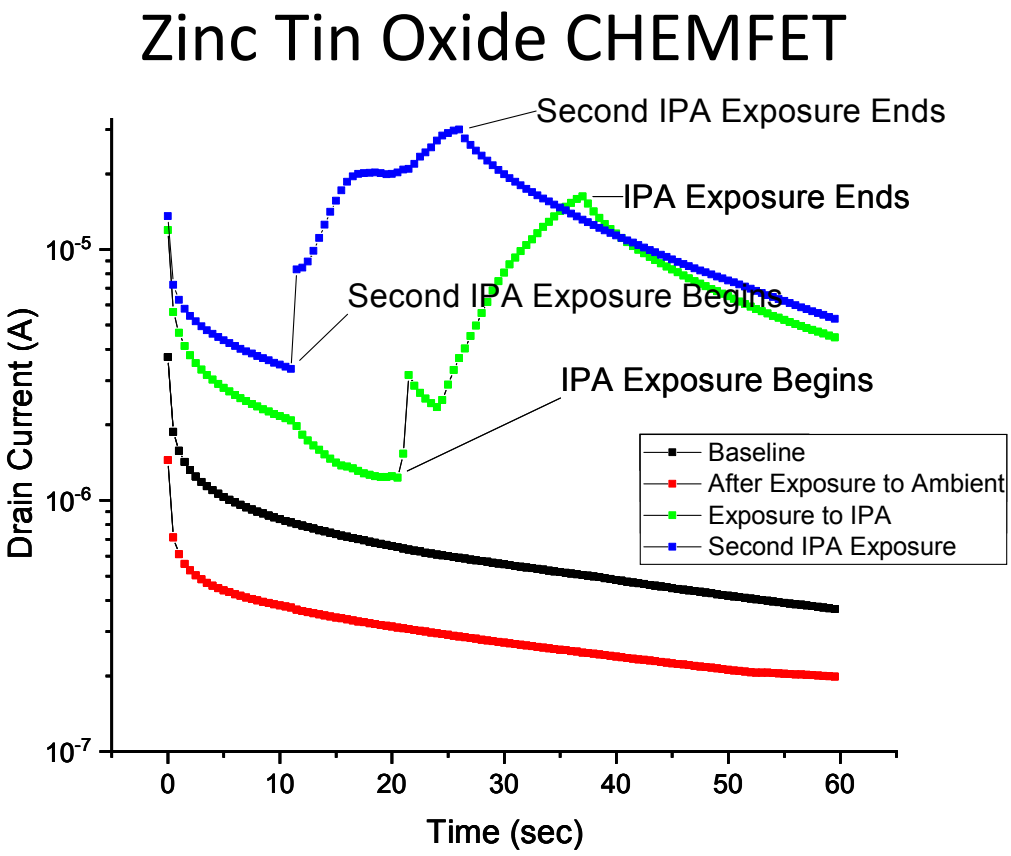

Figure 5.10: ZTO TFT drain current as exposed to air and isopropyl alcohol on a semi-logarithmic scale. The change in baseline is due to charge trapping in ambient atmosphere.

All devices tested displayed a bias stress effect decrease in drain current in atmosphere. This indicates that operation of the device in atmosphere causes a decrease in the charge carrier mobility. This is due to the trapping of organic analytes in the sensing layer, which then function as charge scattering centers. Furthermore, the continued oxidation of the zinc tin oxide thin film when under an electric field in ambient may lead to a decrease in the available charge carriers.

5.4 Functionalized Zinc Tin Oxide Thin Film Transistors

Inorganic metal oxides are most electrically responsive to oxidizing and reducing analytes. Their oxidation states are well-characterized—stannic oxide (tin([V] oxide), stannous oxide (tin[II] oxide), and zinc oxide. In order to increase the specificity of these inorganic metal oxides, small molecule organic receptors were used. These receptors can be added from solution after all high temperature processing is complete, without affecting the underlying TFT chemistry.

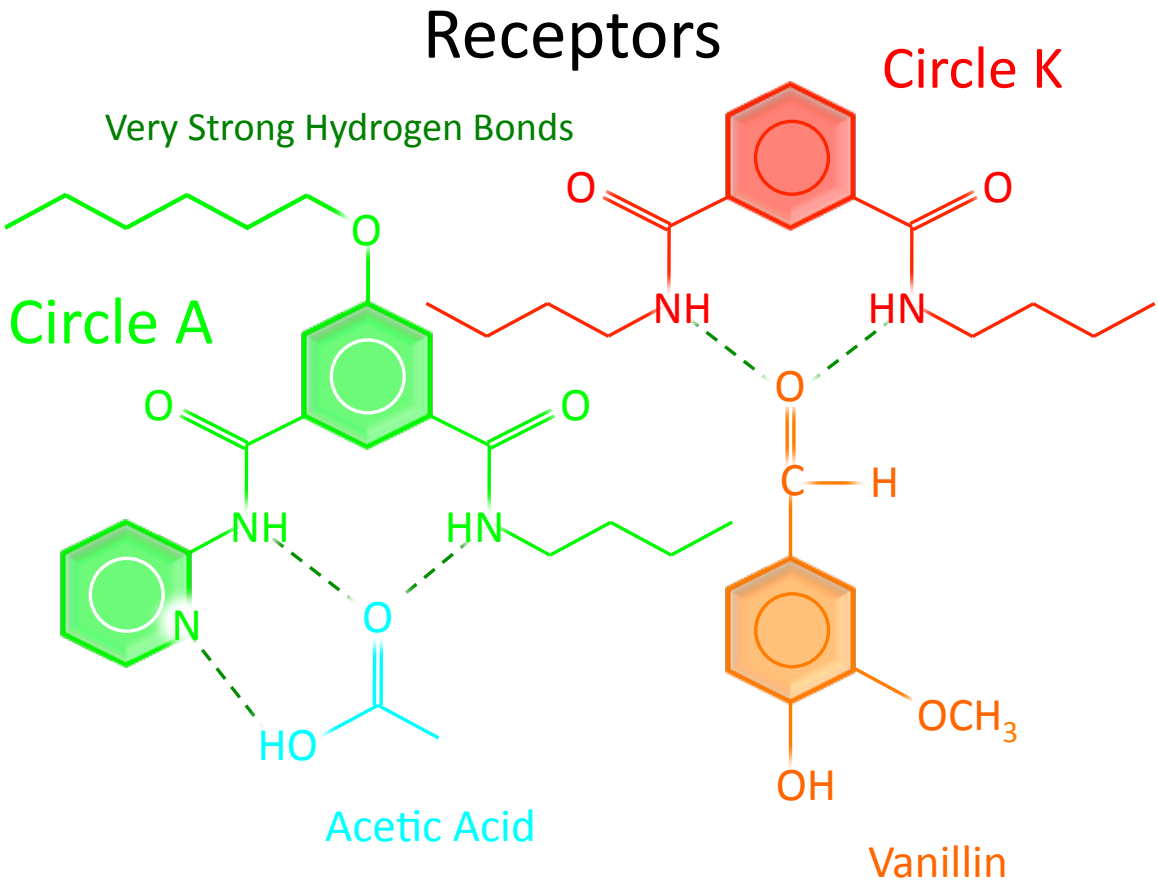

Figure 5.11: The molecular structure of the small molecule organic receptors used to functionalize ZTO. Both Circle A and Circle K interact strongly with organic dipoles through hydrogen bonding.

5.4.1 Fabrication

The deposition of the small molecule receptors was accomplished from solution via spin-coating. The Circle A is dissolved in chloroform and is deposited directly on top of the zinc tin oxide semiconductor TFTs which were fabricated as described previously in section 5.3.1.

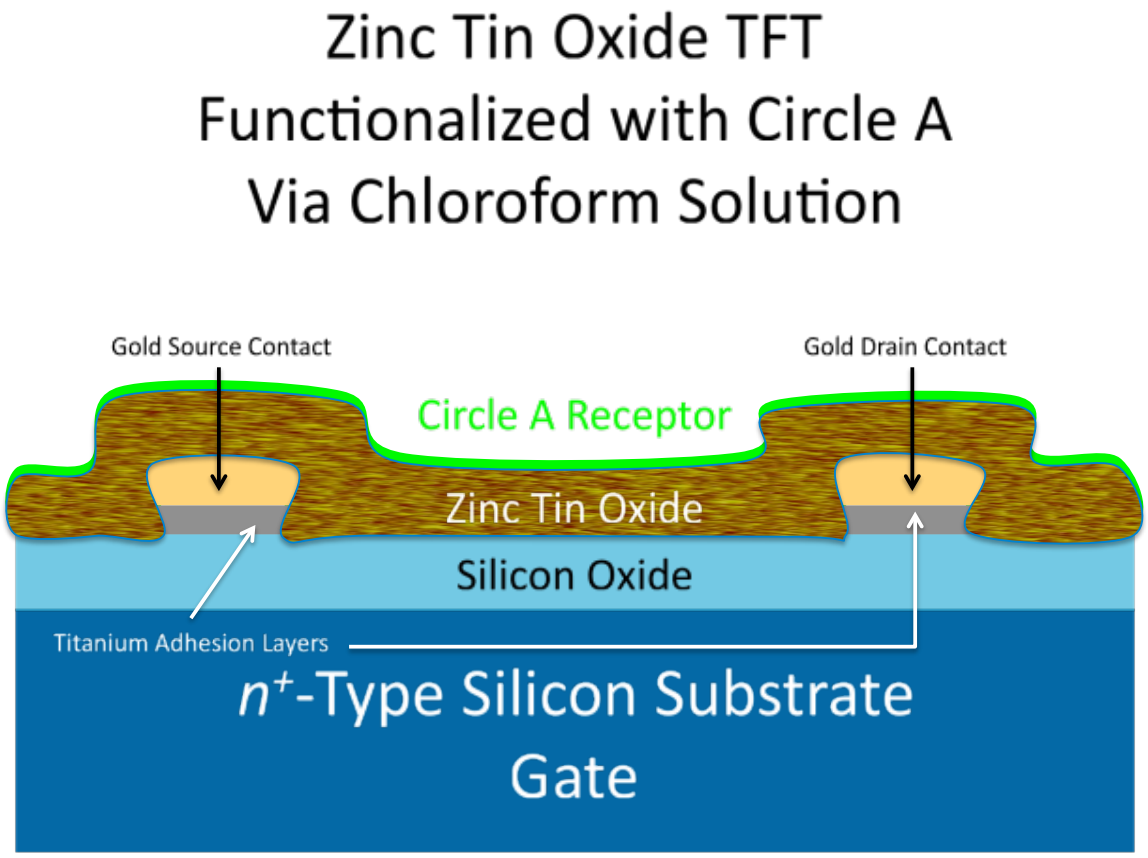

Figure 5.12: The cross-section of a zinc tin oxide TFT with Circle A functionalization.

5.4.2 Operation

The addition of a receptor to the zinc tin oxide TFT has minimal effect on the electrical characteristics. The receptor layer is physically separate from the semiconductor layer. The zinc tin oxide layer is granular, and the Circle A layer is spin-coated on its rough surface. The circle A layer is probably not continuous, and it does not isolate the zinc tin oxide from the analyte.

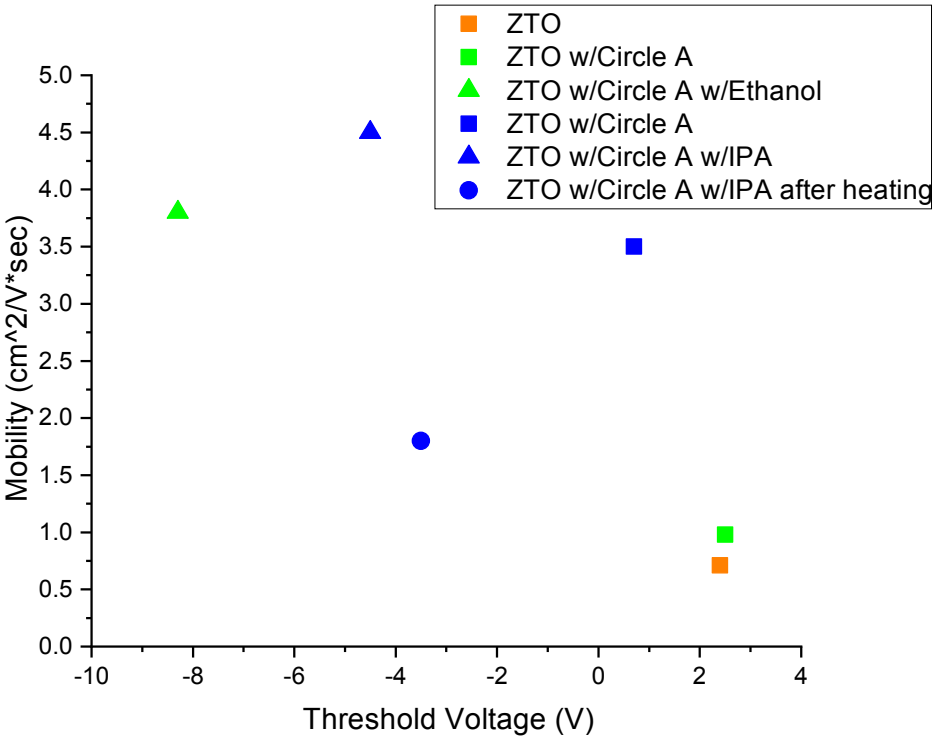

Figure 5.13: Comparison threshold voltage and mobility for ZTO FETs with and without Circle A before and after exposure to various analytes. The devices and colors correspond to those in Table 6.1.

For the zinc tin oxide TFTs with Circle A that were fabricated, the threshold voltage was positive but close to zero. The electron mobility was calculated as $1.1*10^{-3}$ $cm^2/V*sec$, with a threshold voltage of 0.8 V. The saturation region displays a slight linear increase with drain voltage.

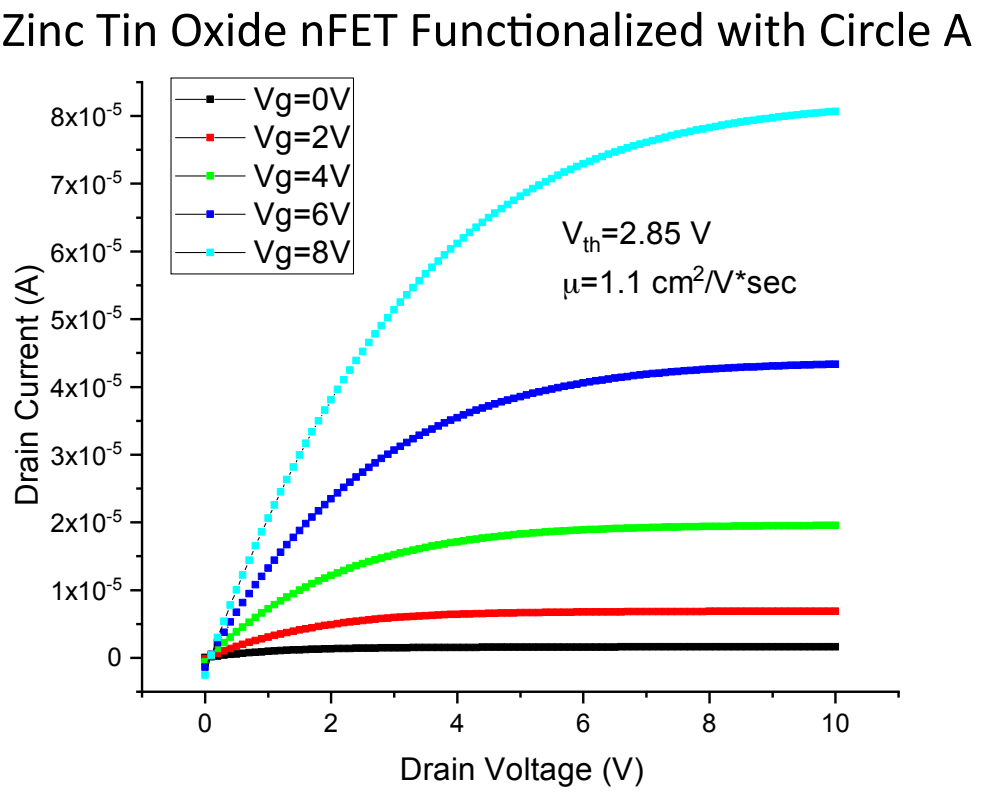

Figure 5.14: The operational characteristics for a ZTO nFET coated with Circle A from solution.

The application of Circle A to ZTO changes the threshold voltage and mobility characteristics of the *n*FET. The changes are described in the following table.

Semiconductor	Receptor	Analyte	Threshold Voltage (V)	Mobility ($cm^2/V*sec$)
ZTO	None	None	2.4	0.71
ZTO	Circle A	None	2.5	0.98
ZTO	Circle A	Ethanol	-8.3	3.8
ZTO	Circle A	None	0.7	3.5
ZTO	Circle A	IPA	-4.5	4.5
ZTO	Circle A	Heated After IPA	-3.5	1.8

Table 5.1: Table displaying the various measured threshold voltages and mobilities calculated for Circle A on ZTO devices. The yellow device is ZTO without Circle A. The green device is ZTO coated with Circle A exposed to ethanol. The blue device is ZTO coated with Circle A exposed to isopropanol.

5.4.3 Testing

The testing for zinc tin oxide with Circle A was identical to that of zinc tin oxide without any functionalization. A peristaltic pump was used to deliver saturated vapor. First a 20 μm pore size filter paper was soaked in the desired liquid. Then the wetted paper was placed into an angled syringe. Finally, nitrogen gas was pushed through the paper, creating an analyte vapor. The syringe itself was aimed towards the channel of the device being tested. Because the channels of the TFT device are so large, they are easy to visually identify.

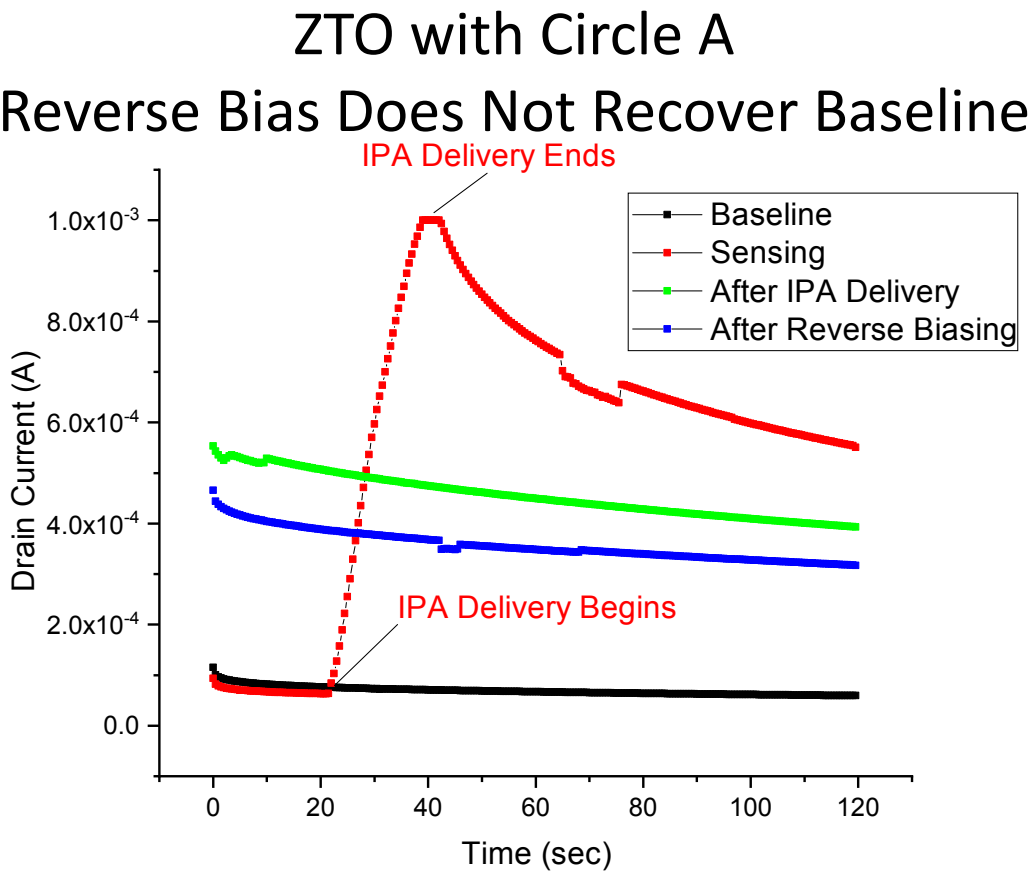

Figure 5.15: The sensing response of a zinc tin oxide TFT coated with Circle A to isopropyl alcohol. The drain voltage does not return to the pre-sensing baseline even with reverse biasing. V_{DS} of 10 V and V_G of 8 V.

One peculiarity of zinc tin oxide with Circle A TFTs is that they are not de-trapped by reverse biasing. The other device studied in this work experiences desorption of trapped charges when the gate is reverse biased. The activation energy of the hydrogen bonding between Circle A and isopropyl alcohol is so great that the isopropyl alcohol remains adsorped to the surface unless heated.

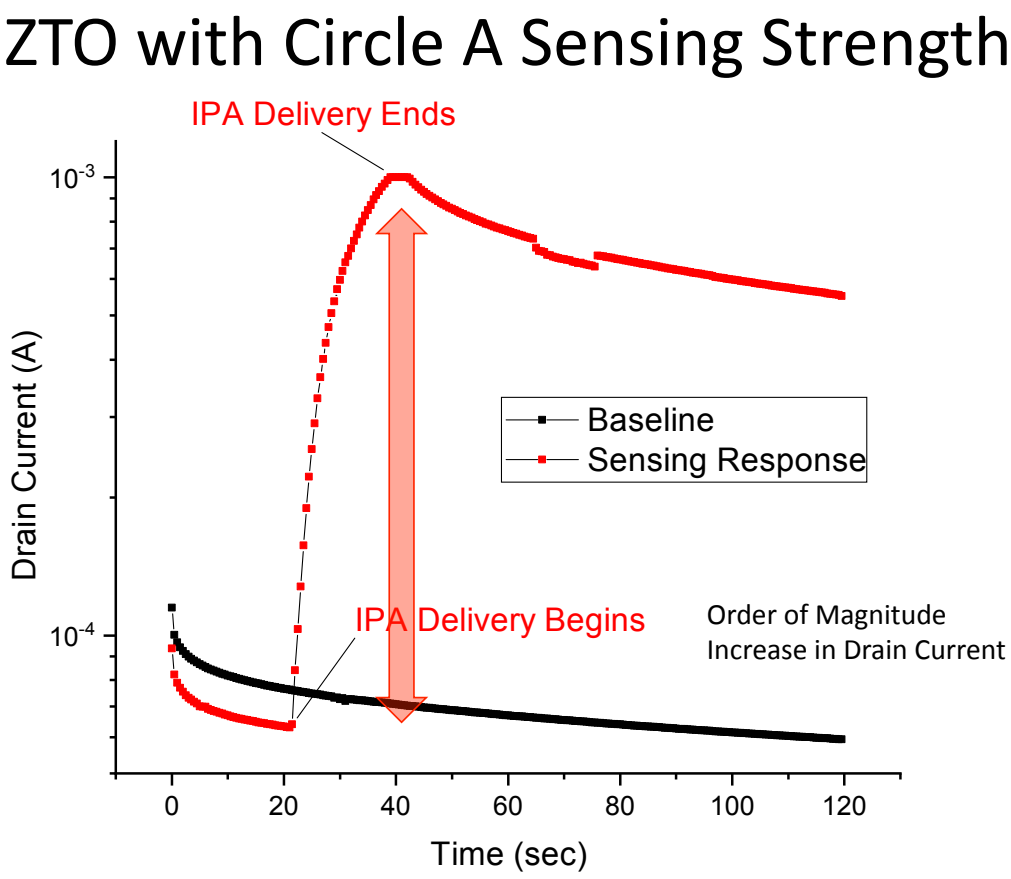

Figure 5.16: The sensing response of a zinc tin oxide TFT coated with Circle A to isopropyl alcohol is an order of magnitude increase in the drain current.

The increase in drain current upon exposure to isopropyl alcohol is about an order of magnitude. That is larger than the corresponding increase in drain current without Circle A.

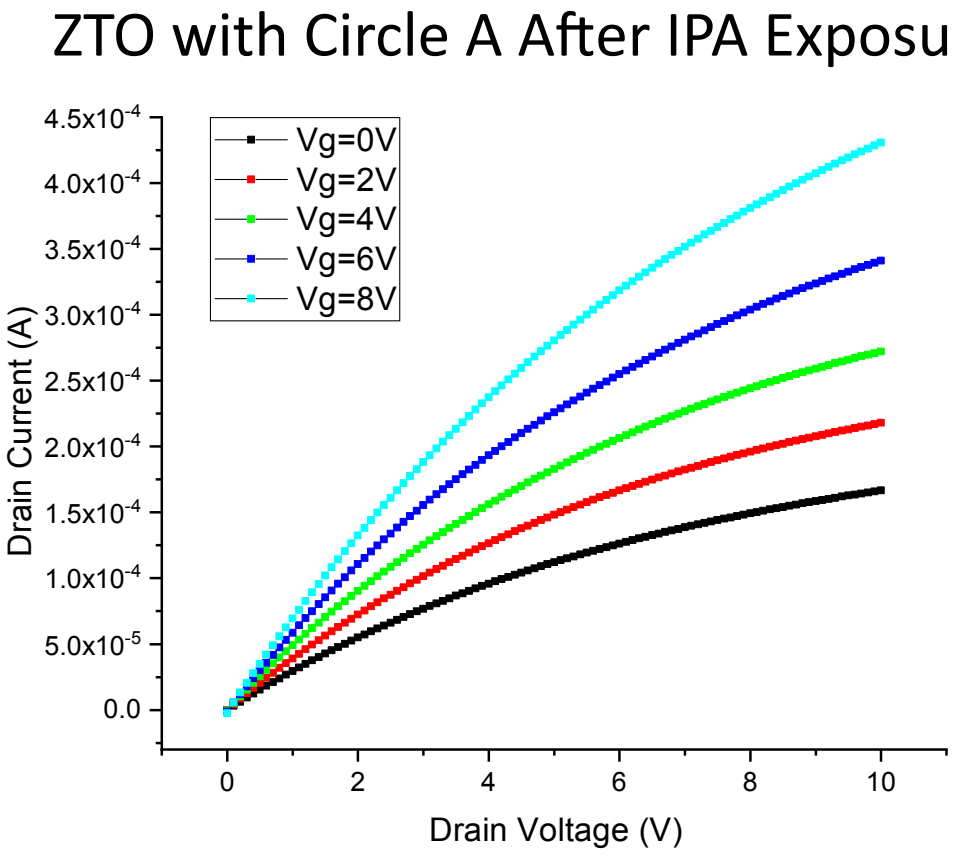

Figure 5.17: The output characteristics of a zinc tin oxide nFET with Circle A after exposure to isopropyl alcohol.

After exposure to isopropyl alcohol, the zinc tin oxide TFT was a calculated threshold voltage of 4.3 V. Before the exposure, the threshold voltage is calculated as 0.8 V. The change in threshold voltage is due to charges that are permanently trapped in the Circle A layer and therefore held close to the zinc tin oxide sensing layer. These trapped charges shift the threshold voltage upwards.

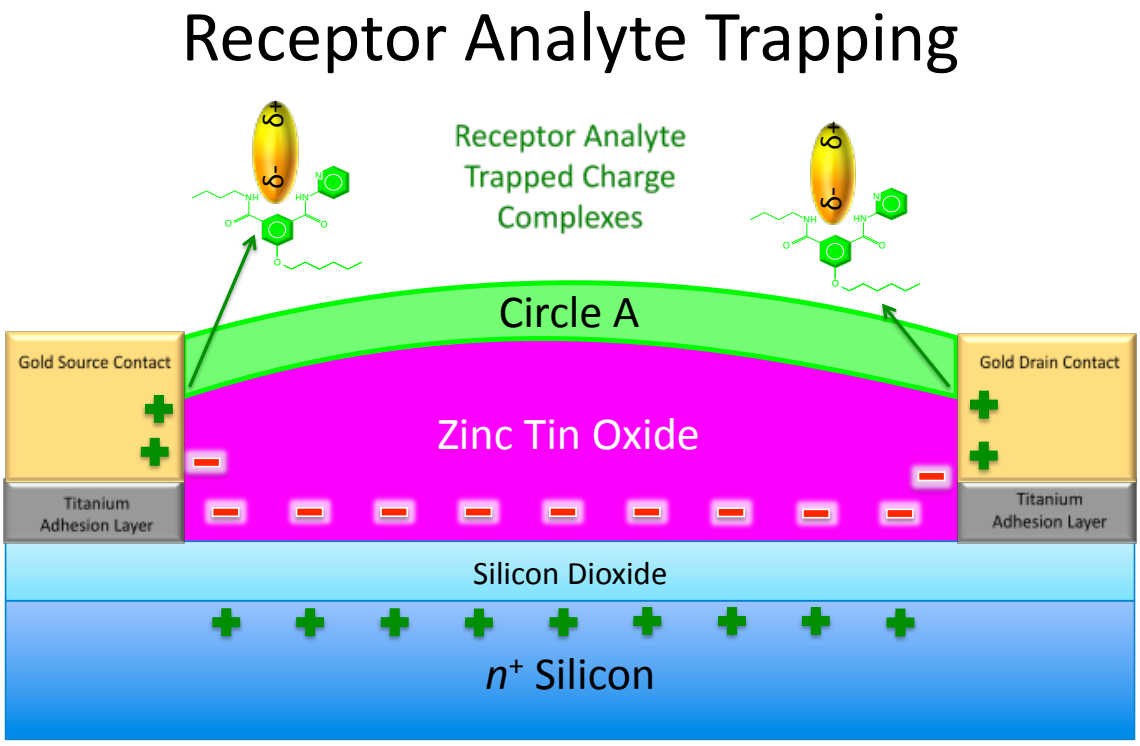

Figure 5.18: Analyte trapping in zinc tin oxide with Circle A. The Circle A receptors bind strongly with the analyte dipole molecules, trapping them at interface with the ZTO layer. Both Circle A and the analyte have a dipole moment that contributes to the dipole mediation of the Schottky charge injection barrier.

The pre-exposure electron mobility was calculated as $1.8*10^{-3}$ $m^2/V*sec$. The mobility after exposure to isopropyl alcohol increases to $2.2*10^{-3}$ $m^2/V*sec$. The increase in mobility can only occur if all the trapped charges that affect the threshold voltage do not also act as charge scattering centers. This means that the trapped charges are located in the Circle A receptor layer, not in the zinc tin oxide thin film.

5.4.3.1 Alternative to Reverse Biasing

Because reverse biasing does not reset the device when Circle A is involved, another method of refreshing the sensor was necessary. It was discovered that heating

the device in a vacuum drives out the trapped charges without destroying the Circle A functionalization. Circle A is a small molecule organic, and it is stable at room temperature, up to body temperature. For this reason, 310 K was used.

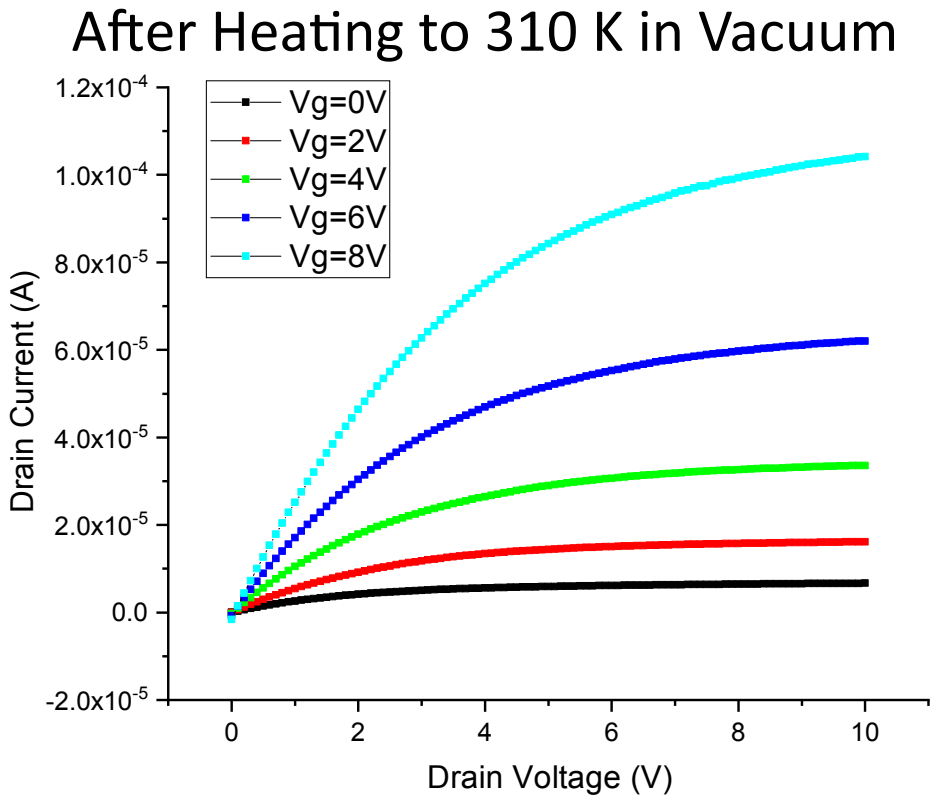

Figure 5.19: The output characteristics of a zinc tin oxide nFET with Circle A after heating to 310 K in vacuum.

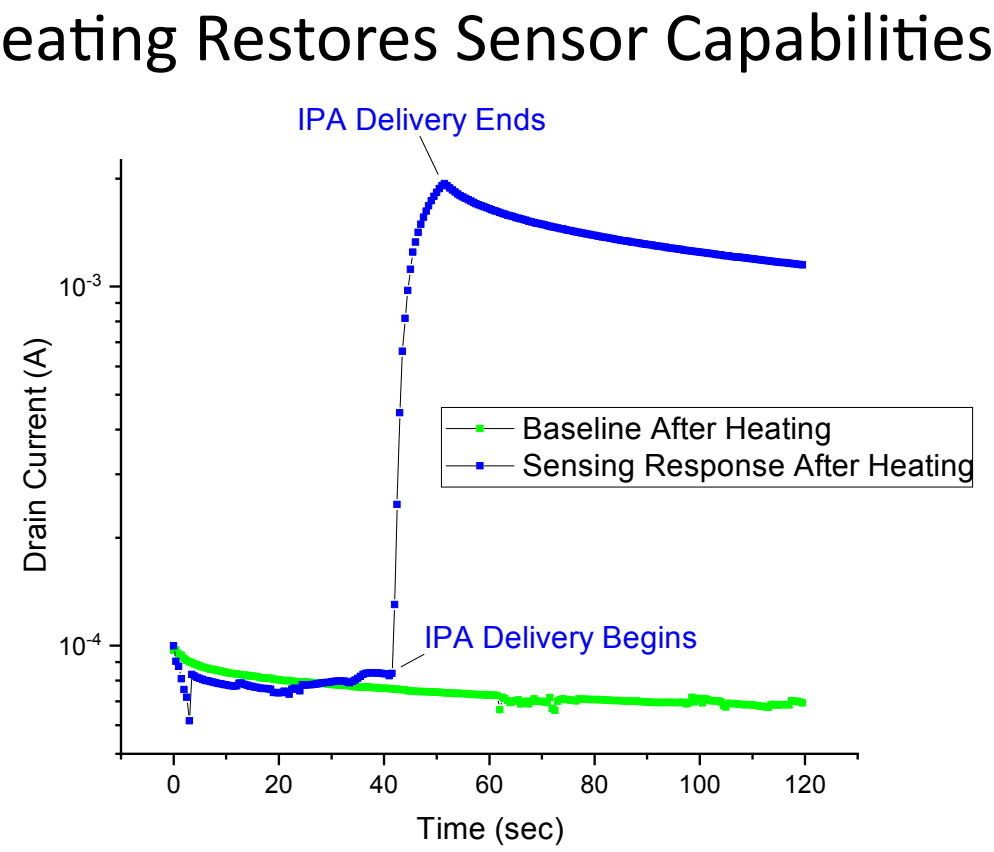

Figure 5.20: Heating the zinc tin oxide TFT with Circle A restores the sensing ability of the TFT. The increase in drain current upon exposure to isopropyl alcohol is over one order of magnitude.

The heating successfully restores sensor capability but contributes to a major threshold voltage shift. After heating, the threshold voltage was calculated at -2.6 V. This threshold voltage shift must be due to changes in the zinc tin oxide itself. The Circle A is not affected enough by the heating to change its sensing mechanism. The zinc tin oxide may experience oxidation or annealing under this heating regime. It is also possible that the threshold voltage shift results from gate leakage due to degradation of

the metal contacts. The gate oxide, silicon dioxide, should be stable at and above much higher temperatures than those used here.

5.5 Transport in Tin Oxide

Tin oxide is a *p*-type semiconductor under most circumstances, while zinc tin oxide is an *n*-type semiconductor. The diode-like behavior of the tin oxide TFTs at high source-drain voltages indicates that there is at least some specious *n*-type transport occurring.

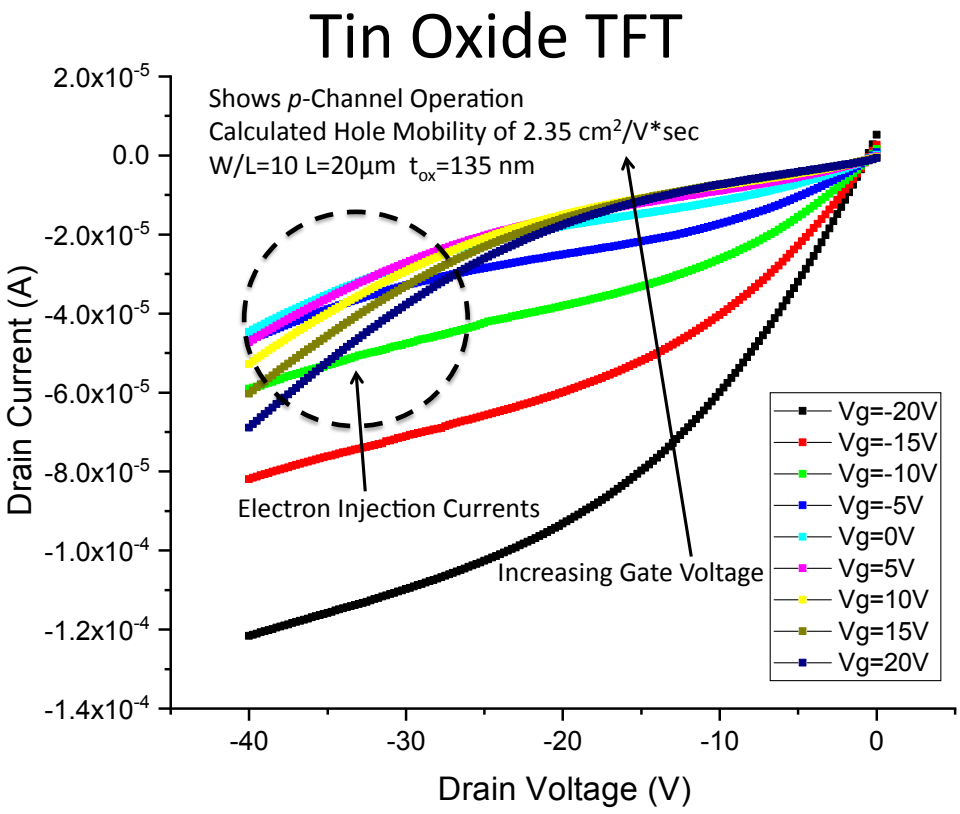

Figure 5.21: Tin oxide TFT pFET output characteristics showing ambipolar transport.

The nFET output characteristics show triode-like behavior with no saturation region. This means that the nFET region shows no inversion region, which is consistent with SnO_x being a hole transporting material.

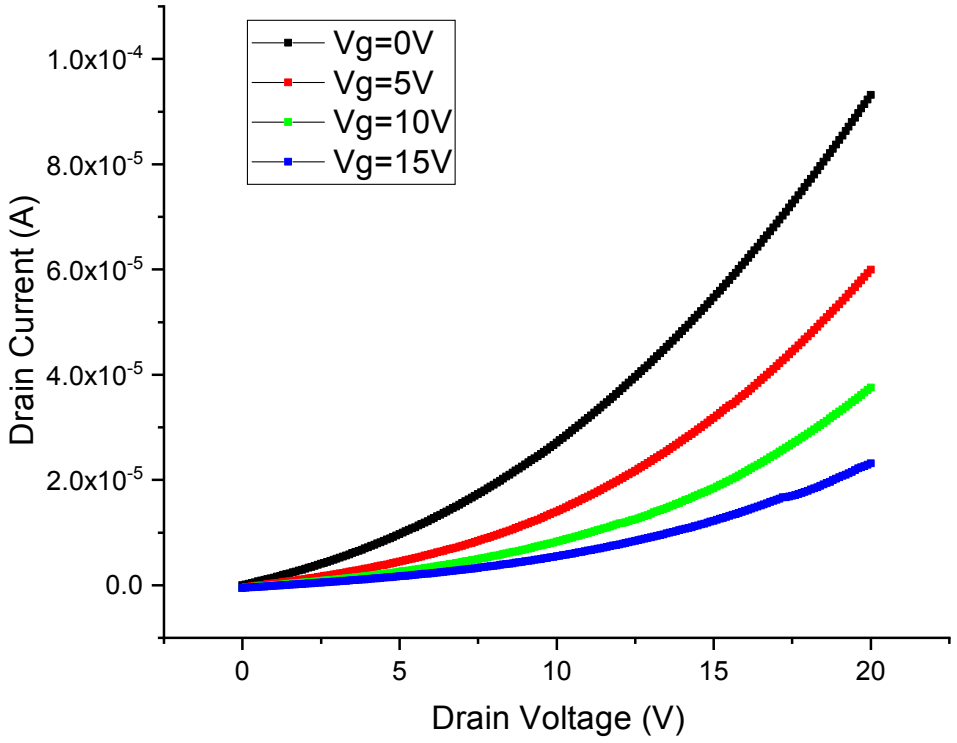

Figure 5.22: Tin oxide TFT showing its nFET output characteristics.

When plotted together, the nFET and pFET output characteristics show some minor evidence of ambipolar behavior. Even in the pFET saturation region, there is a strong increase in drain current with increasing drain voltage indicating a resistive element in the device. The field effect behavior is much stronger for hole transport.

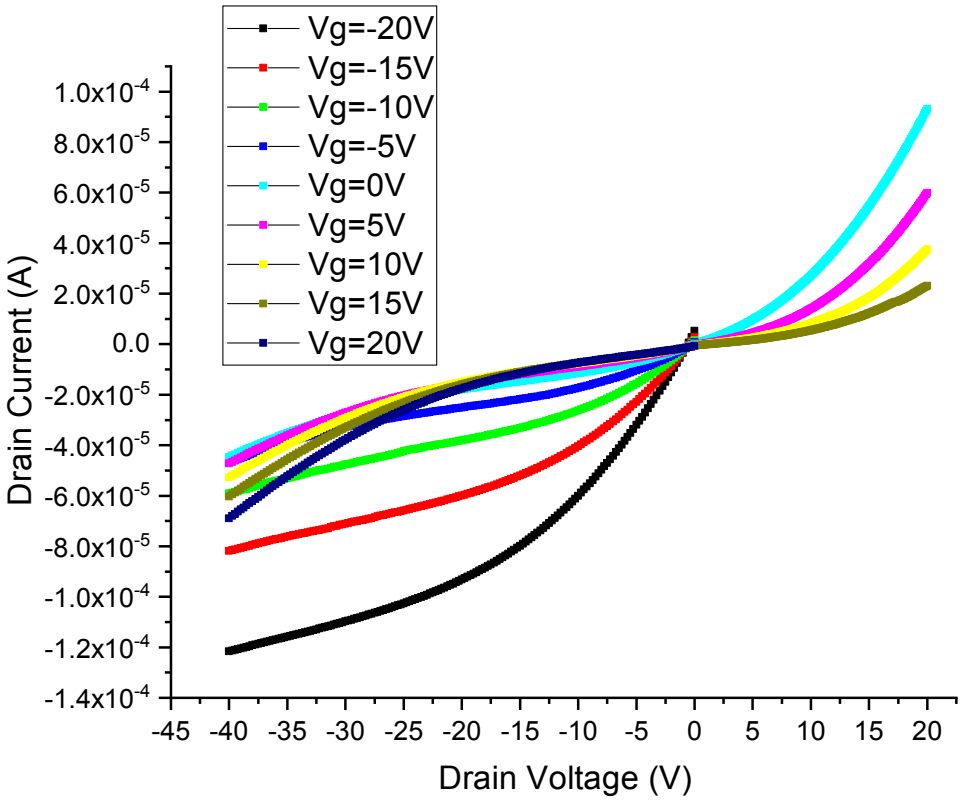

Figure 5.23: Tin oxide TFT output characteristics for both hole and electron transporting regions with $-20V<V_{ds}<20V$.

5.5.1 Orbital Structure

Most inorganic oxide semiconductors are electron-transporting materials, while semiconducting tin oxide is *p*-type with relatively high hole mobility. Tin oxide can transport holes because of the structure of the orbitals contributing to the valence band maximum. In most inorganic oxides, the valence band is made up of the oxygen 2*p* orbitals that have a low overlap, even in crystalline metal oxides as shown in Figure 5.25. Hole transport is therefore restricted to hopping mode with no bandlike transport, which is necessarily low-mobility.

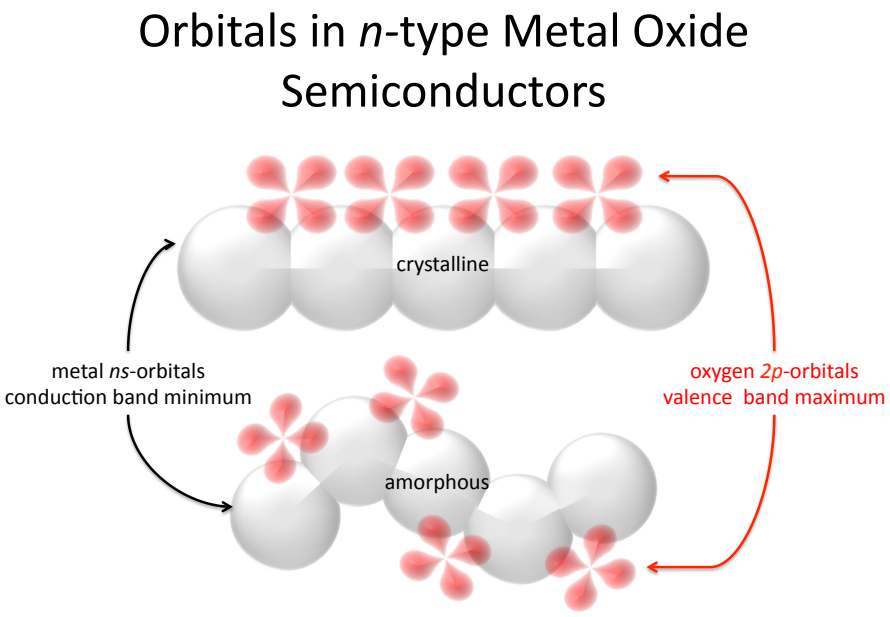

Figure 5.24: The conduction band minimum (CBM) and valence band maximum (VBM) in an *n*-type metal oxide semiconductor.

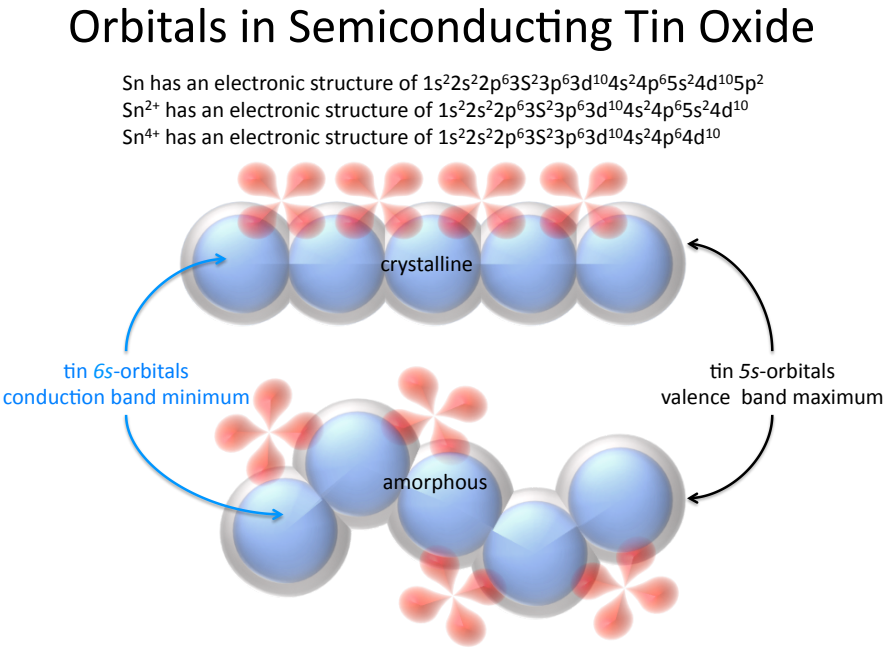

Figure 5.25: The conduction band minimum (CBM) and valence band maximum (VBM) in *p*-type semiconducting tin oxide.

For tin oxide, the valence band is made up of the 5*s* orbitals of Sn^{2+} that are spherically symmetrical [72]. These metal *s* orbitals also have large overlaps whether the metal oxide is crystalline or not as shown in Figure 5.26. Tin oxide forms a PbO-type layered crystalline structure, but for thin films (even after annealing), disordered and strained crystal structures and interfaces dominate over ordered crystalline structure.

5.5.2 Bandgaps in Tin Oxide

The bandgap for tin(II) oxide is composed of a large direct bandgap of 2.7 eV and an indirect bandgap of 0.7 eV, as reported by Ogo *et al* [70].

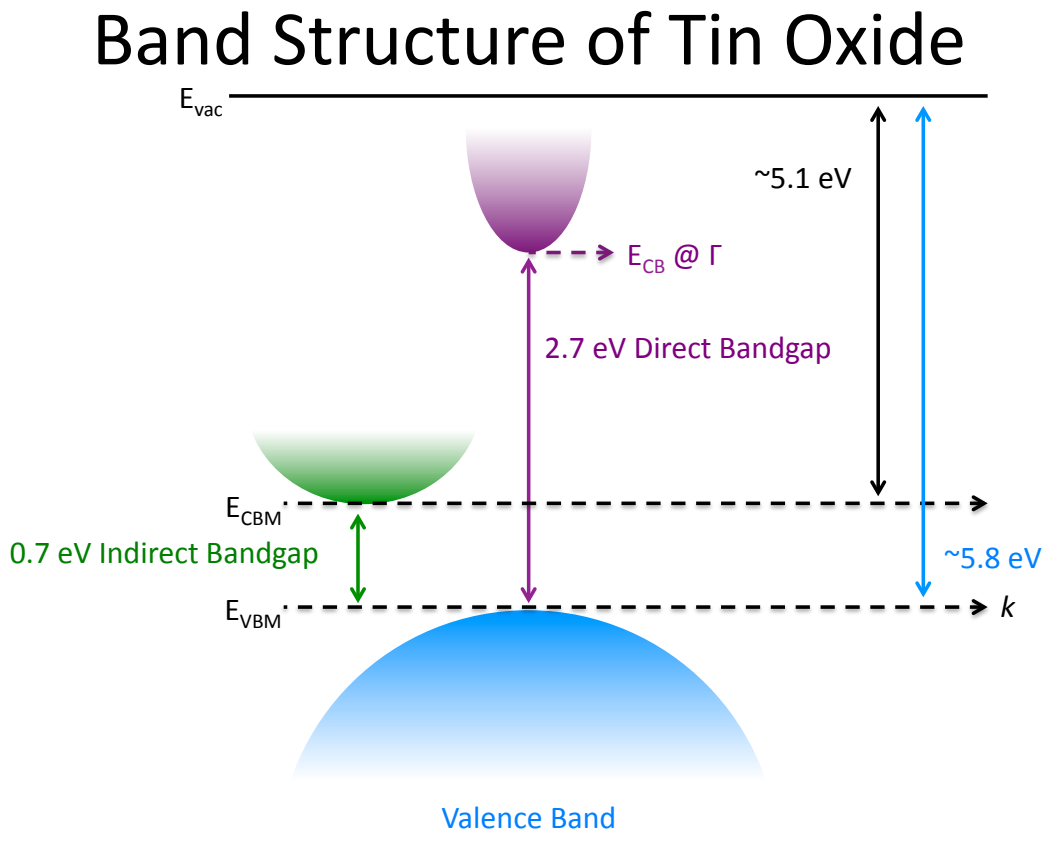

Figure 5.26: The band structure of tin monoxide, showing the direct bandgap of 2.7 eV and the indirect bandgap of 0.7 eV.

However, the as-grown tin oxide from this work demonstrated a different bandgap. Using absorbance spectra for tin oxide grown on glass, the bandgap can be calculated. The absorbance was measured using a Cary 5000UV-VIS NIR and is shown in the figures below.

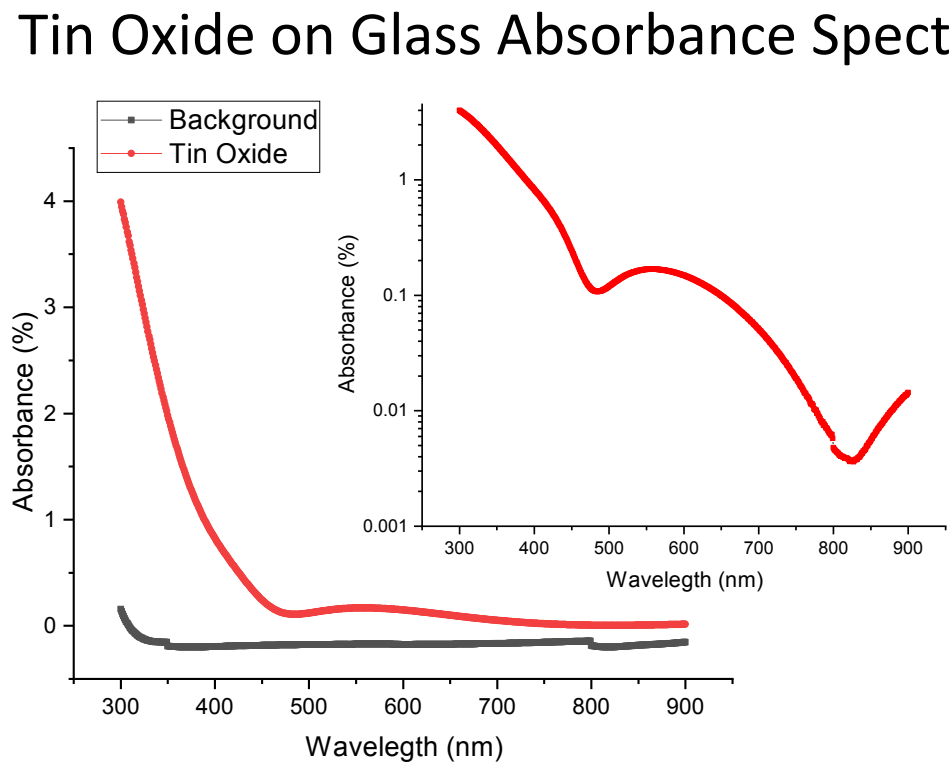

Figure 5.27: Absorbance spectra of tin oxide on glass as a function of wavelength.

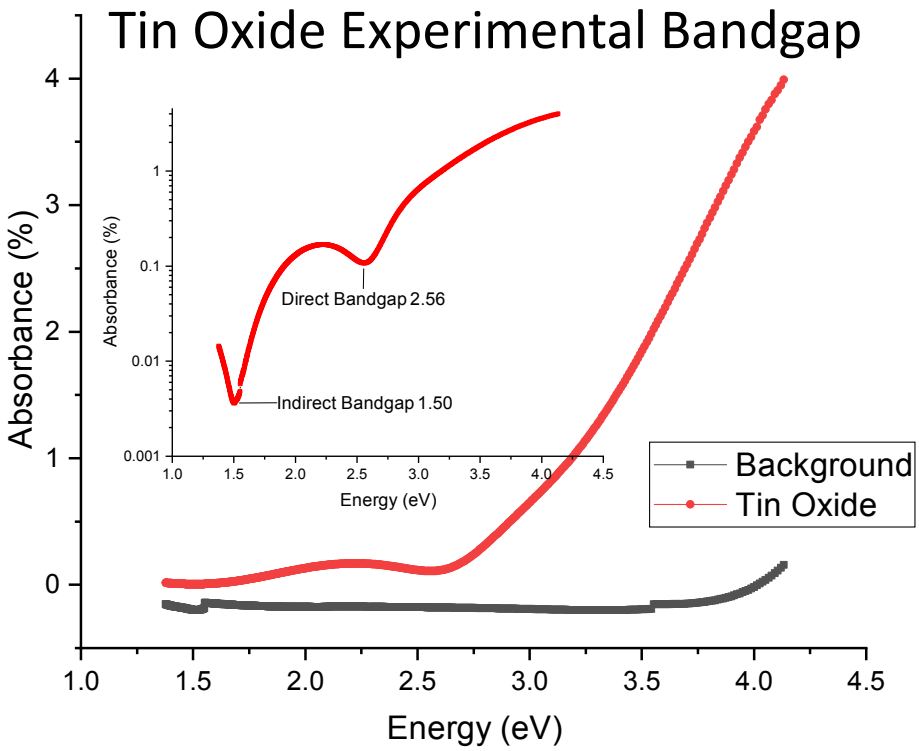

Figure 5.28: Experimental calculations of tin oxide bandgap derived from absorbance spectra for tin oxide on glass.

The logarithmic plot of absorbance as a function of energy in eV shows two separate absorbance minimums. The low energy minimum located around 825 nm (1.5 eV) suggests an indirect bandgap of ~1.5 eV. The high-energy minimum is found at 485 nm or 2.56 eV. This suggests a direct bandgap of ~2.6 eV which is close to the calculated optical bandgap of ~2.7 eV.

The difference in measured bandgap from reported literature may be a result of the substrate on which this tin oxide was grown. Ogo *et al*. reported tin oxide absorbance

from tin oxide powder. This tin oxide was grown on optically clear glass, and amorphous substrate, and therefore experiences more crystalline strain [70].

5.5.3 Oxygen Doping

There is evidence that the oxygen partial pressure under which the tin oxide is grown affects the threshold voltage. This makes sense as the percentage of each oxidation states of tin—tin(IV) and tin(II)—will be affected by the available oxygen during which the tin oxide is grown. Threshold voltage is highly affected by trapped charges, particularly at the interface between SiO_2 and SnO_x and at grain boundaries. SnO and SnO_2 form different crystal structures. SnO forms tetragonal PbO type crystals while SnO_2 forms rutile crystals. The presence of both types of tin oxides in one thin film layer will necessarily produce structural defects, vacancies, and trapped charges.

The partial pressure of oxygen under which the deposition takes place greatly influences the percentage of metallic Sn, Sn^{2+}, and Sn^{4+} that are found in the tin oxide film. The work of Luo *et al* [73] shows that for $O_{PP} > 14.3\%$, the resistivity of tin oxide deposited is so high that TFT performance is impossible. For the tin oxide described in this work, which was deposited before the comprehensive study by Luo, it was impossible to control oxygen partial pressure. The electron beam chamber operates under vacuum with a 6-10 Torr base pressure, with no specific oxygen scrubbing system.

5.5.4 Charge Transport

The narrow bandgap of SnO means that the Fermi level can be shifted from the valence band maximum (VBM) to the conduction band minimum (CBM) using either chemical doping or electrostatic doping [74], [75]. SnO_2 has a larger bandgap. The unipolar transport displayed by the as-fabricated SnO_x thin film transistors indicates that the Fermi level cannot be shifted up to the CBM because of sub-gap traps in the density

of states. These trapping states prevent minority carrier charge injection and hinder electron transport.

5.5.5 Conductivity

Because semiconducting tin oxide was so difficult to reproduce, the conductivity of samples was measured using Tunneling Atomic Force Microscopy (TUNA AFM). As shown in the below figure, some samples displayed small areas of electrical conductivity at 10V of gate bias. For many devices, however, the oxidation of tin oxide was simply too high for any meaningful semiconducting behavior to be observed.

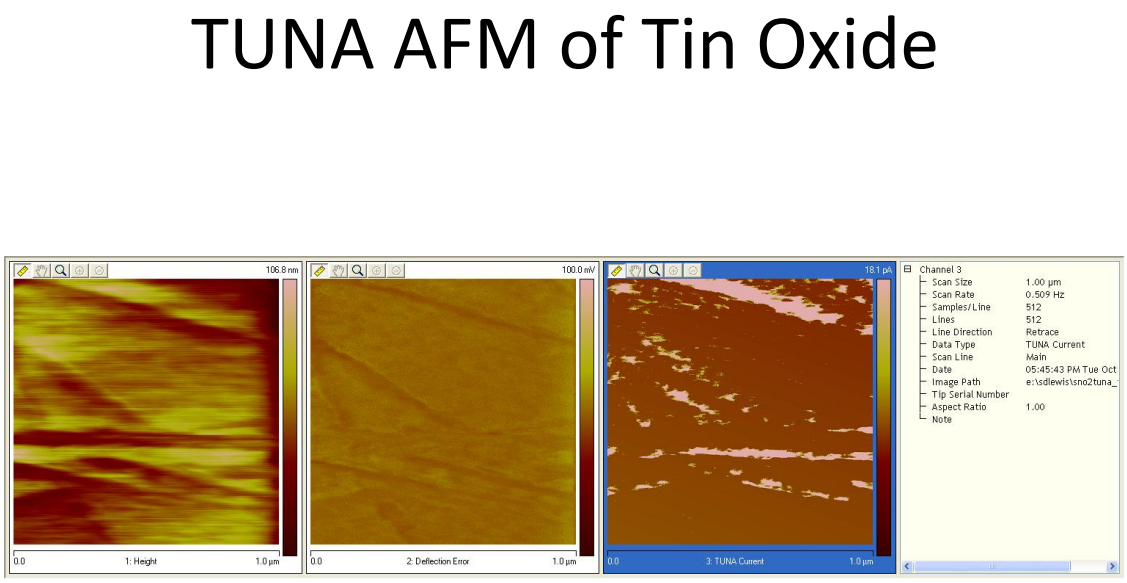

Figure 5.29: Tunneling Atomic Force Microscopy (TUNA AFM) measurements of tin oxide surface.

5.6 SIGNIFICANCE

The tin oxide growth and testing described here was conducted in 2007. Before that time, all oxide thin-film transistors were *n*-channel devices. This includes all the

metal oxides pioneered by Hideo Hosono *et al* [76]. The first paper the Hosono group wrote about *p*-type SnO TFTs was published in 2008.

Chapter 6: Bilayer Devices[1]

Most disordered organic semiconductors transport only one type of charge well under reasonable bias conditions at room temperature—unlike inorganic semiconductors, such as crystalline Si or GaAs that can be biased to transport either holes or electrons [77]. By combining a hole-transporting layer with an electron-transporting layer, it is possible to create an organic device that transports both holes and electrons. These devices are useful for chemical sensing, much like the four-terminal device discussed in the previous chapter.

6.1 Bilayer Device Electronic Band Structure

Most organic semiconductors transport only one type of charge efficiently. By combining appropriately chosen hole and electron transporting materials, it is possible to create devices that can accumulate both holes and electrons. For such a heterostructure to work, the *p*-type material must have a highest occupied molecular orbital (HOMO) energy level which is energetically lower for holes than that of the *n*-type material, and the *n*-type material must have a lowest unoccupied molecular orbital (LUMO) that is energetically lower for electrons that that of the *p*-type material [78]. Additionally, the HOMO states of the *p*-type semiconductor and the LUMO states of the *n*-type semiconductor must compete favorably with deep traps caused by moisture and oxygen. Similar considerations also apply for thin-film inorganic semiconductors such as zinc oxide and zinc tin oxide.

[1] Portions of this chapter have been previously published as "Hybrid organic/inorganic ambipolar thin film transistor chemical sensors" by Soumya Dutta, Shannon Doane Lewis, and Ananth Dodabalapur [77]. The devices described there were designed and fabricated by Dutta and Lewis. Data gathering was performed by Dr. Dutta.

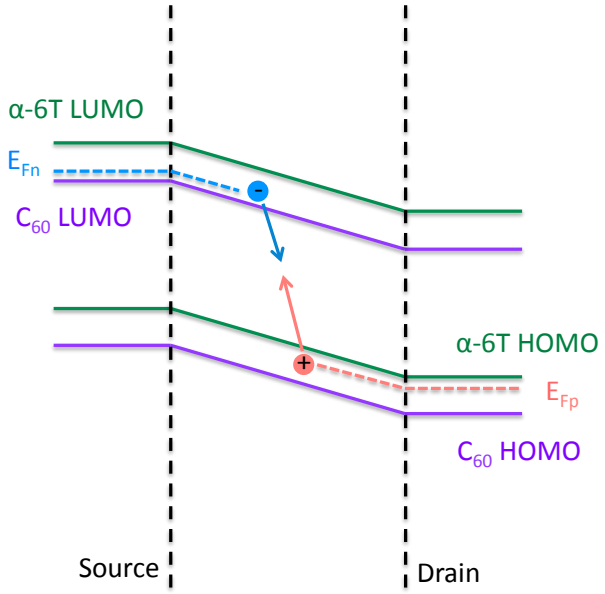

Figure 6.1: The electronic structure of an α-sexithiophene and C_{60} LED under bias conditions that encourages recombination of holes and electrons to produce photons.

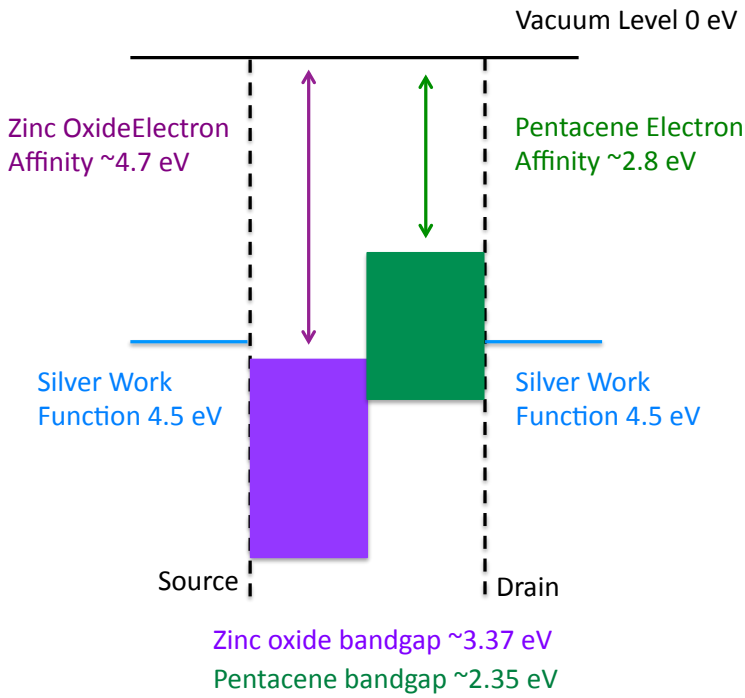

Figure 6.2: The electronic structure of a zinc oxide-pentacene device with silver source and drain contacts at zero bias [47].

These heterostructures can be biased to favor the recombination of holes and electrons in order to produce photon in light emitting diodes (LEDs) or to separate holes and electrons in solar photovoltaic cells [79]. In this application, recombination is not desired but rather ambipolar charge transport.

6.1.1 Heterostructure Geometry

The rate at which holes and electrons recombine is determined by the ease with which they physically approach each other. In order to maximize charge carrier recombination, the *n* and *p* type materials are often physically combined, as in a bulk heterojunction illustrated in Figure 6.3 below. When this effect is not desired, the surface area interaction between the charge transporting layers in minimized. The smallest contact area occurs in a bilayer device. In this construction, one layer is simply deposited on top of the other layer. This allows ambipolar transport and for both materials to be subjected to the same gate voltage and source drain voltage. In a planar heterojunction, there is still some recombination of electrons and holes across the interface, but it is much less than in a bulk heterojunction.

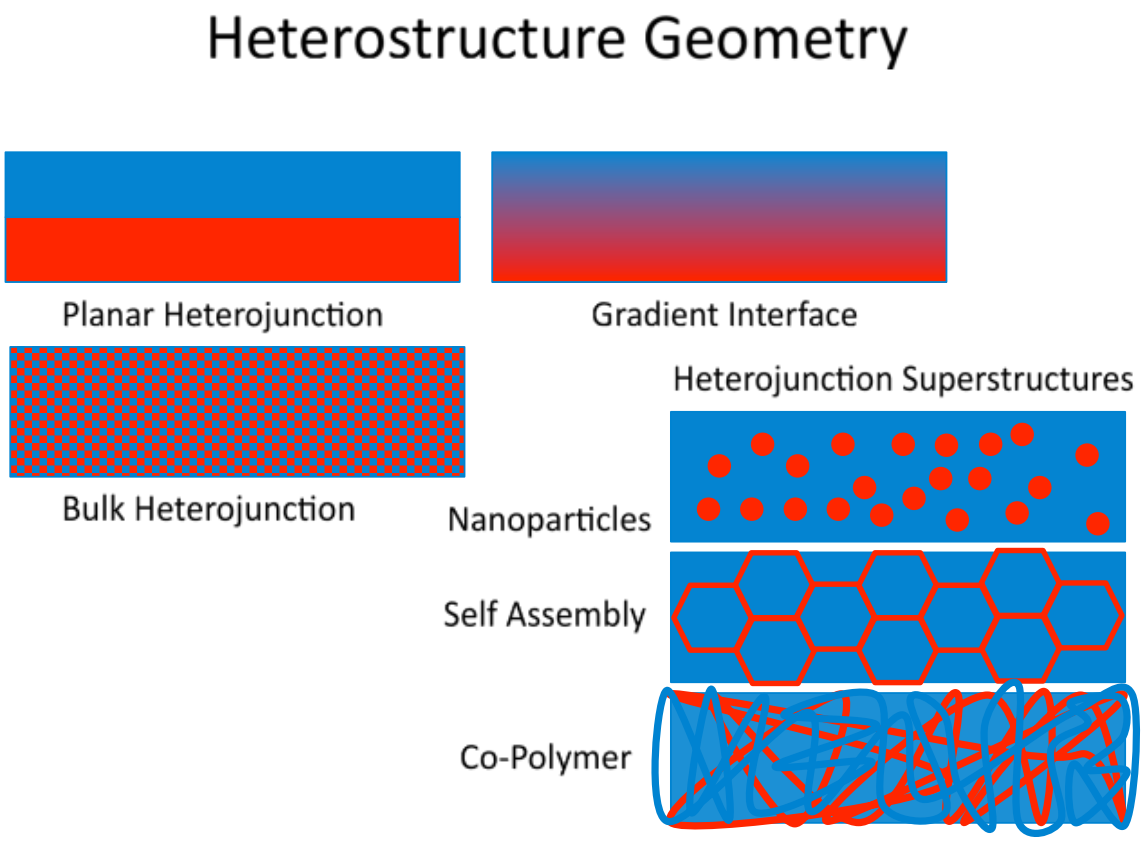

Figure 6.3: Examples of heterostructure geometry for dual semiconductor devices.

Zinc oxide cannot be co-deposited with pentacene. The zinc oxide is deposited via electron beam deposition, while pentacene is an organic and must be deposited by sublimation in vacuum. The bilayer device geometry is the easiest to produce for these two materials.

6.1.2 Electron Traps in Organic Semiconductors

There is evidence that organic semiconductors are also capable of transporting electrons when appropriate hydroxyl-free gate dielectrics are used [80]. The Cavendish laboratory has reported electron mobilities of 10^{-3} to 10^{-2} cm^2 V^{-1} sec^{-1} for organic nFETs. The reason organic semiconductors directly on silicon dioxide are predominantly *p*-type is because of the deep state trapping of electrons at the semiconductor-dielectric

interface. The interface silanol (SiOH) groups trap free electrons electrochemically as surface Si-O^- ions. This trapped layer of negative ions shifts the threshold voltage such that electron transport is effectively quenched for organic semiconductors with small electron affinity.

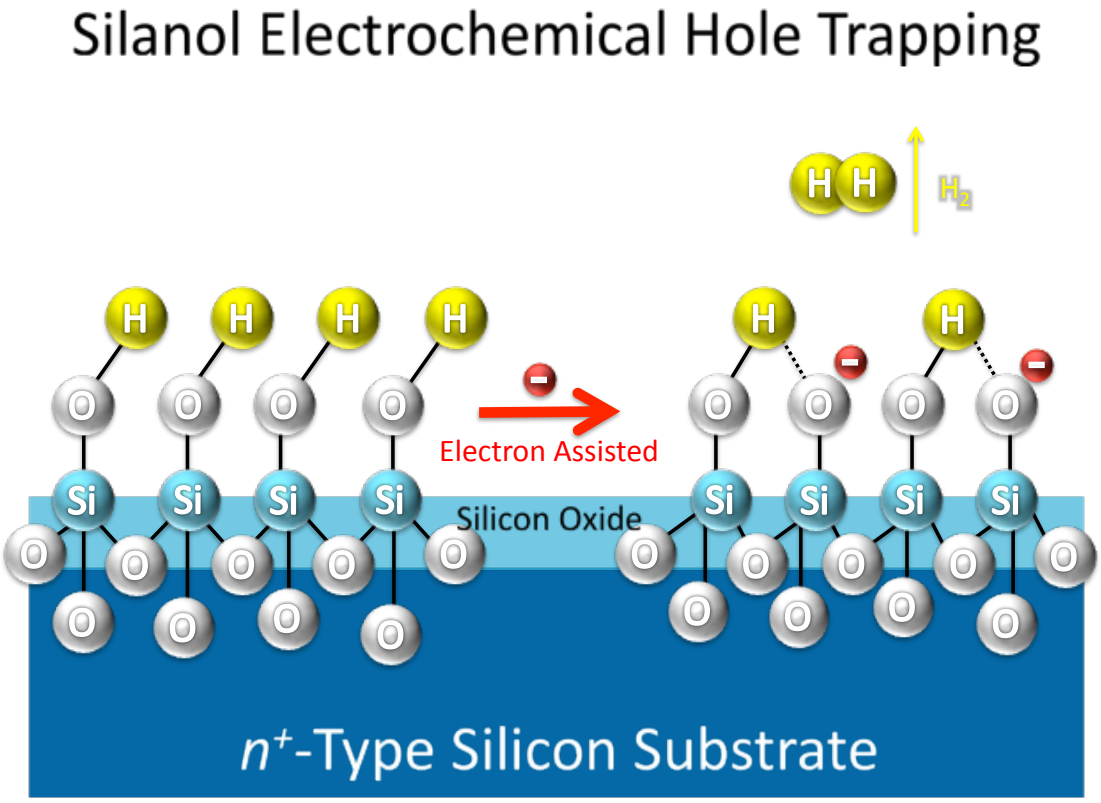

Figure 6.4: Proposed mechanism for silanol electrochemical hole trapping at the silicon oxide and organic semiconductor interface [80].

These SiOH electron traps are one reason to deposit zinc oxide directly onto the gate dielectric. Zinc oxide, because of its larger electron affinity, is a better electron transporting material, unlike pentacene, and can therefore produce an electron density large enough to both fill the traps states at the dielectric and contribute to mobile charge accumulation in the nFET.

6.2 Bilayer Organic And Inorganic Oxide Devices

In this application, the *n*-type material is pentacene, and the *p*-type material is zinc oxide. Zinc oxide is an electron transporting material and an inorganic oxide semiconductor already used as a chemical sensor, as described in the second chapter.

6.2.1 Bias Stress Effect

Zinc oxide does not experience the same degree of bias stress effect that degrades hole transport in organic semiconductors. However, it does experience some bias stress degradation in drain current when in nFET configuration [81]. This degradation has been shown to result from oxygen-facilitated charge trapping at the dielectric interface. However, unlike in organic semiconductors, the bias stress effect does not reduce mobility. The negative ions trapped at interface do not create charge scattering centers, both because they are the same polarity as the electrons being transported and because the zinc oxide charge transport is not polaronic. Charges in polycrystalline zinc oxide are more delocalized than those in typical organic semiconductors, resulting in higher carrier mobilities. The trapped charge layer mediates the effect of the gate charge and adds capacitance that effects threshold voltage. This charge trapping happens on a longer time scale than that in pentacene, so for these devices, it is possible to ignore the bias stress contribution from the zinc oxide portion of the device.

$$\Delta V_{th}(t) = [V_{th}(\infty) - V_{th}(0)]\left[1 - e^{-\left(\frac{t}{\tau}\right)\beta}\right]$$

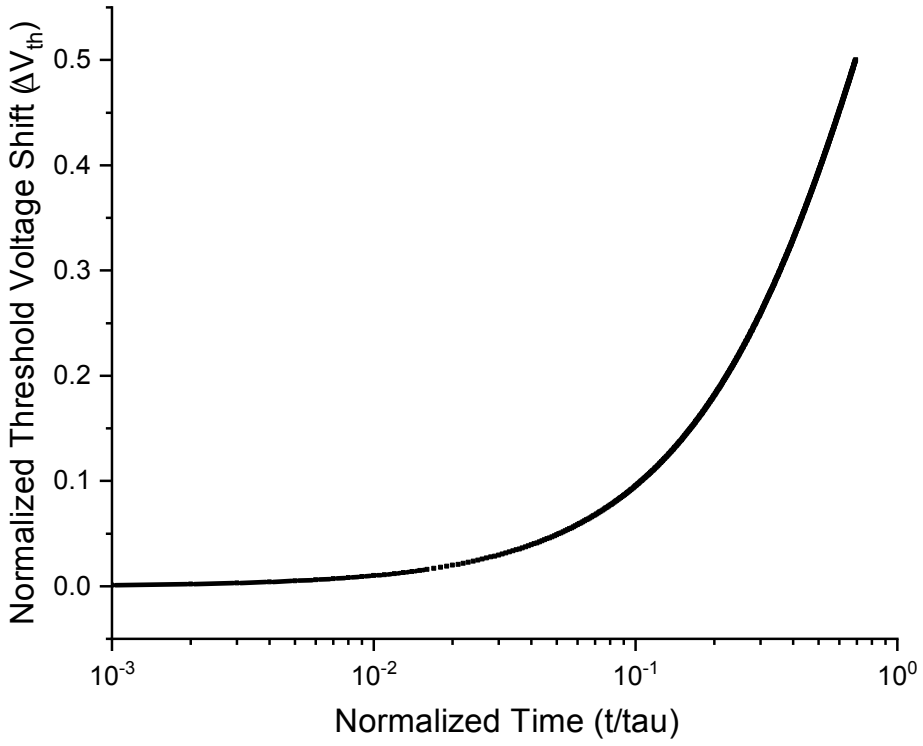

Figure 6.5: The shift in threshold voltage for an organic semiconductor as a function of time using the equation from Zschieschang *et al* [23].

Pentacene, like most organic semiconductors, experiences a noticeable bias stress effect when under bias in ambient atmosphere. This effect was discussed in Chapter 2.

6.3 Dual Channel Device Design

The bilayer device structure was developed to in order to produce an ambipolar chemical sensor that can be operated with minimal bias stress effect.

6.3.1 Ambipolar Transport

The bilayer device transports both holes and electrons. This ambipolar transport allows for several modes of operation. The organic semiconductor, in this case

pentacene, transports holes and interacts with the atmosphere. The zinc oxide layer transports electrons. The zinc oxide layer is gated by voltage applied to the silicon substrate, but also experiences induced mirror charges due to charges present in the organic top layer. Total charge transport across the device is a combination of both hole and electron transport through their respective charge transporting layers.

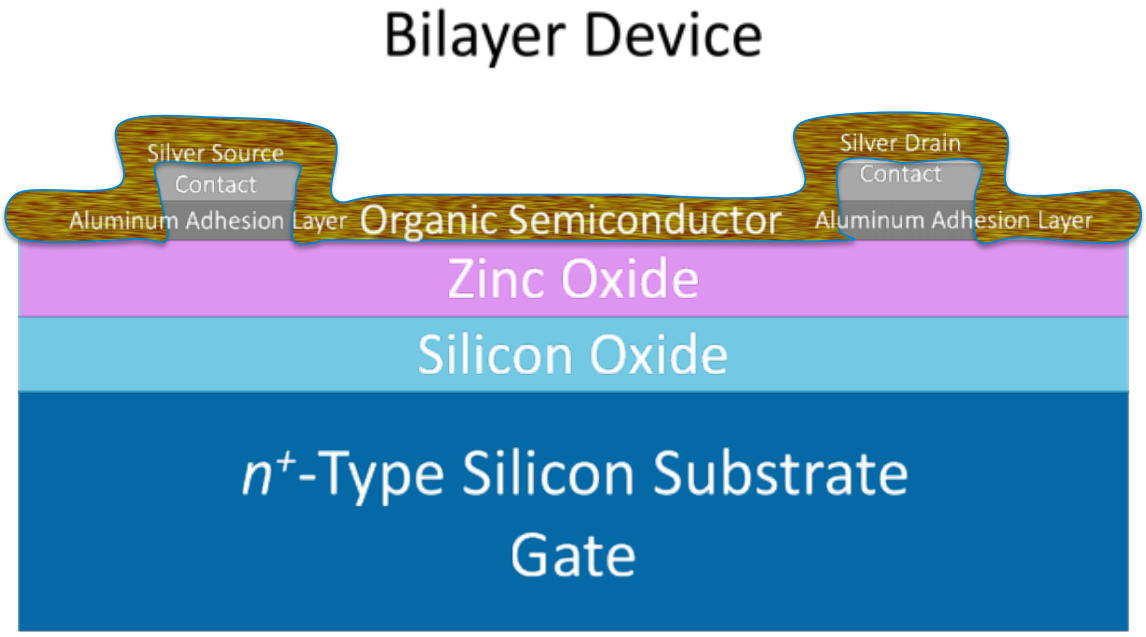

Figure 6.6: Cross-section of the zinc oxide and pentacene bilayer device.

6.4 Device Fabrication

The bilayer device was fabricated in-house at the Microelectronics Research Center at the J. J. Pickle Research Campus of the University of Texas at Austin.

6.4.1 Mask Design

The fabrication of the bilayer device required the development of one shadow mask. The device was fabricated on purchased silicon wafers coated with thermally grown SiO_2. These wafers are readily available and well-characterized and therefore easy

to use as substrates. The entire surface of each sample was covered with zinc oxide. A shadow mask was used to deposit the metal contact layers, which functioned as the source and drain electrodes. Then the entire substrate was again covered with pentacene. This allowed the development of a device that required only the one shadow mask and no etching or photoresist processing.

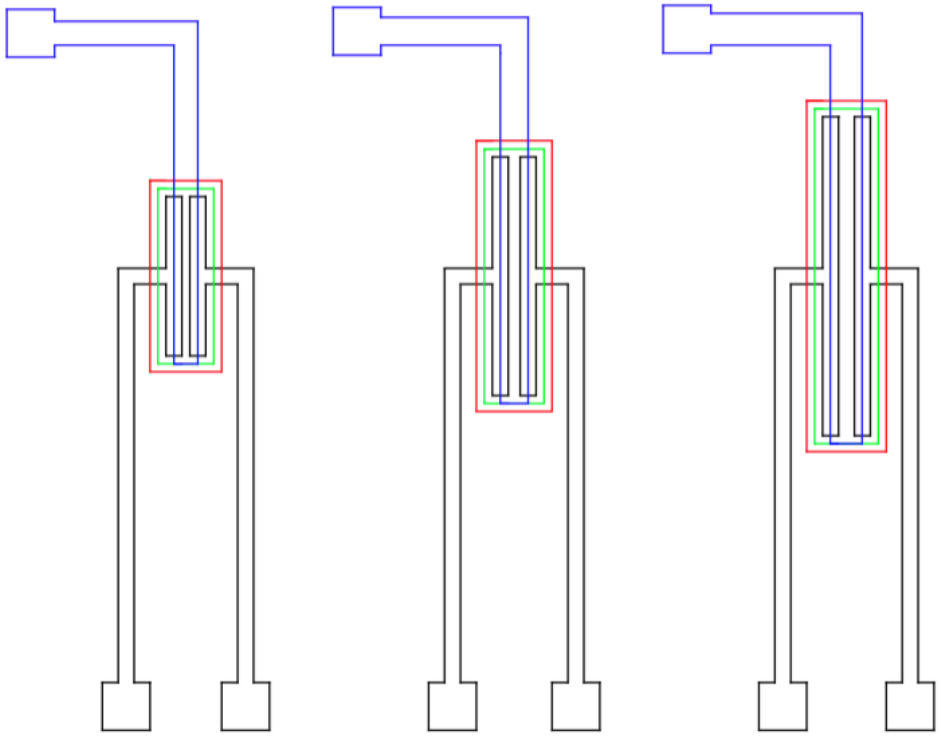

Figure 6.7: Top view of the shadowmask designs used to create the bilayer devices. The black layer contains the source and drain arms, while the blue layer is an optional additional channel electrode mask.

6.4.2 Silicon Processing

The bilayer device fabrication begins with the purchase of a heavily doped n^+ silicon (Si) (100) substrate with 150 nm of thermally grown silicon oxide (SiO_2). These

substrates are readily available and cost-effective. The commercially grown oxide is good quality and reliable in both thickness and resistivity.

The substrate is cleaned by five minutes of ultrasonification each in acetone, isopropyl alcohol, and deionized water. The acetone, isopropyl alcohol, and water together with ultrasonic agitation remove most polar and nonpolar surface contaminants. The surface is not etched because the silicon functions as a gate and substrate layer with its existing oxide. No new oxide is grown.

6.4.3 Inorganic Oxide Deposition

Zinc oxide (ZnO_x) was deposited directly on top of the cleaned silicon oxide by electron beam deposition. Zinc oxide was purchased as 99.9% pure tablets from Kurt J. Lesker for use in e-beam deposition. 35 nm of zinc oxide were deposited and then the substrate was annealed at 700 C for one hour under oxygen ambient.

6.4.4 Metal Contact Deposition

The source and drain contacts for both the organic and inorganic semiconductor were deposited directly on top of the zinc oxide using a shadow mask. All contacts were created using a single shadow mask and consist of approximately 30 nm of aluminum (Al) followed by approximately 30 nm of silver (Ag). The aluminum forms an adhesion layer on top of the zinc oxide that allows the silver to stick to the substrate. Silver has a more favorable work function for charge injection into pentacene. The work function of Al is 4.06-4.2 eV and that of Ag is 4.26-4.74 eV. Gold has a work function of 5.10-5.47 eV and is an even better contact for pentacene but reacts negatively with the necessary aluminum adhesion layer.

6.4.5 Organic Semiconductor Deposition

Pentacene is deposited via thermal evaporation under vacuum on top of the metal contact layer. The thermal evaporation was limited to 0.1 Å/sec in order to create a well-ordered material with high hole mobility. The pentacene layer thickness was approximately 35 nm.

6.5 OPERATION

The bilayer devices operate in four different modes depending on the source drain voltage (V_{DS}) and gate voltage (V_G). These modes are named after the type of charge that is transported and the region of the FET characteristic curve in which the device is operating.

Mode	Charge Transportation Material	Charge Type	V_G	V_{DS}
n-Channel Accumulation	Zinc Oxide	Electron	$V_G > 0$	$V_{DS} > 0$
p-Channel Triode	Pentacene	Hole	$V_G \sim 0$	$V_{DS} > 0$
n-Channel Triode	Zinc Oxide	Electron	$V_G < 0$	$V_{DS} < 0$ $V_{DS} > V_G$ and $V_{DS>0}$
p-Channel Accumulation	Pentacene	Hole	$V_G < 0$	$V_{DS} < 0$ $V_{DS} < V_G$

Table 6.1: The various conditions for the four modes of operation of the bilayer device.

6.5.1 *n*-Channel Accumulation

In *n*-channel accumulation mode, $V_{DS} \geq 0$ and $V_G > 0$. In this region, electrons are accumulating in the zinc oxide semiconductor region, and the FET displays distinct linear and saturation regions for drain current.

6.5.2 *p*-Channel Triode

The *p*-channel triode mode dominates for $V_{DS} \geq 0$ when $V_G \sim 0$. In this regime, charge transport is dominated by the injection of holes into the pentacene layer. The drain current increases superlinearly with V_{DS} for $V_{DS} > V_G$. The triode regime extends when $V_G < 0$ as well.

Because hole mobility in pentacene is lower than electron mobility in zinc oxide, electron conduction dominates hole conduction.

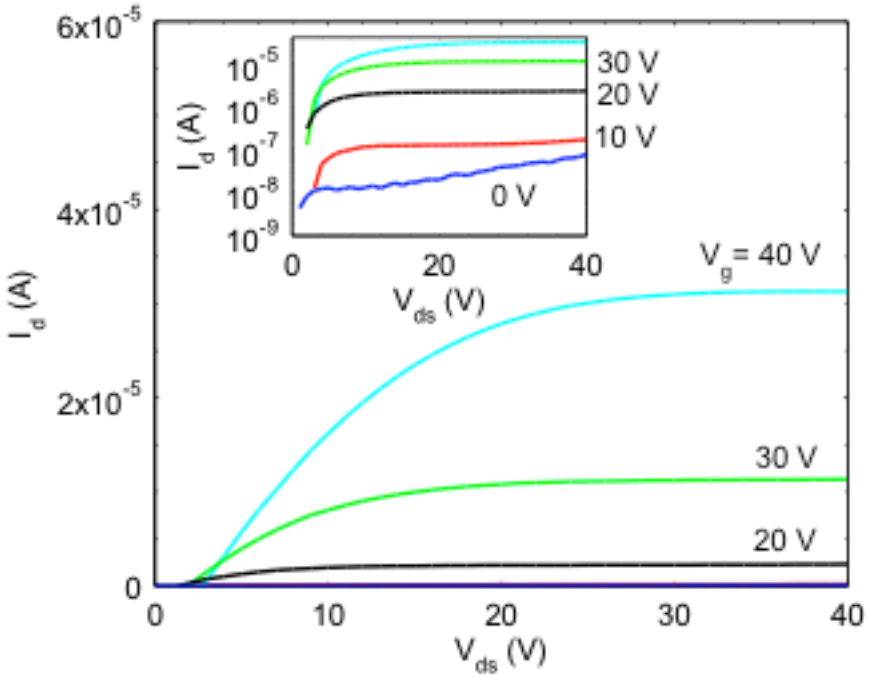

Figure 6.8: Output characteristics of the bilayer device for $V_{ds} > 0$.

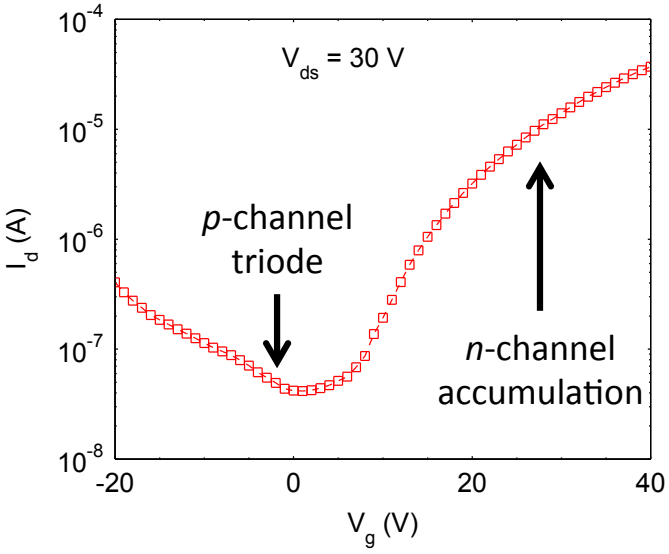

Figure 6.9: Semi logarithmic graph of transfer characteristics of the bilayer device under $V_{ds} > 0$, showing *p*-channel triode and *n*-channel accumulation modes.

6.5.3 *n*-Channel Triode

When both V_{DS} and V_G are negative, and $V_{DS} > V_G$, the device enters *n*-channel triode mode. This mode persists for V_{DS} positive. Electrons in the zinc oxide layer carry most of the current. For a fixed V_{DS} the drain current decreases in magnitude as V_G increases. This mode is the most stable chemical sensor. The chemical analyte interacts with the holes in the organic semiconductor, causing a corresponding change in the electron current in the inorganic oxide *n*-type semiconductor. Because the *n*-channel is functioning as a triode, a small increase in the electron concentration causes a large change in the drain current I_D.

6.5.4 *p*-Channel Accumulation

P-channel accumulation mode occurs when both V_G and V_{DS} are negative but $V_{DS} < V_G$. In this region, holes are accumulating in the channel of the pentacene organic semiconductor, and drain current increases in magnitude as V_G increases. This mode is

the second most effective sensing region. The current is predominantly hole-transport in the organic semiconductor, so the device functions very similarly to a typical organic thin film transistor (OTFT) sensor.

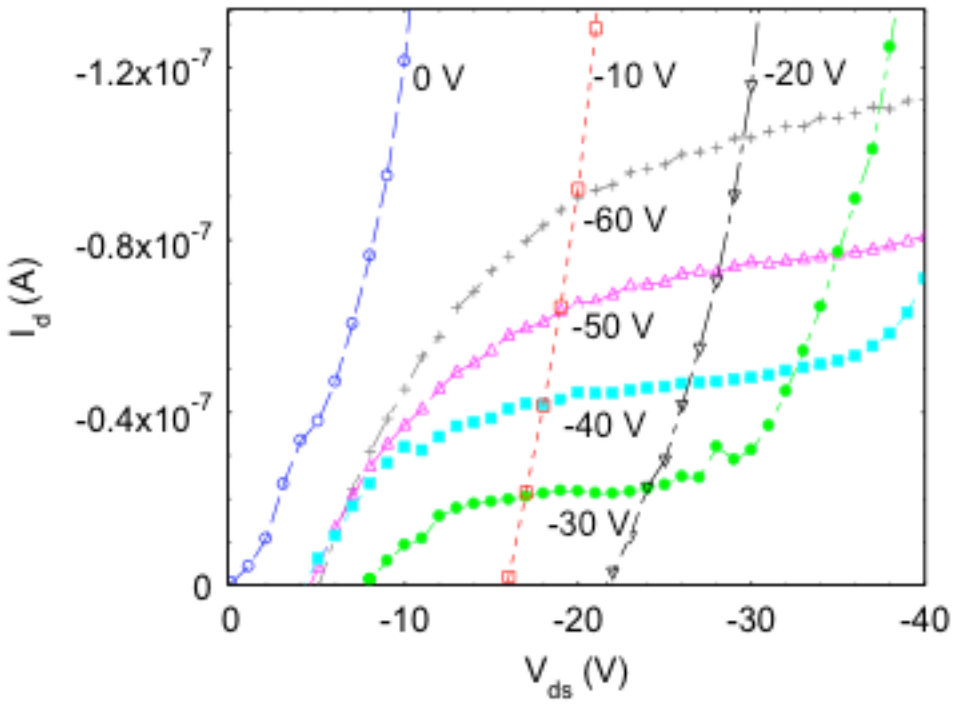

Figure 6.10: Output characteristics for the bilayer device when $V_{ds} < 0$.

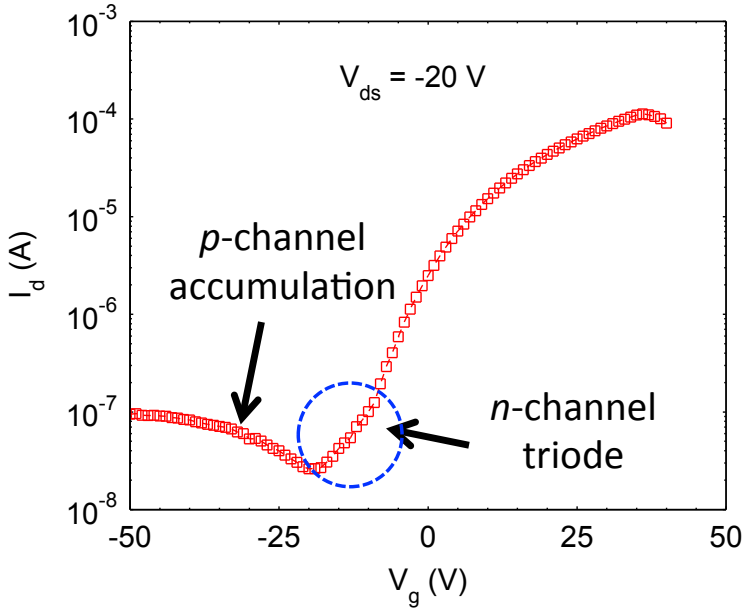

Figure 6.11: Semi-logarithmic graph of transfer characteristics of the bilayer device under $V_{ds} < 0$ showing *p*-channel accumulation and *n*-channel triode modes.

6.6 TESTING

The sensing characteristics of the device were evaluated using ethanol vapor (2000 ppm) at a set V_{DS} and V_G and measuring drain current.

6.6.1 *p*-Channel Accumulation Mode

The device was tested in *p*-channel accumulation mode with V_{DS} = -20 V and V_G = -40 V. Under these testing conditions, a large bias stress effect was observed. The magnitude of the bias stress effect may be due to the large amount of disorder at the zinc oxide/pentacene interface. The capacitive effect of the gate voltage is reduced because the pentacene is physically removed from the silicon dioxide gate by the presence of the zinc oxide, but this does not seem to affect the bias stress effect charge trapping mechanism. The bilayer device response to analytes in this region of operation is remarkably similarly to the response of OTFT sensors.

The physical separation of the pentacene from the silanol trap states at the silicon oxide-zinc oxide interface does not eliminate the bias stress effect. As shown by Hausermann and Batlogg, most of the traps that cause the bias stress effect occur at the grain boundaries and are filled by oxygen hole donation from the ambient atmosphere [82].

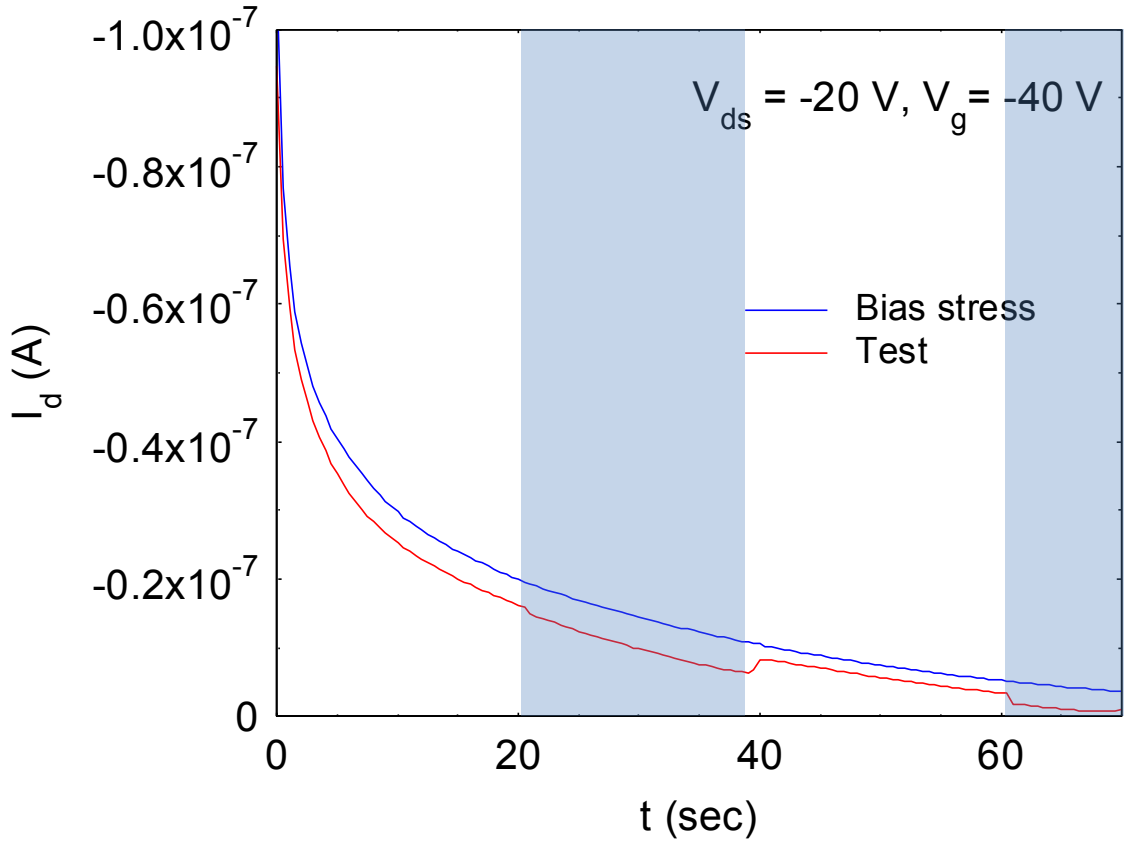

Figure 6.12: Sensor response of the bilayer device in *p*-channel accumulation mode as compared to the bias stress baseline. Analyte (ethanol) delivery occurred during the shaded time segments.

The device was also tested in *n*-channel triode mode with V_{DS} = -20 V and V_G = -10 V. In the triode mode, where electron transport dominates, the bias stress effect is

much less prevalent. There was an initial drop in drain current, but the long-term baseline is relatively flat.

The response to ethanol delivery was an immediate increase in drain current. When the analyte delivery was stopped, the current returned quickly to the baseline value. There was little current degradation due to the bias stress effect, even in the presence of ethanol, and no large increase in gate leakage current. In this mode, therefore, the bilayer device sensor shows several large advantages over typical OTFT sensors.

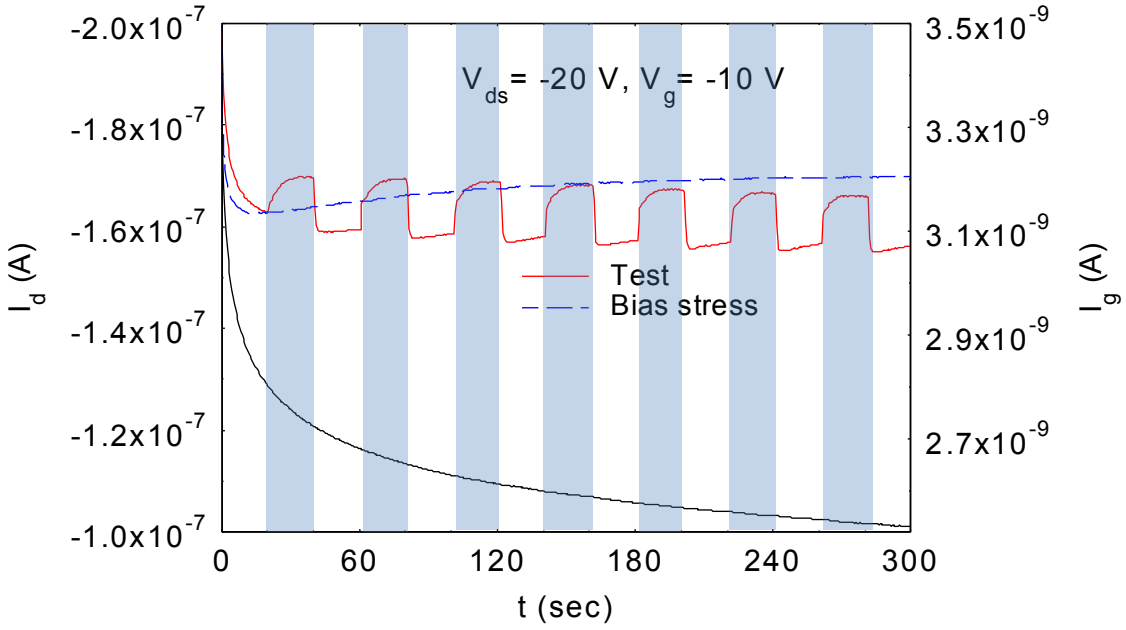

Figure 6.13: Sensor response of the bilayer device in *n*-channel triode mode as compared to the bias stress baseline. Ethanol analyte was delivered during shaded time segments. The right axis shows gate leakage current as a function of time.

6.7 Charge Trapping Mechanism

The different response to analyte delivery in the various modes can be explained by the proposed charge trapping mechanisms. The ethanol analyte dipole is delivered to

the top of the device, the pentacene layer. Ethanol is a polar molecule with a dipole moment of 1.69 Debye.

6.7.1 *p*-Channel Accumulation Mode

In the *p*-channel accumulation mode, charge transport is dominated by holes in the pentacene layer. These holes are likely to be induced near the zinc oxide/pentacene interface, which is as physically close to the gate dielectric as these charges can get. The large difference in ionization potential between the ZnO and pentacene creates a large potential barrier at this interface that confines the holes in the pentacene. When the analyte is delivered, its dipole moment is attracted to these holes, and it diffuses through the pentacene grain boundaries to the interface and functions as a charge trap state. As a result of this trapping, the current through the pentacene is reduced. Charge in most organic semiconductors is polaronic in nature, and the presence of polar molecules in the vicinity of charge carriers enhances trap depths and lowers mobilities. This results in a reduction in channel current during exposure of the sensor to the analyte.

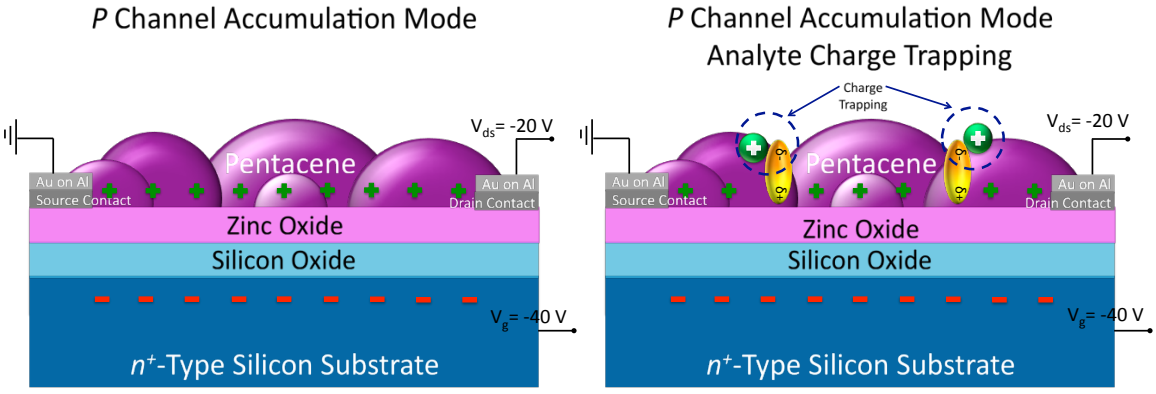

Figure 6.14: Charge trapping in the bilayer device operating in *p*-channel accumulation mode. Trapped charges in the pentacene layer lower mobility through the organic semiconductor because they inhibit hole transport by increasing trap depth.

6.6.2 *n*-Channel Triode Mode

In the *n*-channel triode mode, drain current is predominately the result of electron transport through the zinc oxide layer. In this mode, there are induced holes in the pentacene channel whose concentration and location is determined by the details of the bias conditions. Hole accumulation is prevalent when the gate-to-channel potential is negative and exceeds the pentacene threshold voltage. When polar analytes such as ethanol are delivered, the electrostatic conditions are disturbed, leading to enhanced electron injection into the channel and resulting in an increase in measured current as seen in Fig. 6.13 below.

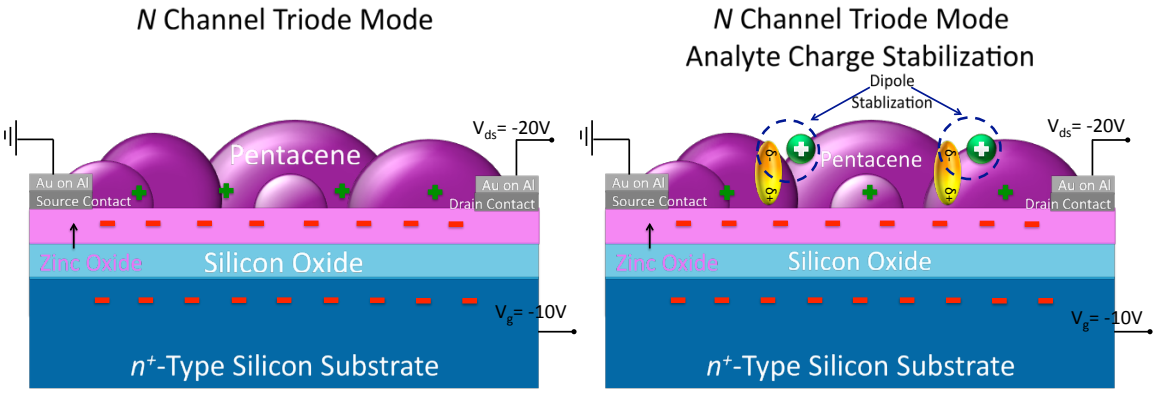

Figure 6.15: Charge trapping in the bilayer device operating in *n*-channel triode mode. Charges trapped in the pentacene layer induce additional charges in the zinc oxide layer that increase current through the inorganic oxide.

In this model, it is assumed that the analyte only interacts with pentacene—that zinc oxide itself is indifferent to the analyte molecule. This bilayer sensor is a unique combination of the chemical sensitivity of pentacene and charge transport in zinc oxide. The net result is that the sensor response is more stable and less susceptible to bias stress effects.

References

[1] H. Shirakawa, "Discovery of Polyacetylene Film: The Dawn of an Era of Conducting Polymers (Nobel Lecture)," *Angew. Chem. Int. Ed.,* vol. 40, pp. 2574-2580, 2001.

[2] N. F. Mott, "Conduction in non-crystalline systems IX. The minimum metallic conductivity," *Philosophical Magazine*, vol. 26, pp. 1015-1026, 1972.

[3] H. Shirakawa, E. J. Louis, A. G. MacDiarmid, C. K. Chiang, and A J. Heeger, "Synthesis of Electrically Conducting Organic Polymers: Halogen Derivatives of Polyacetylene, (CH)x." *J.C.S. Chem. Comm.,* iss. 16, pp. 578-580, 1977.

[4] π Systems. Organic Chemistry at Penn State. http://courses.chem.psu.edu/chem210/mol-gallery/pi-systems/pisystems.html. Accessed October 20, 2015.

[5] M. R. Bryce, "Recent Progress on Conducting Organic Charge-Transfer Salts," *Chem. Soc. Rev.*, vol. 20, pp. 355-390, 1991.

[6] S. D. Wang, X. Dong, C. S. Lee, and S. T. Lee, "Molecular Orientation and Film Morphology of Pentacene on Native Silicon Oxide Surface," *J. Phys. Chem. B*, vol. 109, no. 20, pp. 9892-9896, Apr. 2005.

[7] P. H. Lippel, R. J. Wilson, M. D. Miller, C. Woll, and S. Chiang, "High-Resolution Imaging of Copper-Phthalocyanine by Scanning-Tunneling Microscopy," *Phys. Rev. Lett.* vol. 62, pp. 171-174, Jan. 1989.

[8] M.C. Tanese, D. Fine, A. Dodabalapur, and L. Torsi, "Organic thin-film transistor sensors: Interface dependent and gate bias enhanced responses," *Microelectronics Journal*, vol. 37, pp. 837-840, 2006.

[9] A. Dodabalapur and L. Torsi, "Organic thin film transistors as plastic analytical sensors," *Analytical Chemistry*, vol. 77, pp. 380-387, 2005.

[10] S. V. Nadkarni, *Organic transistor based circuits as drivers for planar microfluidic devices* (Doctoral dissertation), The University of Texas at Austin, Austin, Texas, 2007.

[11] Z. Bao and J. Locklin, *Organic Field-Effect Transistors*, CRC Press, May 17, 2007. Print.

[12] V. Coropceanu, J. Cornil, D. A. da Silva Filho, Y. Olivier, R. Silbey, and J.-L. Brédas, "Charge Transport in Organic Semiconductors," *Chemical Reviews*, vol. 107, no. 4, pp. 926-952, 2007.

[13] T. Sakanoue and H. Sirringhaus, "Band-like temperature dependence of mobility in a solution-processed organic semiconductor," *Nature Materials*, vol. 9, pp. 736-740, 2010.

[14] N. Karl *et al*., "Fast electronic transport in organic molecular solids?," *Journal of Vacuum Science & Technology A,* vol. 17, pp. 2318-2328, 1999.

[15] Z. Bao, "Printable organic and polymeric semiconducting materials and devices," *Journal of Materials Chemistry,* vol. 9, pp. 1895-1904, 1999.

[16] R. H. Friend *et al*., "Electroluminescence in conjugated polymers," *Nature*, vol. 397, pp. 121-128, 1999.

[17] H. Sirringhaus, "25th Anniversary Article: Organic Field-Effect Transistors: The Path Beyond Amorphous Silicon," *Advanced Materials*, vol. 26, pp. 1319-1335, 2014.

[18] K. Myny *et al*. "Organic RFID transponder chip with data rates compatible with electronic product coding," *Organic Electronics*, vol. 11, no. 7, pp. 1176-1179, Jul. 2010.

[19] H. Klauk, "Organic thin-film transistors," *Chemical Society Reviews*, vol. 39, no. 7, pp. 2643-2666, Apr. 2010.

[20] H. Hoppe and N. S. Sariciftci, "Organic solar cells: An overview," *Journal of Materials Research,* vol. 19, pp.1924-1945, Jul. 2004.

[21] *Research Cell Efficiency Records*. Solar Energy Technologies Office. https://www.energy.gov/eere/solar/downloads/research-cell-efficiency-records. Accessed on January 22, 2017.

[22] K. K. Ryu *et al*., "Bias-Stress Effect in Pentacene Thin-Film Transistors," *IEEE Transactions on Electronic Devices*, vol. 57, pp. 1003-1008, 2010.

[23] U. Zschieschang, R. T. Weitz, K. Kern, and H. Klauk, "Bias stress effect in low-voltage organic thin-film transistors," *Applied Physics A,* vol. 95, pp. 139-145, 2009.

[24] T. Someya, A. Dodabalapur, J. Huang, K. C. See, and H. E. Katz, "Chemical and Physical Sensing by Organic Field-Effect Transistors and Related Devices," *Advanced Materials*, vol. 22, pp. 3799-3811, Jul. 2010.

[25] http://www.semi.org/en/node/57526

[26] Y. Sun and J. A. Rogers, "Inorganic Semiconductors for Flexible Electronics," *Advanced Materials*, vol. 19, pp. 1897-1916, 2007.

[27] T. Minami, "Transparent Conducting Oxide Semiconductors for Transparent Electrodes," *Semiconductor Science and Technology,*. vol. 20, no. 4, pp. S35-S44, Mar. 2005.

[28] K. Nomura, H. Ohta, A. Takagi, T. Kamiya, M. Hirano, and H. Hosono, "Room-temperature fabrication of transparent thin-film transistors using amorphous oxide semiconductors," *Nature*, vol. 432, pp. 488-492, Nov. 2004.

[29] E. Comini, "Metal oxide nano-crystals for gas sensing," *Analytica Chimica Acta*, vol. 568, no. 1-2, pp. 28-40, May 2006.

[30] J. S. Suehle, R. E. Cavicchi, M. Gaitan, and S. Semancik, "Tin Oxide Gas Sensor Fabricated Using CMOS Micro-Hotplates and *In-Situ* Processing," *IEEE Electron Device Letters,* vol. 14, no. 3, pp. 118-120, Mar. 1993.

[31] A. Maddalena, R. Dal Maschio, S. Diré, and A. Raccanelli, "Electrical conductivity of tin oxide films prepared by the sol-gel method," *Journal of Non-Crystalline Solids*, vol. 121, no. 1-3, pp. 365-369, May 1990.

[32] M. Batzill and U. Diebold, "The surface and materials science of tin oxide," *Progress in Surface Science,* vol. 79, no. 2-4, pp. 47-154, 2005.

[33] S.-C. Chang, "Oxygen chemisorption on tin oxide: Correlation between electrical conductivity and ERP measurements," *Journal of Vacuum Science and Technology*, vol. 17, no. 1, p. 366, Jan. 1980.

[34] G. Huang, L. Duan, G. Dong, D. Zhang, and Y. Qiu, "High-mobility solution-processed tin oxide thin-film transistors with high-κ alumina dielectric working in enhancement mode," *ACS Applied Materials and Interfaces*. vol. 6, no. 23, pp. 20786-20794, Nov. 2014.

[35] S. Gomri, J.-L. Seguin, J. Guerin, and K. Aguir, "A mobility and free carriers density fluctuations based model of adsorption-desorption noise in gas sensor," *J. Phys. D: Appl. Phys.*, vol. 41, no. 6, p. 065501, Feb. 2008.

[36] A. Rothschild and Y. Komem, "Numerical computation of chemisorption isotherms for device modeling of semiconductor gas sensors," *Sensors and Actuators B*, vol. 93, pp. 362-369, Aug. 2003.

[37] H. Q. Chiang and J. F. Wager, "High mobility transparent thin-film transistors with amorphous zinc tin oxide channel layer," *Applied Physics Letters,* vol. 86, no. 1, p. 013503, Dec. 2004.

[38] S. Dutta and A. Dodabalapur, "Zinc tin oxide thin film transistor sensor," *Sensors and Actuators B: Chemical*, vol. 143, no. 1, pp. 50-55, Dec. 2009.

[39] R. L. Hoffman, "Effects of channel stoichiometry and processing temperature on the electrical characteristics of zinc tin oxide thin-film transistors," *Solid State Electronics*, vol. 50, no. 5, pp. 784-787, May 2006.

[40] M. K. Jayaraj, K. J. Saji, K. Nomura, T. Kamiya, and H. Hosono, "Optical and electrical properties of amorphous zinc tin oxide thin films examined for thin film transistor application," *Journal of Vacuum Science and Technology B*, vol. 26, no. 2, pp. 495-501, Mar. 2008.

[41] B. Sykora and H. von Seggern, "Hybrid top-gate transistors based on ink-jet printed zinc tin oxide and different organic dielectrics," *Applied Physics Letters*, vol. 112, pp. 053503-1 – 053503-5, Jan. 2018.

[42] S. T. Shishiyanu, T. S. Shishiyanu, and O. I. Lupan, "Sensing characteristics of tin-doped ZnO thin films as NO_2 gas sensor," *Sensors and Actuators B*, vol. 107, no. 1, pp. 379-386, May 2005.

[43] S.-J. Seo, G. C. Choi, Y.H. Hwang, and B. S. Bae, "High performance solution-processed amorphous zinc tin oxide thin film transistors," *Journal of Physics D: Applied Physics*, vol. 42, p. 035106, Dec. 2008.

[44] C.-G. Lee, S. Dutta, and A. Dodabalapur, "Solution-Processed ZTO TFTs With Recessed Gate and Low Operating Voltage," *IEEE Electron Device Letters*, vol. 31, no. 12, pp. 1410-1412, Dec. 2010.

[45] A. Janotti and C. G. Van de Walle, "Fundamentals of zinc oxide as a semiconductor," *Reports on Progress in Physics*, vol. 72, p. 126501, Oct. 2009.

[46] A. Janotti, J. B. Varley, J. L Lyons, and C. G. Van de Walle, "Controlling the Conductivity in Oxide Semiconductors," in *Functional Metal Oxide Nanostructures,* J. Wu *et* al., Eds. Springer, 2012, pp. 23-35. <http://www.springer.com/978-1-4419-9930-6 >.

[47] Y. Zhang *et al*., "Zinc oxide nanorod and nanowire for humidity sensor," *Applied Surface Science*, vol. 242, no. 1-2, pp. 212-217, Mar. 2005.

[48] Y. Anno *et al*., "Zinc-oxide-based semiconductor sensors for detecting acetone and capronaldehyde in the vapor of consommé soup," *Sensors and Actuators B*, vol. 25, no. 1-3, pp. 623-627, Apr. 1995.

[49] M. S. Wagh, G. H. Jain, D. R. Patil, and L. A. Patil,"Modified zinc oxide thick film resistors as NH_3 gas sensor," *Sensors and Actuators B*, vol. 115, pp. 128-133, May 2006.

[50] B. B. Roa, "Zinc oxide ceramic semi-conductor gas sensor for ethanol vapour," *Materials Chemistry and Physics*, vol. 64, no. 1, pp. 62-65, Mar. 2000.

[51] B. Crone *et al*., "Electronic sensing of vapors with organic transistors," *Applied Physics Letters,* vol. 78, pp. 2229-2231, Apr. 2001.

[52] H. K. Patel, *The Electronic Nose: Artificial Olfaction Technology*. New Delhi: Springer, 2014.

[53] J. Fu, G. Li, Y. Qin, and W. J. Freeman, "A pattern recognition method for electronic noses based on an olfactory neural network," *Sensors and Actuators B*, vol. 125, no. 2, pp. 489-497, Aug. 2007.

[54] W. Göpel, "Chemical imaging: I. Concepts and visions for electronic and bioelectronics noses," *Sensors and Actuators B*, vol. 52, no. 1, pp. 125-142, Sep. 1998.

[55] J. B. Chang, V. Liu, and V. Subramian, "Printable polythiophene gas sensor array for low-cost electronic noses," *Journal of Applied Physics*, vol. *100*, pp. 014506, Jul. 2006.

[56] W. Shi, J. Yu, and H. E. Katz, "Sensitive and selective pentacene-guanine field-effect transistor sensing of nitrogen dioxide and interferent vapor analytes," *Sensors and Actuators B: Chemical*, vol. 254, pp. 940-948, Jan. 2018.

[57] L. Torsi *et al*, "A sensitivity-enhanced field-effect chiral sensor," *Nature Materials*, vol. 7, pp. 412-417, May 2008.

[58] I. Shackery *et al*, "Few-layered α-$MoTe_2$ Schottky junction for a high sensitivy chemical-vapour sensor," *Journal of Materials C*, 2018.

[59] R. G. Endres, C. Y. Fong, L. H. Yang, G. Witte, and C. Woll, "Structural and electronic properties of pentacene molecule and molecular pentacene solid," *Computational Materials Science*, vol. 29, no. 3, pp. 362-370, Mar. 2004.

[60] D. Sharma, "Combining silicon and organic/polymer semiconductors in a new class of sensor devices," M.S. thesis, Dept. Electron. Eng., The University of Texas at Austin, Austin, TX, 2005.

[61] Janata, Jiri and Mira Josowicz. "Conducting polymers in electronic chemical sensors." *Nature Materials* **2**, 19-24 (2003).

[62] Podzorov, V. *et al*. "Single-crystal organic field effect transistors with hold mobility ~8 cm^2/Vs." *Applied Physics Letters* **83**, 3504 (2003).

[63] *Diffused Ion Implantation Profile Calculator and Graph*. Brigham Young University Department of Electrical & Computer Engineering Cleanroom Home. http://www.cleanroom.byu.edu/implantcal.phtml. Accessed March 26, 2017.

[64] A. Ortiz-Conde *et al*., "A review of recent MOSFET threshold voltage extraction methods," *Microelectronics Reliability*, vol. 42, no. 4-5, pp. 583-596, Apr. 2002.

[65] F. Liao, "Organic TFTs as gas sensors for electronic nose applications," *Sensors and Actuators B: Chemical,* vol. 107, no. 2, pp. 849-855, June 2005.

[66] L. Wang, D. Fine, D. Sharma, L. Torsi, and A. Dodabalapur, "Nanoscale organic and polymeric field-effect transistors as chemical sensors," *Analytical and Bioanalytical Chemistry*, vol. 384, no. 2, pp. 310-321, Jan. 2006.

[67] S. Sharma, L. Wang, C. Burnham, D. Fine and A. Dodabalapur, "Organic and hybrid organic/inorganic transistors for chemical and bio sensing," *IEEE International Electron Devices Meeting*, 2005. *IEDM Technical Digest*., Washington, DC, 2005, pp. 4, pp. 453.

[68] D. H. Fine, *Approaches and Evaluation of Architectures for Chemical and Biological Sensing Based on Organic Thin-Film Field-Effect Transistors and*

Immobilized Ion Channels Integrated with Silicon Solid-State Devices (Doctoral dissertation), The University of Texas at Austin, Austin, Texas, 2007.

[69] A. Kolmakov, Y. Zhang, G. Cheng, M. Moskovits, "Detection of CO and O_2 Using Tin Oxide Nanowire Sensors," *Advanced Materials*, vol. 15, no. 12, pp. 997-1000, 2003.

[70] Y. Ogo *et al*., "*P*-Channel Thin-Film Transistors Using *p*-Type Oxide Semiconductor, SnO," *Applied Physics Letters*, vol. 93, no. 3, p. 032113, 2008.

[71] F. J. Arlinghaus, "Energy bands in stannic oxide (SnO_2)," *Journal of Physics and Chemistry of Solids*, vol. 35, no. 8, pp. 931-935, 1974.

[72] K. Nomura, T. Kamiya, and H. Hosono, "Ambipolar Oxide Thin-Film Transistor," *Advanced Materials*, vol. 23, no. 30, pp. 3431-3434, Aug. 2011.

[73] H. Luo, L. Liang, H. Cao, M. Dai, Y. Lu, and M. Wang, "Control of Ambipolar Transport in SnO Thin-Film Transistors by Back-Channel Surface Passivation for High Performance Complementary-like Inverters," *ACS Applied Materials & Interfaces*, vol. 7**,** pp. 17023-17031, 2011.

[74] G. Gupta, B. Rajasekharan, and R. J. E. Hueting, "Electrostatic Doping in Semiconductor Devices," *IEEE Transactions on Electronic Devices*, vol. 64, no. 8, June 2017.

[75] A. H. Nguyen, *at al*, "Electrical performance enhancement of p-type tin oxide channel thin film transistors using aluminum doping," *Thin Film Solids*, vol. 641, pp. 24-27.

[76] H. Hosono and T. Kamiya, "Material characteristics and applications of transparent amorphous oxide semiconductors," *NPG Asia Materials*, vol. **2**, no. 1, pp. 15-22, Jan. 2010.

[77] S. Dutta, S. D. Lewis, and A. Dodabalapur, "Hybrid organic/inorganic ambipolar thin film transistor chemical sensors," *Applied Physics Letters*, vol. 98, no. 21, p. 213504, May 2011.

[78] A. Hinderhofer and F. Schreiber, "Organic-Organic Heterostructures: Concepts and Applications," *ChemPhysChem*, vol. 13, pp. 628-643, Jan. 2012.

[79] A. Dodabalapur, H. E. Katz, L. Torsi, and R. C. Haddon, "Organic field-effect bipolar transistors," *Applied Physics Letters*, vol. 68, p. 1108, 1996.

[80] L.-L. Chua *et al*., "General observation of n-type field-effect behavior in organic semiconductors," *Nature,* vol. 434, pp. 194-199, Mar. 2005.

[81] R. B. M. Cross and M. M. De Souza, "Investigating the stability of zinc oxide thin film transistors," *Applied Physics Letters*, vol. 89, no. 26, p. 26313, Dec. 2006.

[82] R. Häusermann and B. Batlogg, "Gate bias stress in pentacene field-effect-transistors: Charge trapping in the dielectric or semiconductor," *Applied Physics Letters*, vol. **99**, no. 8, p. 083303, Aug. 2011.

Vita

Shannon Doane Lewis was born in Washington, D.C. She graduated from Georgetown Visitation Preparatory School in 2001 and received her B.S. in Chemical Engineering (Materials) from the California Institute of Technology in 2005. She received her M.S.E.E. in Electrical Engineering (Solid State Electronics) from the University of Texas at Austin in 2007. She then completed her research towards a Ph.D. in Electrical Engineering under the supervision of Dr. Ananth Dodabalapur at the Microelectronics Research Center at the J. J. Pickle Research Campus of the University of Texas at Austin.

Permanent email: sdlewis@utexas.edu

This dissertation was typed by the author.